University of Alberta

Advances in Stochastic Surface and Facies Modeling of Deepwater
Depositional Systems

by

Xingquan Zhang

©

A thesis submitted to the Faculty of Graduate Studies and Research
in partial fulfillment of the requirements for the degree of

Master of Science

in

Mining Engineering

Department of Civil and Environmental Engineering

Edmonton, Alberta
Fall 2007

Canada

Abstract

Numerical reservoir models are constructed by cell-based techniques or by stochastically placed geometric objects. Description of spatial structures needs three-point or even higher order of statistics, but traditional geostatistical tools are limited to reproduce one and two-point statistics. Stochastic surface-based modeling allows for improved integration of geological information in deepwater clastic turbidite reservoir models. Surface-based methods model stratigraphic layers to fill available accommodation space. Stacking patterns and hierarchies of trends related to sedimentary processes are reproduced by construction.

Deepwater surface-based methods are not mature. This thesis documents new developments, such as automatic surface-picks identification, deterministic and stochastic surface placement, global and local base levels modeling, improved hierarchical trend modeling and, global and depositional erosion events modeling, which result in more practical workflows and greater integration of deepwater geologic information. The result is improved numerical reservoir models of deepwater systems and, therefore, an expectation of improved reservoir performance forecasting and management.

Acknowledgements

I would like to thank Professor Clayton V. Deutsch for his support and encouragement. Dr. Deutsch led me to the world of Geostatistics. As a new research field, my M.Sc. has been a great learning experience. Without his efforts and help, it is impossible for me to think as a geostatistician now.

I would also like to thank Dr. Michael J. Pyrcz for his help and discussions. I had been working on the programs developed by him, including *Alluvsim*, *Surfsim*, *Turbsim* and others. I gained much knowledge by reading his source codes.

I appreciate the support of my colleges at Centre for Computational Geostatistics (CCG), specifically Dr. Weishan Ren who was another source of new ideas.

I dedicate this thesis to my family for their love and encouragement. My wife, Yuling, and daughter, Angelina, are a tremendous source of joy and stability.

Table of Contents

List of Tables

List of Figures

Chapter 1

Introduction

Depositional systems can be classified as continental depositional systems, coastal and nearshore depositional systems, continental shelf depositional systems and deep-sea depositional systems (DSD) based on their position. Each depositional systems can be further classified (Figure 1-1) on basin scale. Global hydrocarbon resources are unequally distributed in these depositional systems (Figure 1-2). Siliciclastic shoreline systems (SSL), and carbonate shelf systems and reefs (CSR) are the most important hydrocarbon bearing and production depositional systems due to their tectonic positions and proximity to hydrocarbon source locations. Discovered hydrocarbon reserves in deep-sea depositional systems (DSD) account for the smallest part of discovered global hydrocarbon resources (Figure 1-3): (1) deep-sea environments were inaccessible to the petroleum industry for many years, and (2) depositional mechanisms are very complicated. There are still many aspects of deepwater depositional systems at second-order lobe scale that are poorly understood until now. Therefore, there are many different geologic "models" for deepwater environment (Stow, 1992). However, with the development of new equipments and techniques, drilling in deeper water area becomes possible. As a result, deepwater environments will be more and more important in hydrocarbon exploration. It will be an important supplement to world hydrocarbon production.

Deepwater turbidite systems have become important exploration targets since the successful exploration in 1970s (Stow, 1992; Stelting *et al.*, 2000). Research in deepwater turbidite has been active since then. An accurate geological model is important to minimize the development risk due to the high development costs. The inaccessibility of deepwater environments and complicated spatial structures result in a high grade of uncertainty. Under this situation, stochastic simulation approaches are widely applied in investigating deepwater turbidite reservoir to quantify the uncertainty by building multiple equiprobable realizations.

Conventional stochastic facies, porosity and permeability models are usuallly cell based. These models are generally limited to reproduce one- and two-point statistics, therefore complicated spatial structures cannot be well reproduced because the descript of spatial structures needs three-point or even higher order of statistics (Pyrcz, 2005; Deutsch, 2006). However, the inference of multiple-point statistics of surfaces is difficult with limited data (Strebelle, 2002). The desire to reproduce more geologically realistic models naturally leads to the development of object- and surface-based simulation approaches. Object-based techniques were pioneered by Hal-

1

dorsen and Lake (1984), Haldorsen and Chang (1986), and Stoyan *et al.* (1987). Surface based techniques were introduced recently (Xie and Deutsch, 2000; Deutsch *et al.*, 2001; Pyrcz and Deutsch, 2003, 2004, 2005). The development of object- and surface-based simulation techniques has been important targets for many years.
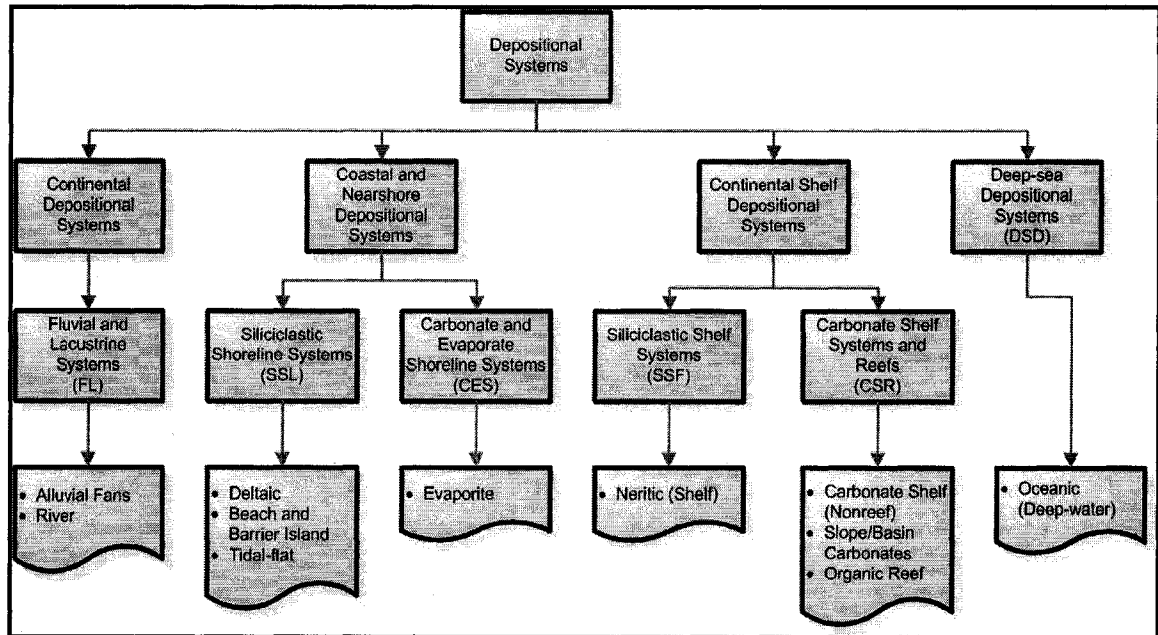
Figure 1-1: A diagram showing the depositional systems classification scheme used in this research (after Boggs, 2001 and Allen *et al.*, 2005)

Figure 1-2: The world hydrocarbon resources distribution (data from American Energy Information Administration; until January, 2006). Data are collected on countries and districts basis. The circle size represents the relative importance of that country / district in the world hydrocarbon resources. The red, yellow and blue colors represent oil, gas and coal resources, respectively.

2
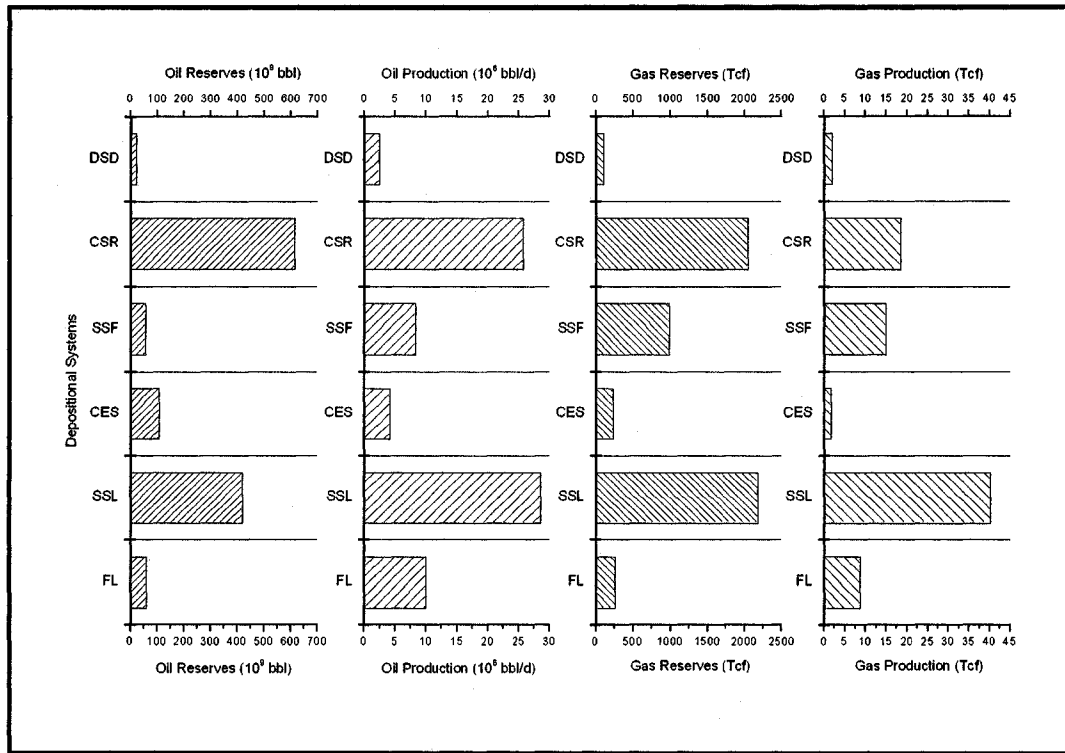
Figure 1-3: The world hydrocarbon resources distribution in different depositional systems.

1.1 Research background

There are many object- and surface-based turbidite modeling algorithms available in public domain. The development in this thesis is based on the following programs developed at the Centre of Computational Geostatistics (CCG) at the University of Alberta.

The *LobeSim* program, an object-based turbidite reservoir modeling program, was developed by Deutsch and Tran in 1999. A "simple" surface template was proposed and followed by later surface-based modeling techniques. This program was based on simulated annealing technique; both surface geometries and facies components can be well honoured, but the algorithm is quite slow.

Xie and Deutsch (2000) proposed a surface-based modeling program, *SurfSim*, which is based on a rule-based scheme to enforce data conditioning. The proposed methodology stochastically builds a surface model and honours available surface picks; rules are based on volume filling, types of stratal termination and the reproduction of within unit trends. The generated surface model mimics the appearance of actual geologic bounding surfaces and it was successfully applied in an outcrop with tabular units.

Pyrcz and Deutsch (2003) proposed a hierarchical surface modeling program, *TurbSim*, which builds models based on user-specified surface geometry parameters. The large-scale ge-

3

ometry may be a third-order lobe or bounding surfaces extracted from seismic. The fine-scale geometry is a second-order lobe. Surface model may be built hierarchically, that is, both large- and small-scale lobes may be built. A rejection algorithm was proposed for well conditioning, but the convergence may be slow with many wells. Facies are not simulated directly. As an alternative, a surface-based hierarchical petrophysical trend modeling approach was proposed to simulate reservoir petrophysical properties that followed the modeled reservoir spatial structures.

A limitation of *TurbSim* is that it assumes only single source location for all lobe events within given bounding surfaces. To extend the application of surface-based techniques in common geological settings without modeling third-order lobes, firstly, *LE_model* program was designed by Deutsch in 2006. Surfaces extracted from seismic image were applied directly as bounding surfaces and multiple source locations might be specified. Besides the flexibility, the limitations of *LE_model* are also apparent: (1) the entry position of a candidate surface is randomly picked without any constraints; therefore the simulated surface may not follow local bathymetry very well, and (2) the program is unconditional, that is, it cannot reproduce intersections at local wells.

The research in this thesis is based on the programs described above. For convenience, the development is based on the *LE_model* program, so the developed surface-based turbidite lobe events modeling program is still called *LE_model*.

1.2 Research motivation

The goal of this research is (1) to develop an algorithm that overcomes many of the limitations that have been identified, and (2) to extend the application of surface-based techniques to other geologic bodies with similar spatial structures, such as alluvial fans and delta fans. The initial motivation of this research is to solve the volume missing problem at the later simulation stage.

To avoid surface stacking artifact, a candidate surface is positioned on a reference surface instead of on the former surface. The volume below the former surface is truncated, so some volume will be lost. It is acceptable as long as the remaining volume is not too small. However, much volume is lost at the later simulation stage with the original algorithms of *LE_model* program. Figure 1-4 shows a case study example with the original algorithms. After 75% of filling proportion, large amount of surfaces are needed to fill the remaining volume, which means that volume missing becomes serious.

The reasons for volume missing problem at the later simulation stage are (1) a horizontal plane with the global minimum elevation of the former surface is selected as the reference surface, and (2) the influence of angle of permissible deposition. The angle of permissible deposition is

4

used to quantify basin boundary (Figure 1-5). At the later simulation stage, the global minimum elevation may be located out of the influence area, but it is difficult for this area to accept deposition. Therefore, the global minimum elevation will stop updating and the volume missing problem arises.
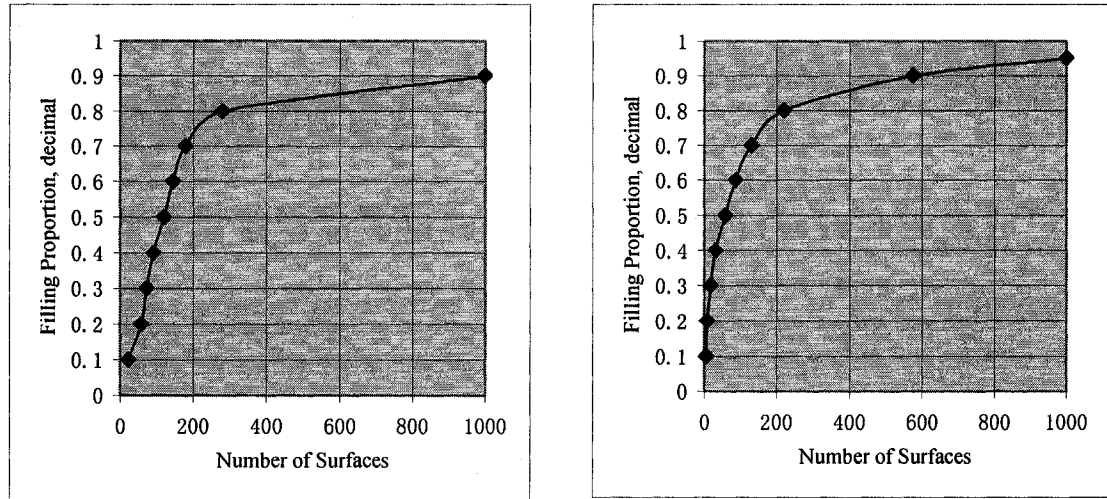
Figure 1-4: The cross plots of number of surfaces and filling proportion. Left: original surface placement rules without base surface transformation; Right: original surface placement rules with flattening base surface.
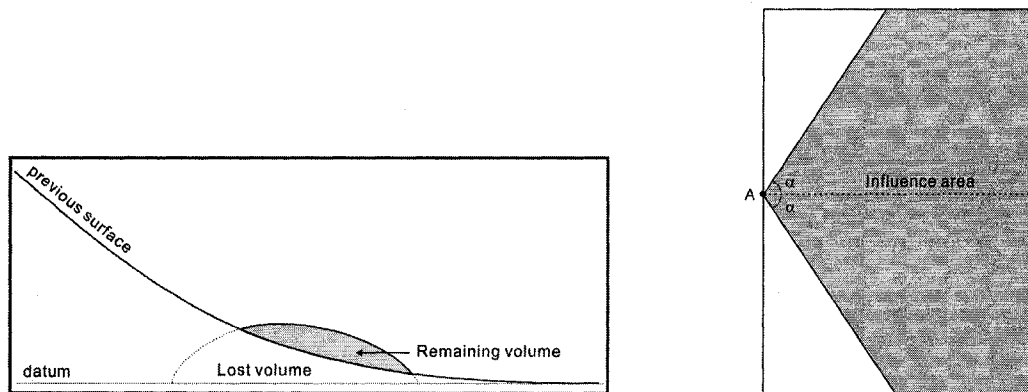
Figure 1-5: Schematic diagrams illustrating the volume missing problem at the later simulation stage. Left: the original vertical surface positioning rule. Right: the influence of angle of permissible deposition. Point "A" represents for a source location. Angle of permissible deposition, α, is used to quantify the basin boundary.

1.3 The need for surface-based modeling technique

The geological reality cannot be well known with limited data; therefore, the "truth" will never be known in practice. Figure 1-6 shows an idealized deepwater turbidite model representing a geological truth. The top and base surfaces are tilted and they pinch out towards north and west edges. Such pinch outs are common in continental slope environments. Since flow energy diminishes along streamlines, a special facies depositional sequence, the Bouma sequence, may form in a

5

flooding event. In the conceptual model, facies relationship is very strict and clear. In practice, facies relationship can only be coarsely honoured due to flow energy fluctuations. 36 wells are regularly sampled in the conceptual model with 1000 m well distance. The well positions are shown in Figure 1-7 with the corresponding stratigraphic thickness distribution. In practice, such dense well pattern seldom exists due to high drilling costs in deepwater environments. A cross surface section and the corresponding facies section are shown in Figure 1-8 and Figure 1-9, respectively. It is important to note that the lobe thickness diminishes quickly along flow direction. Therefore, the curvilinear shape of facies distribution is very clear and follows the shape of surfaces.
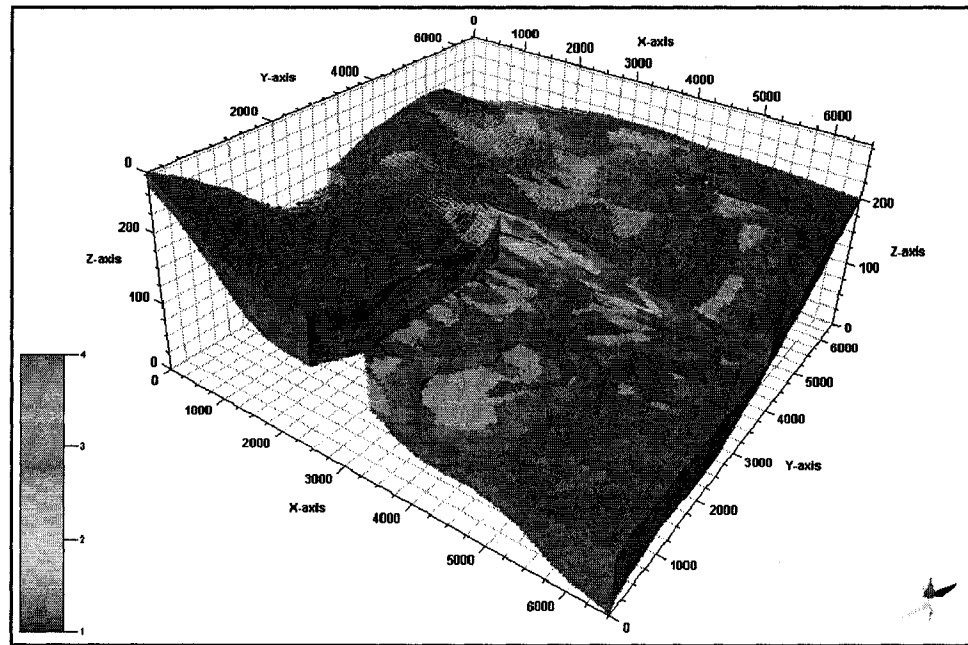
Figure 1-6: A conceptual deepwater turbidite depositional model showing the idealized 3D facies distribution. Note the curvilinear shape in both directions.
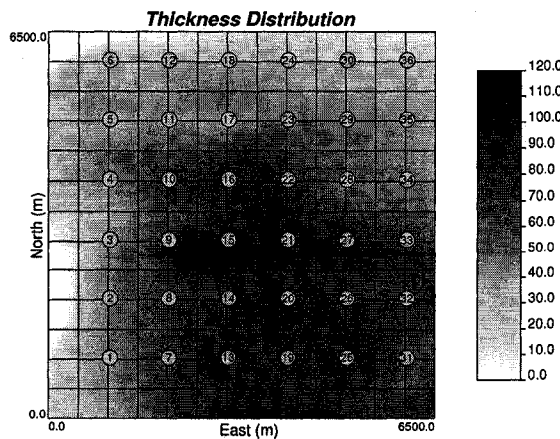
Figure 1-7: The well locations map with stratigraphic thickness distributions as background information.

6
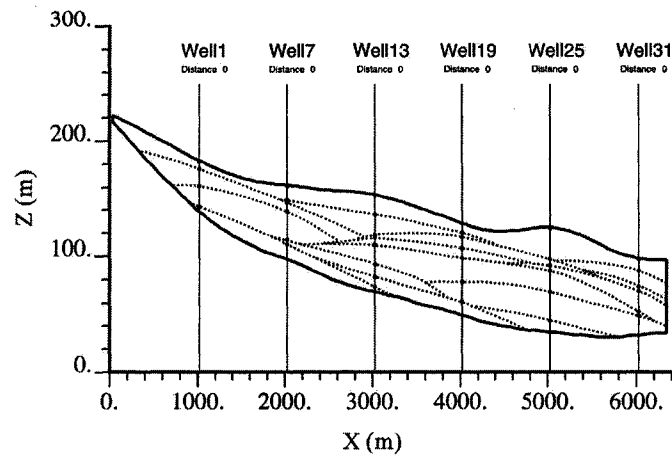
Figure 1-8: A cross section from the depositional model shown in Figure 1-6. Note the curvilinear surface shape and the scale of continuity. The lobe thickness also presents great variability.
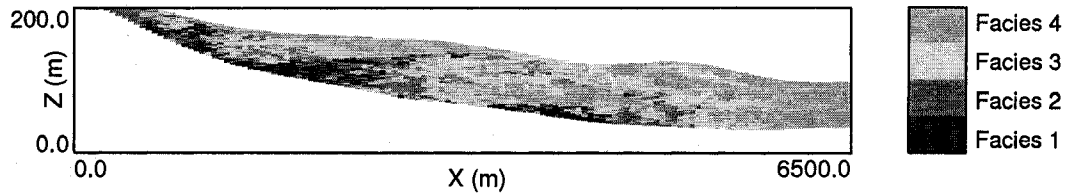
Figure 1-9: A possible facies distribution within the surface model shown in Figure 1-8. The curvilinear shape of the facies model is also very clear and follows the geometry of surface / lobe model.

1.3.1 Uncertainty on well correlations

Conventionally, reservoir structure is modeled with a series of well correlation diagrams, horizontal facies distribution maps and layer thickness distribution maps. Well sections with similar well log characteristics and lithology features are usually grouped into a geologic layer. In modern analysis, this is done within a sequence stratigraphic context.

Surface picks identification. Surface picks are the intersections of surfaces/lobes with well trajectories. Each interval between two surface picks is a Bouma sequence. This sequence is usually incomplete due to lateral facies changes and depositional erosions. Surface picks with similar depositional characteristics may be grouped as larger-scale depositional unit.

Well correlation diagrams plotting. The correlation is often based on surface picks and/or seismic image. Building a fine-scale 3D reservoir structural model by hand is difficult because the information of fine-scale surfaces on seismic is incomplete. Descriptive language is used often instead of giving a quantitative structure model. With the same identified surface picks, different correlation maps may be plotted based on different geological understandings. In practice,

7

usually only one correlation map is made because the procedure is tedious and time-consuming when large amount of wells are available. Figure 1-10 shows a hand-contoured well correlation map.
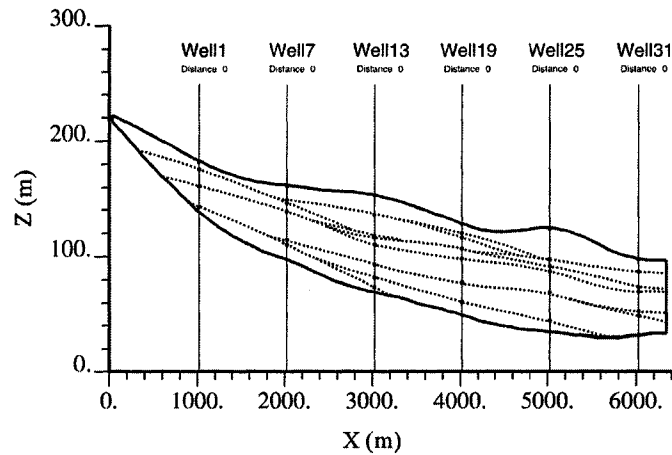
Figure 1-10: The identified surface picks and a hand-contoured well correlation map based on surface picks.

The limitations of above approach are apparent, (1) the correlation maps are usually built deterministically, and (2) the procedure is tedious and time consuming. It is inefficient to build multiple correlation diagrams by hand if there are many wells available. The correlation procedure is subjective, which has the advantage of integration of expert knowledge; however, the procedure is tedious and the scale of identified geological body may be unreasonable if average well distance is sparse comparing with lobe size. Therefore, the inference of the spatial distribution of turbidite lobes is difficult and ambiguous. In practice, the spatial structure is commonly built at larger scale. Several Bouma sequences may be grouped together as a stratigraphic unit. Each unit is equivalent to a third-order lobe. The curvilinear shape of lobes is awkward to map by hand. Therefore, the result may look more like a "layer-cake" model and the spatial continuity inference may be incorrect.

Sequence stratigraphy may be applied to guide for building consistent reservoir structure. When seismic data are available, the stratigraphic framework building in large-scale is relatively straightforward. However, the resolution of seismic data is usually not good enough for fine-scale structure identification. Therefore, the solution for fine-scale reservoir structure model may not be unique.

In a word, the lack of control results in great uncertainty on fine-scale reservoir structure construction/modeling, which cannot be quantified by conventional approaches.

8

1.3.2 Uncertainty on facies distribution

The distribution of facies controls the distribution of petrophysical properties, such as porosity and permeability. Therefore, the prediction of facies distribution is an important topic in reservoir modeling. Large-scale facies distribution may be visualized on high-resolution seismic image; however, fine-scale facies can only be identified on wells and outcrops, which cannot be continuously traced through seismic. 2D mapping methodologies are frequently applied to map areal facies distributions, such as kriging and minimum curvature. These maps are deterministic and they are the average of a layer; therefore, they are only trend maps and cannot be used to quantify the uncertainty of a specific location. Another type of facies trend map is hand-contoured conceptual facies distribution map (Figure 1-11), which are deterministic; therefore, uncertainty is not quantified.
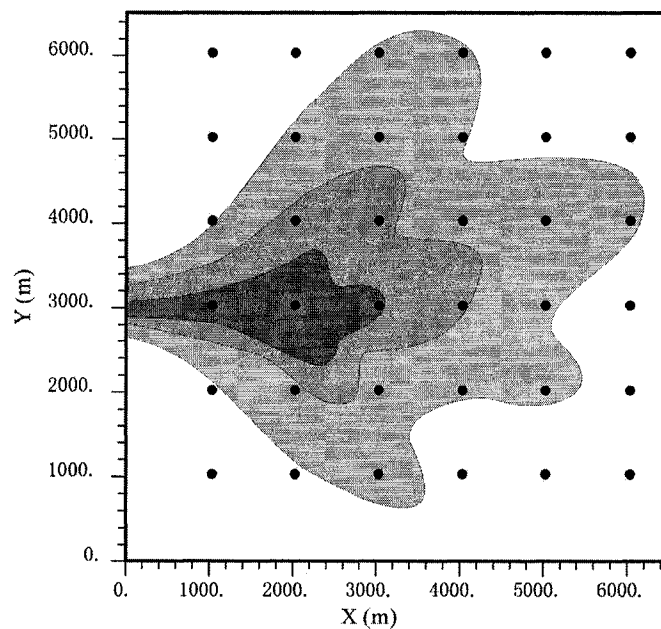
Figure 1-11: A hand-contoured facies distribution map based on well data and well correlation results.

Cell-based stochastic modeling techniques may be applied to quantify the uncertainty of facies distribution. The major limitation of cell-based facies modeling techniques is that only one- and two-point statistics can be reproduced, so the complicated reservoir structure cannot be captured because the description of spatial structures needs three-point or even higher order of statistics. Figure 1-12 shows a typical SIS-based facies cross section based on 36 wells data. Although there are plenty of wells and average well distance is only 1 kilometre, the curvilinear shape of facies still cannot be well captured. In this research, a depositional trend-based facies modeling

9

method is proposed. The method is also cell-based. The depositional coordinates of each cell are calculated and facies proportions are calculated based on specified trend template. Therefore, continuous surface information is transformed to discrete cell-based facies proportions information, which can be integrated by many SIS-based facies modeling techniques, such as truncated Gaussian simulation (*GTSIM*), blocked sequential indicator simulation (*BlockSIS*) and sequential indicator simulation with local means (*sisim_lm*).

In a word, uncertainty of facies distribution results from (1) the uncertainty of fine-scale reservoir structures, and (2) the uncertainty of cell-based facies modeling methodologies.

Based on above analysis, we can see that the curvilinear lobe distribution is the major drive for turbidite facies distribution, which cannot be well reproduced with conventional geostatistical tools. Therefore, we need surface-based modeling techniques to integrate limited information and geological knowledge.
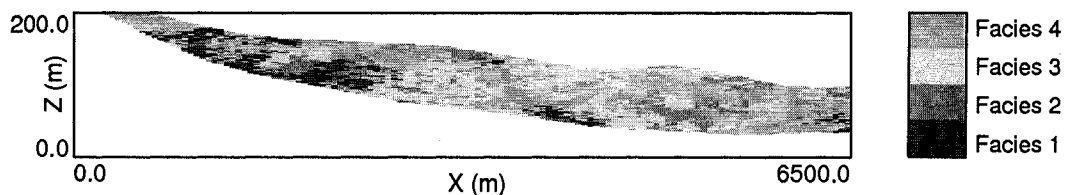
Figure 1-12: A conventional SIS-based facies section based on well data. Although there are many wells available, the spatial structure is not realistic and does not follow the shape of the conceptual depositional model.

1.4 Dissertation outline

Chapter 2 is an overview of the geological background of deepwater depositional systems. Section 2.1 reviews deep sea environments. Section 2.2 illustrates the deepwater turbidite classification used in this thesis and their major characteristics. Section 2.3 illustrates the major components of turbidity current. Section 2.4 presents the idealized vertical profile, Bouma sequence, and its characteristic of each division. Section 2.5 discusses the large-scale controlling parameters on turbidite distribution.

Chapter 3 illustrates the advances in surface based modeling made in this research. Section 3.1 presents an automatic procedure for surface identification based on well logs. Section 3.2 presents the advances in lobe events modeling. Section 3.3 illustrates the advances on strataform surface simulation.

Chapter 4 demonstrates a possible application of constructed facies models and the surface-based facies modeling approach. Section 4.1 introduces the conceptual turbidite model used in this thesis. Section 4.2 presents how to integrate vertical facies trends with conceptual facies

10

model, that is, the idealized areal facies distribution. Section 4.3 illustrates how to integrate statistical trends with honouring global facies proportions. Section 4.4 compares two popular cell-based facies modeling approaches that can integrate facies proportions information. Section 4.5 presents a geologically realistic case study to explain the application of surface-base modeling approach.

Chapter 5 presents a turbidite case study. A geostatistical workflow is presented. The reservoir is located in a typical deepwater environment with 36 synthetic wells. Known conditioning data include surface picks, facies, porosity and permeability well logs. 25 stochastic surface models are built with honouring all surface picks. All available facies, porosity and permeability data are honoured in coming reservoir properties modeling stage.

Chapter 6 presents conclusions and discusses the limitations of this research.

11

Chapter 2

Geological Background

There are three fundamental deepwater depositional environments, (1) slope aprons, (2) submarine fans, and (3) basin plains. Second-order turbidite lobe focus of this thesis is an important component of deepwater submarine fans. The chief characteristics of deepwater submarine fans are illustrated in this chapter, (1) a brief introduction of deep sea environment, (2) the classification and basic characteristics of deepwater submarine fans, (3) major components of large-scale turbidity current, (4) components of idealized vertical profile, the Bouma sequence, and (5) major controlling parameters on the morphology of deepwater depositional systems.

2.1 Deep sea environment

The deep sea can be subdivided into several topographical units, (1) deep-sea grabens, (2) ocean basins, and (3) continental margins. Most submarine fans are located along continental margins. The bottom gradient of typical submarine fans is usually less than 0.5 degrees (Table 2-1). Submarine canyons play an important role in carrying large amount of sediments across continental margins to form submarine fans. These canyons and channels are easily visualized on high resolution seismic.

Location	Bottom gradient in degrees
Submarine canyons	1.0 – 3.0
Upper fan channels	0.2 – 0.5
Middle fan lobes	0.1 – 0.4
Lower fan	0.1 – 0.2

Table 2-1: Typical gradients of submarine fans (after Pickering *et al.*, 1989)

Reineck and Singh (1980) summarized the important transport systems in the continental shelf, margin and ocean basins, which produce characteristic types of deep-sea deposits:

1) Fluvial mixed transport and separation of sand and lutum.
2) Transport and deposition of sand, including longshore transport, canyon and distributary transport.
3) Low-velocity, low-density turbidity currents.
4) High-velocity, high-density turbidity currents.
5) Sediment slides of larger dimensions.
6) Transport through contour currents.

12

From above, we can see that transport systems of deep sea environment are complicated; therefore, a universal process-based turbidite modeling program development is difficult.

Although the transport mechanisms may be different, many transport systems form similar deposition structures. Middleton and Hampton (1976) distinguished four types of sediment gravity flow and their possible deposition forms:

1) Turbidity current flow → turbidite.

2) Liquefied sediment flow → turbidite.

3) Grain flow → resedimented conglomerate and some fluxo turbidite.

4) Debris flow → pebbly mudstone.

Therefore, surface-based modeling technique development is practical by neglecting specific depositional mechanisms and modeling lobe geometry instead. As a geometry-based simulation approach, surface-based modeling technique may be applied in many types of turbidite depositional systems with similar spatial structures.

2.2 Deepwater turbidite classification

Each turbidite system has unique tectonic setting, sediment supply and oceanographic controls (Stow, 1992). For simplicity, an idealized end-member classification is applied in this research. There are two types of deepwater submarine fans, radial fan and elongate fan. Radial fan includes three regions, upper fan, mid-fan and lower fan. Upper fan region is dominated by a single feeder channel or canyon that is flanked by distinct levees; mid-fan region is characterized by distributory channels and depositional lobes; lower fan is smooth with low-gradient. Radial fans are usually sand-rich fans. Elongate fans extend longitudinally away from a relatively broad head region, either perpendicular to or sub-parallel to the source-area margin. Two or more main fan channels may be developed with distinct confined levees and these channels meander across an extensive mid-fan area. Large terminal lobes form in a smooth lower fan region. The facies distribution is more elongate than concentric. These fans are often referred to as mud-rich fans. The research in this thesis focuses on second-order lobes, which may be middle fan lobes of a radial fan or distal fan lobes of an elongate fan.

The classification of smaller-scale architectural elements of turbidite environment is also complicated. Many classifications were proposed for specific research purposes or based on different geological settings. For example, the Reading and Richards (1984) scheme was based on grain size and feeder system and it was proposed to describe various architectural element associations. The Ghosh and Lowe (1993) scheme, a hierarchical process-based architectural elements classification scheme, is applied in this research. According to this classification, individual ho-

13

mogeneous component is identified as first-order architectural elements, including individual division of the Bouma sequence and other coarser components. A single or the collection of first-order elements forms a second-order element, which represents products of a flow event. Third- and fourth-order architectural elements represent reservoir-scale features, such as lobes and channel-levee systems. These elements can be visualized and continuously traced on high-resolution seismic, thus they are treated as boundary conditions in this research. Note that because of the resolution of seismic, the distribution of bounding surfaces may have some uncertainties.

2.3 Components of large-scale turbidity current

As mentioned above, turbidity current is an important transport system in deepwater environment. Small-scale turbidity currents have great variability, so the prediction of the product of small-scale turbidity currents is difficult. Large-scale turbidity current may be distinguished into head, body and tail components (Figure 2-1). Head is the thickest part that is the region of erosion and formation of scour marks; body is rather uniform in thickness through its length; and tail is where flow thins out and becomes dilute. Dense medium (sediment-water mixture) must be continuously supplied in the head to compensate for the losses caused by turbulence (Middleton and Hampton, 1976). If loss is larger than compensation, the turbidity current slows down and begins forming a new lobe.

d_B = depth of body
d_H = depth of head
U_B = velocity of body
U_H = Velocity of body
ⒸC = Coarse load
ⒻF = Fine load
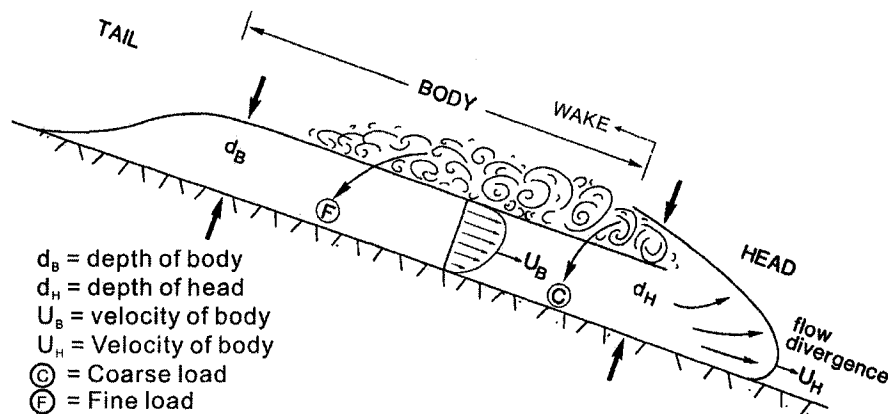
Figure 2-1: Simplified sketch of a large turbidity current, divided into head, body and tail regions. Setting from the wake behind the head produces a lateral size grading in the flow (after Pickering *et al.* 1989).

2.4 Components of Bouma sequence

Bouma (1962) made a comprehensive study of ancient turbidites and developed a vertical facies model, the well-known Bouma sequence (Figure 2-2). An idealized turbidite sequence is made up of five divisions with specific sedimentary structures:

14

1) **Graded interval**, the lowest part. It shows more or less distinct graded bedding. No other sedimentary structures exist. It is sandy or gravelly in nature. The contact to the former deposition is usually erosional.

2) **Lower interval of parallel lamination**. It shows predominantly thick parallel laminae of sand. The contact to the graded interval is gradual.

3) **Current ripple lamination interval**. It is made up of fine sand and silty sediments and shows small-current ripple bedding. An indistinct grading is present from bottom to top.

4) **Upper interval of parallel lamination**. It is a very fine sandy to silty clay zone showing a distinct parallel lamination.

5) **Pelitic interval**. This is a clayey sediments interval. No distinct sedimentary structures exist.

These intervals are seldom completely observed due to lateral facies change and depositional erosions. Note that Bouma sequence is idealized. Many researchers modified it based on geological settings, such as Hesse (1992), Pickering (1989).
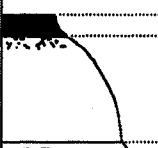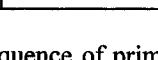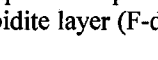
Grain size (ø)			Time of deposition	Bouma sequence (1962)		Devisions	Interpretation
8	4	2 0 -1					
Clay	Silt	Sand					
	Md.	Max.					Erosion by turbidity current
			1 to 10³y Months(?)		F	(Hemi-)pelagic	Interturbidite
					E	Pelitic	Deposition from low-density tail of burbidity current setting of pelagic or hemipelagic particles
			Hours		D	Upper parallel laminated	Shear sorting of grains and flocs
					C	Ripples, climbing ripples or convolute laminated	Lower part of lower flow regime
					B	Lower parallel laminated	Upper flow regime plane bed
2µm	62µm	2mm	Minutes		A	Massive or graded	Rapid deposition with no traction transport, possible quick (liquefied) bed

Figure 2-2: Modified Bouma sequence of primary sedimentary structures in an ideal turbidite showing a pelagic (or hemipelagic) interturbidite layer (F-division) separated from the pelitic E-division (after Pickering *et al.* 1989).

2.5 Large-scale controlling parameters on turbidite morphology

The natural development of surface models involves geological processes that occur over a range of time-scales. Stow *et al.* (1996) and Baas *et al.* (2005) summarized the major long-scale parameters controlling the morphology of deep-water depositional systems (Table 2-2). In general, the shape and internal organization of deep-water systems vary according to grain size, sea-level, basin configuration and degree of basin confinement, number and distribution of sediment input

15

points and tectonic settings. Grain size represents flow energy which controls the lobe geometry and scale, such as lobe shape, length and width. In LE_model program developed in this thesis, lobe geometries are randomly drawn from user specified distributions. From Figure 2-2, it is very clear that turbidite flow events are driven by processes on annual or sub-annual time-scale. Therefore, long-scale controlling parameters, such as sea-level changes, basin configuration, degree of basin confinement and tectonic settings are assumed stable during stochastic lobe events modeling. In particular, sea-level changes result in different surface stacking patterns, such as aggradation, progradation and retrogradation, and large-scale thickness trend. The number and distribution of sediment input points can be specified explicitly in LE_model program. The sediment input points are located on one edge of the model. A coordinate transform could be applied to rotate the spatial coordinates to align the model with the paleocurrent.

Long-scale controlling parameters	Short-scale controlling parameters
Regional basin tectonics	Local tectonics
	Basin bathymetry
	Basin and basin margin geometry
	Entry point distribution
Sea-level fluctuations	Eustatic changes
	Tectonically induced changes
	Variations in clastic input
Rate, type and source of sediment supply	Depositional process
	Hinterland type and climate
	Nearshore system, type and shape
	Shelf systems, type and shape

Table 2-2 Major parameters controlling the morphology of deepwater clastic depositional systems (after Baas *et al.* 2005)

16

Chapter 3

Advances in Surface Based Modeling

The research in this thesis focuses on two modeling targets, (1) second-order lobes, and (2) strataform surfaces. Lobe events modeling is mainly based on the *LE_model* and *TurbSim* programs. Strataform modeling is based on the *Surfsim* program developed by Pyrcz in 2004.

Section 3.1 illustrates an automatic surface picks identification approach that can be used as the data preparation process for surface modeling; Section 3.2 illustrates advances in lobe events modeling; Section 3.3 presents advances in strataform modeling aiming at making it more flexible and powerful.

3.1 Automatic surface picks identification

Surface picks are the intersections of surfaces with wells. Third-order surfaces can be clearly visualized on high-resolution seismic, but the identification of second-order surface picks is problematic. Due to the scale, second-order surface picks can only be identified on well logs, core and outcrops. In general, there is no directly relevant outcrop data to a particular deepwater reservoir. Core is limited due to cost. Therefore, well logs are the common information used for surface picks identification. Experienced geologists can identify them with specific well logs, such as *RT* (resistivity), *Gr* (Gamma) and/or *SP* (spontaneous potential). In many cases, the accessible logs are interpreted petrophysical property logs instead of raw logs. These logs may be facies proportions, $Fac(z)$, porosity, $\phi(z)$, and shale content, $Vsh(z)$. The proposed methodology can be applied to raw or interpreted log, and it may be easily modified to utilize multiple well logs to minimize misidentification.

Commonly, bed thickness within a turbidite lobe presents a thinning-upward trend. There are two types of idealized sequence with thinning-upward trend, (1) gradual and progressive thinning-upward trend, and (2) step-like thinning-upward trend (Figure 3-1). The probability of gradual and progressive thinning-upward trends is very small (Pickering, 1989). The proposed approach can handle both trends.

A core profile of the Cumberland Bay Formation (CBF) of South Georgia is selected to illustrate the proposed methodology (Figure 3-2). CBF is a thick sequence of turbidite sandstones deposited in a linear back-arc basin (MacDonald, 1992). The selected profile is a shale abundant vertical sequence located in distal turbidite. A synthetic porosity curve is constructed that is shown as the solid line in Figure 3-3. Lamination information is discarded and only lithofacies

17

information is kept. Texture information may be important in surface picks identification; however, it is very hard to obtain directly from well logs. Two lithofacies are assumed based on original profile, sandstone and mudstone.
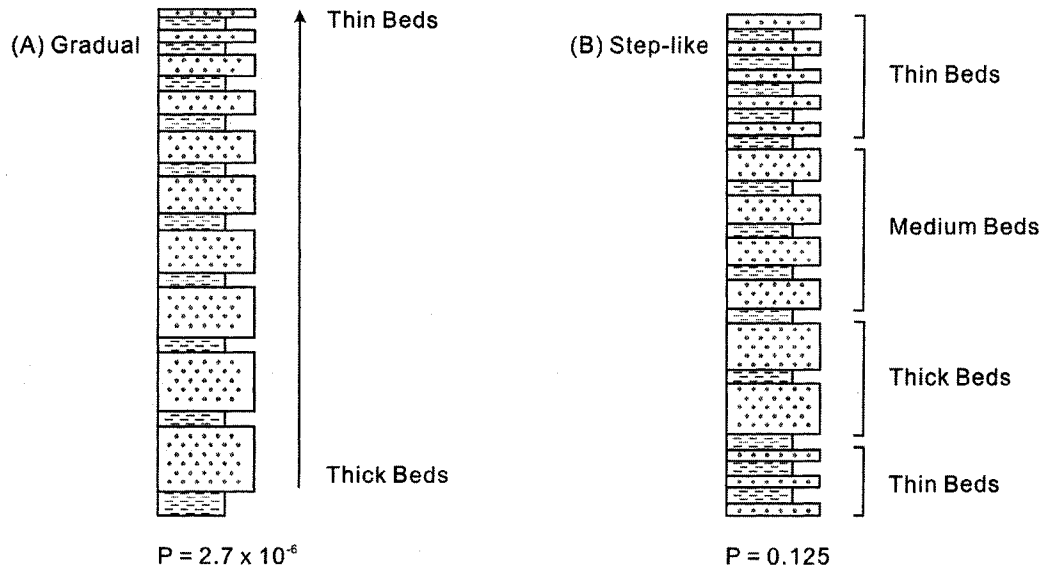
Figure 3-1: Idealized types of sequence shown as thinning-upward trends, (a) gradual, and (b) step-like (Pickering *et al*. 1989). The calculated probability of happening is shown below each sequence.
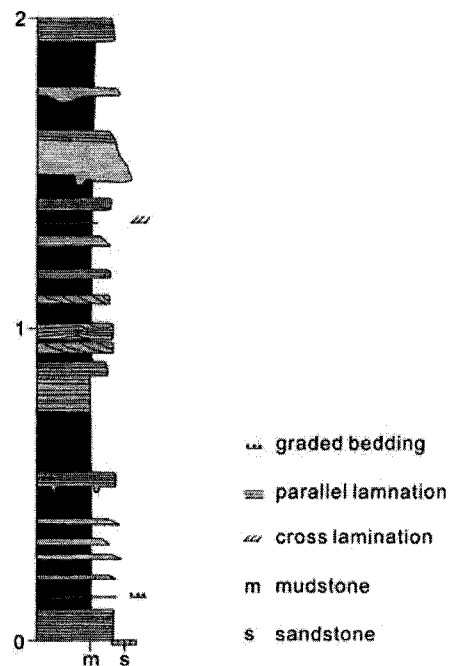
Figure 3-2: A representative sedimentological profile of the Cumberland Bay Formation (CBF) of South Georgia (after, MacDonald, 1992).

graded bedding

parallel lamnation

cross lamination

m mudstone

s sandstone

18
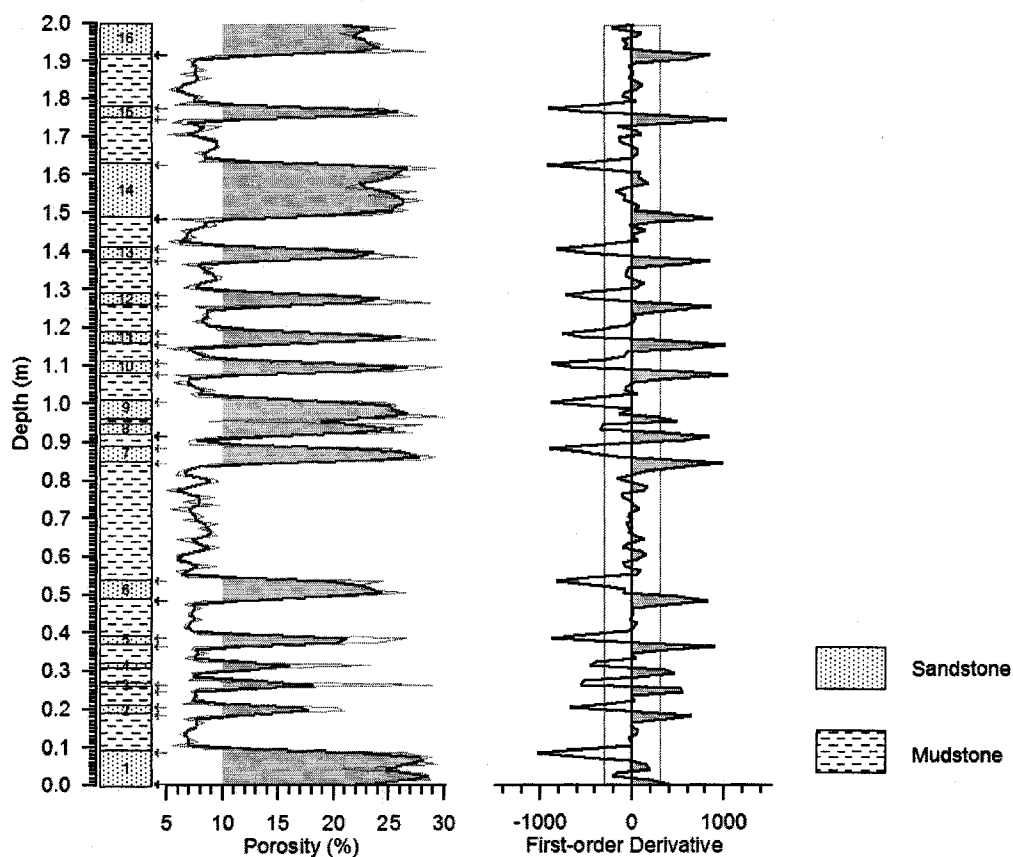
Figure 3-3: A diagram illustrating the vertical lithofacies profile, synthetic porosity curve and auto surface pick identification results. Reference profile is plotted on the left with 16 sandstone layers. The identified rock type picks are shown with gray left arrows, and the identified surface picks are illustrated with dark left arrows. The original porosity is plotted with thin solid line, and the smoothed porosity is illustrated with heavy solid line. High porosity (> 10%) is filled for highlighting. The positive first-order derivative of porosity is also highlighted.

3.1.1 Rock type picks identification

The first step in automatic surface picks identification is rock type picks identification. The identification is based on the fact that effective porosity in sandstone is generally higher than that in mudstone. Therefore, porosity has steeper slope on sandstone boundary. The transition will be very clear if silty deposition is clean.

a. Smooth original curves

Usually, short-scale variability exists within all rock types. It may lead to misidentification. Therefore, a smoothing approach is implemented as a preprocessor. A simple solution is to smooth the original well log with moving windows. To retain the major curve characteristics, an unequal-weighted moving window smooth methodology is applied.

19

The method can be expressed as:

$$a_1' = 0.5 \cdot a_1 + 0.25 \cdot (a_0 + a_2) \tag{3.1}$$

where a_1 is the currently processed value, a_1' is the smoothed value, a_0 and a_2 are the adjacent values. The smoothed porosity curve is plotted as the heavy solid line in Figure 3-3. Alternative smoothing algorithms or different window sizes could be considered if the resulting picks are too frequent or appear to be missed.

b. Rock type picks identification

Rock type picks identification is based on the fact that sandstone has higher porosity values and there is a significant rate of change in porosity at a boundary.

First-order derivative of the smoothed curve is calculated to quantify the rate of change:

$$a_0' = (a_1 - a_0)/(d_1 - d_0) \tag{3.2}$$

where a_0 is the currently processed data point, a_0' is its first-order derivative value, a_1 is the data value of the upper adjacent position, d_0 and d_1 are the depth of a_0 and a_1, respectively. In practice, petrophysical properties are usually interpreted from well logs that are regularly sampled, so $d_1 - d_0$ is usually constant. This procedure may be repeated several times for a smoother curve. There are other numerical schemes to calculate the derivative of regularly spaced data; however, this simple approach is considered adequate in most cases.

The lower sandstone boundary has a positive derivative, and the upper boundary has a negative derivative (the right plot of Figure 3-3). Lower and upper cutoffs of the derivatives can be specified to identify surface picks. The cutoffs selection is problem related. In the case study, -300.0 and 300.0 are selected, respectively. All 16 sandstone picks are accurately identified (Figure 3-3). There will always be a need for the geological modeler to tune these thresholds and other calculation parameters to attain surface picks that match their interpretation.

3.1.2 Surface picks identification

The proposed methodology is based on identifying thinning-upward depositional trend. Because of flow energy fluctuations, grain size and thickness fluctuation are inevitable. Therefore, an un-equal-weighted moving-window smoothing approach may be applied to eliminate the fluctuations. A drawback of the smoothing is that a thicker sequence may screen adjacent thinner sequences. The modeler has to make the decision on what kind of smoothing to apply. Trial-and-error is required. The thickness distribution of the case study is shown on the left plot in Figure 3-4. The first-order derivative of the example described above is shown on the right plot in Figure 3-4.

20
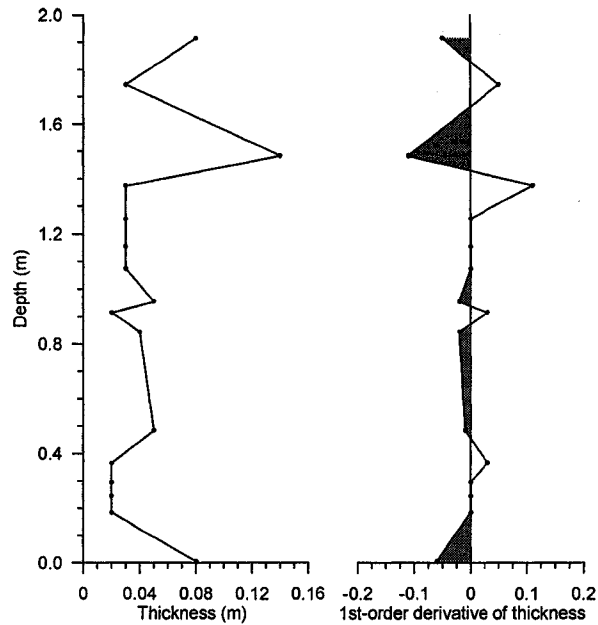
Figure 3-4: Thickness curve and first-order thickness derivative curve. First-order derivatives with negative values are highlighted on the map to show the identified surface picks. The picks are denoted as black left arrows in Figure 3-3.

3.1.3 An example parameter file of *SB_pick*

A Fortran 90 program, *SB_pick*, was written to perform the proposed methodologies described above. An example parameter file (following GSLIB conventions) is shown below. An explanation of each parameter is provided in Table 3-1.

Parameters for *SB_pick*:	
1. por.dat	- file with property values
2. 3 5	- depth column, property column
3. smooth.out	- file with smoothed property & derivative
4. pick.out	- file with surface picks
5. -500.0 500.0	- lower and upper cutoff of derivatives
6. 0	- smooth thickness? (0=no, 1=yes)

Line	Description
1	Input file with property values.
2	Column numbers for depth and proper curve.
3	Output file with smoothed property values and its derivatives.
4	Output file with identified surface picks.
5	Lower and upper cutoff of derivatives.
6	Indicator for performing thickness smoothing or not, 0 = no, 1 = yes.

Table 3-1: A description of the *SB_pick* parameter file.

21

3.1.4 Some comments on *SB_pick*

1. In practice, $\phi(z)$ is a function of grain size, sorting and diagenesis. Therefore, porosity may not be a good indicator for surface picks identification. $Fac(z)$ and $Vsh(z)$ may have better geological response than $\phi(z)$. Some raw well logs such as RT, Gr and SP may also be used. SP log may indicate permeability changes and may be a good sand/shale indicator.

2. The cutoff of first-order derivative of porosity should be adjusted in different problem settings. If the cutoff is set too large, some thinner layers may not be identified.

3. The analysis should be performed separately within each stratigraphic layer.

3.2 Advances in lobe events modeling

3.2.1 Surface template

During modeling, surfaces are stochastically generated based on a proposed analytical surface template. A simplified lobe geometry template is applied to define the idealized surface shape.

In plan view, the lobe boundary is defined by,

$$W(x) = 4 \cdot wmax \cdot \left(1 - \frac{x}{length}\right)^b \cdot \left[1 - \left(1 - \frac{x}{length}\right)^b\right] \tag{3.3}$$

where $W(x)$ is the width from the centerline, x is the distance along centerline, $wmax$ and $length$ is the maximum lobe width and length drawn from user-specified distribution, respectively, $b = -\ln(2)/\ln(1-a)$, where a is the relative position of maximum width (Figure 3-5).

The lobe geometry is quantified by a gridded surface of thickness. The thickness determination methodology adopted from the channel cross-section geometry determination methodology developed by Deutsch and Wang (1996). Thickness distribution along center line is quantified first; cross-section thickness is determined based on the thickness at centerline location.

Thickness along center line is defined geometrically by,

$$t(x) = 4 \cdot tmax \cdot \left(1 - \frac{x}{length}\right)^b \cdot \left[1 - \left(1 - \frac{x}{length}\right)^b\right] \tag{3.4}$$

where $t(x)$ is the thickness along centerline, $tmax$ is the maximum thickness drawn from user-specified parameter, $b = -\ln(2)/\ln(1-a)$, where a is the relative position of maximum width.

Cross-section geometry is defined geometrically by,

$$t(y) = 4 \cdot t(x) \cdot \left(\frac{y}{2 \cdot W(x)}\right)^b \cdot \left[1 - \left(\frac{y}{2 \cdot W(x)}\right)^b\right] \tag{3.5}$$

22

where $t(y)$ is the thickness along a cross section, y is the distance to lower boundary, $y \in [0, 2 \cdot W(x)]$, $b = -\ln(2)/\ln(a)$, where a is the relative position of maximum thickness.

During simulation, *length*, *wmax* and *tmax* are drawn from user-specified distributions; a is deterministic, which is 0.66 in Equations (3.3) and (3.4) and 0.5 in Equation (3.5), which means that the position of maximum width and thickness are at 2/3 of lobe length and the geometry of cross sections is symmetric (Figure 3-6).

No channels are constructed and the starting width of a lobe is zero. The centerline of lobe is constructed by lobe width, instead of by local maximum gradient direction. Therefore, the center-line may not be consistent with local maximum gradient.

There is no unique way for object-based lobe parameterization. Surface shape may be modified to fit specific geologic settings. The parameterization could easily get more elaborate at the cost of additional parameters that must be inferred from limited observational data. For example, ruguosity or inter-fingering may be added to the lobe geometry.
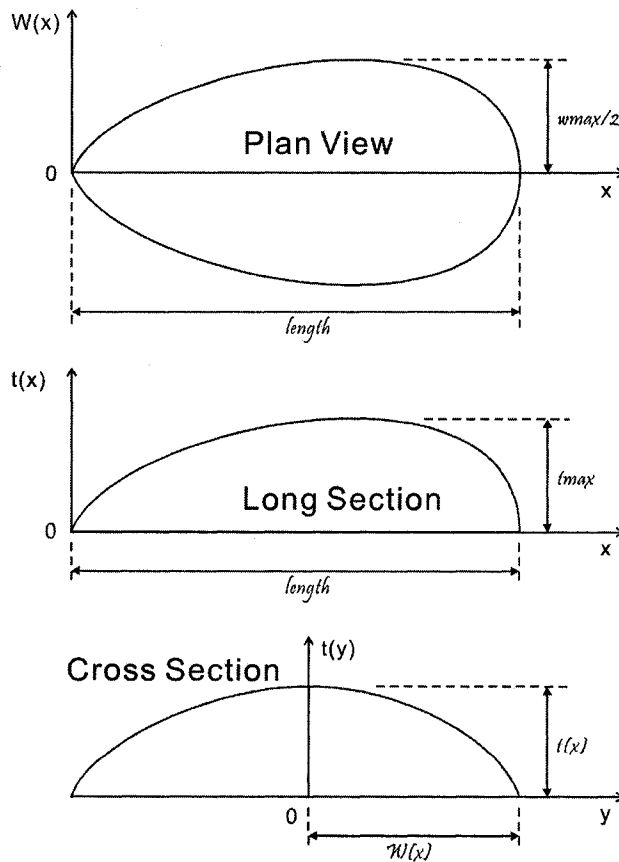
Figure 3-5: Parameters needed to describe the 3-D lobe geometry.
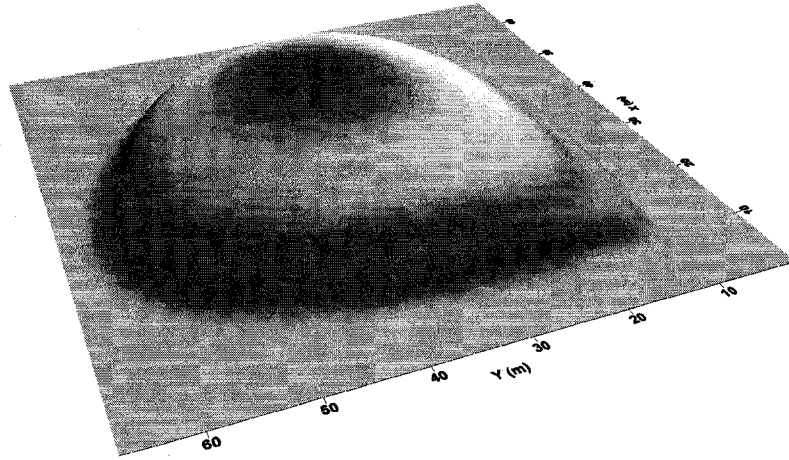
Figure 3-6: A lobe built with proposed analytical surface templates.

3.2.2 Initial bathymetry

As a gravity-driven mass flow, the shape and orientation of turbidite are strongly controlled by sea floor bathymetry; therefore, the initial base surface bathymetry inference is important in surface-based modeling approaches. However, paleobathymetry is difficult to infer, especially in the presence of complicated tectonic history. Basin modeling or tectonic inversion based on seismic data and reasonable assumptions may be used. When no information is available to make reasonable assumptions, a simple surface simulation/transformation approach may be applied to rebuild the idealized initial base surface bathymetry. Three base surface transform approaches are applied in *LE_model* program.

1) Flatten base surface

The simplest solution is to flatten the base surface. The transformed stratigraphic coordinate can be expressed as (Deutsch, 2002):

$$z_{rel} = \frac{z - z_{cb}}{z_{ct} - z_{cb}} \cdot T \tag{3.6}$$

where z_{rel} is the relative stratigraphic coordinate, z_{cb} is the elevation of base level, z_{ct} is the elevation of top surface, and T is the average thickness of the strata. The coordinate z_{rel} is 0.0 at stratigraphic base and equals the thickness at stratigraphic top.

This transform may be reversed by:

$$z = z_{cb} + \frac{z_{rel}}{T} \cdot (z_{ct} - z_{cb}) \tag{3.7}$$

While, this transform is not recommended when there is additional information on the reservoir thickness and geometry.

24

2) Transform base surface to a paraboloid

The base surface may be transformed to an idealized shape based on global base surface bathymetry. The transformed base surface works as a trend surface that removes high frequency and possible unreliable noise in the bathymetry.

The proposed method is to approximate the base surface by an analytical surface of second order:

$$z = ax^2 + bxy + cy^2 + dx + ey + f \tag{3.8}$$

The coefficients of the paraboloid are obtained by least-squares solution of an over-determined system of linear equations, given the coordinates of a set of points in the neighborhood of the point of interest:

$$\mathbf{X}\mathbf{A}^\mathrm{T} = z \tag{3.9}$$

where $\mathbf{A} = [a,b,c,d,e,f]$ are the parameters of the paraboloid; $\mathbf{X} = [x,y,z]$ are the coordinates of a surface point; and $z = [z_1, z_2, \cdots, z_n]$ are the elevations of base surface (after Krsek *et al.*, 1998).

The stratigraphic coordinates are transformed based on the difference between the base level and the fitted paraboloid. That is,

$$z_{rel} = z - (z_{cb} - z_{parab}) \tag{3.10}$$

where z_{parab} is the elevation of the fitted paraboloid.

This transform may be reversed by:

$$z = z_{rel} + z_{cb} - z_{parab} \tag{3.11}$$

3) Transform base surface to an incline

When the paleogeometry is approximately linear, an incline may be more suitable for simulating the idealized base surface. The analytic surface of first order is expressed as:

$$z = ax + by + c \tag{3.12}$$

The incline transform and back transform procedures are similar to the paraboloid transform.

The paraboloid or incline base surface transform are recommended because: (1) the global bathymetry is kept after transform, (2) resulting surface models are more realistic, and (3) honouring stacking patterns becomes possible. The modeler may plot the base surface and visualize it in 3D to select the proper transformation approach, paraboloid or incline.

The stratigraphic framework is always tilted in deepwater turbidite environments, although the gradient may be very low in the mid-fan area. Empirical studies with the research code have shown that paraboloid and incline transforms are stable in common

25

geological settings, even in high gradient environments, and the resulting surface model is geologically realistic and free from visual artifacts. Therefore, the program may be applied for alluvial fans and delta fans modeling.

(a)

(b)

(c)
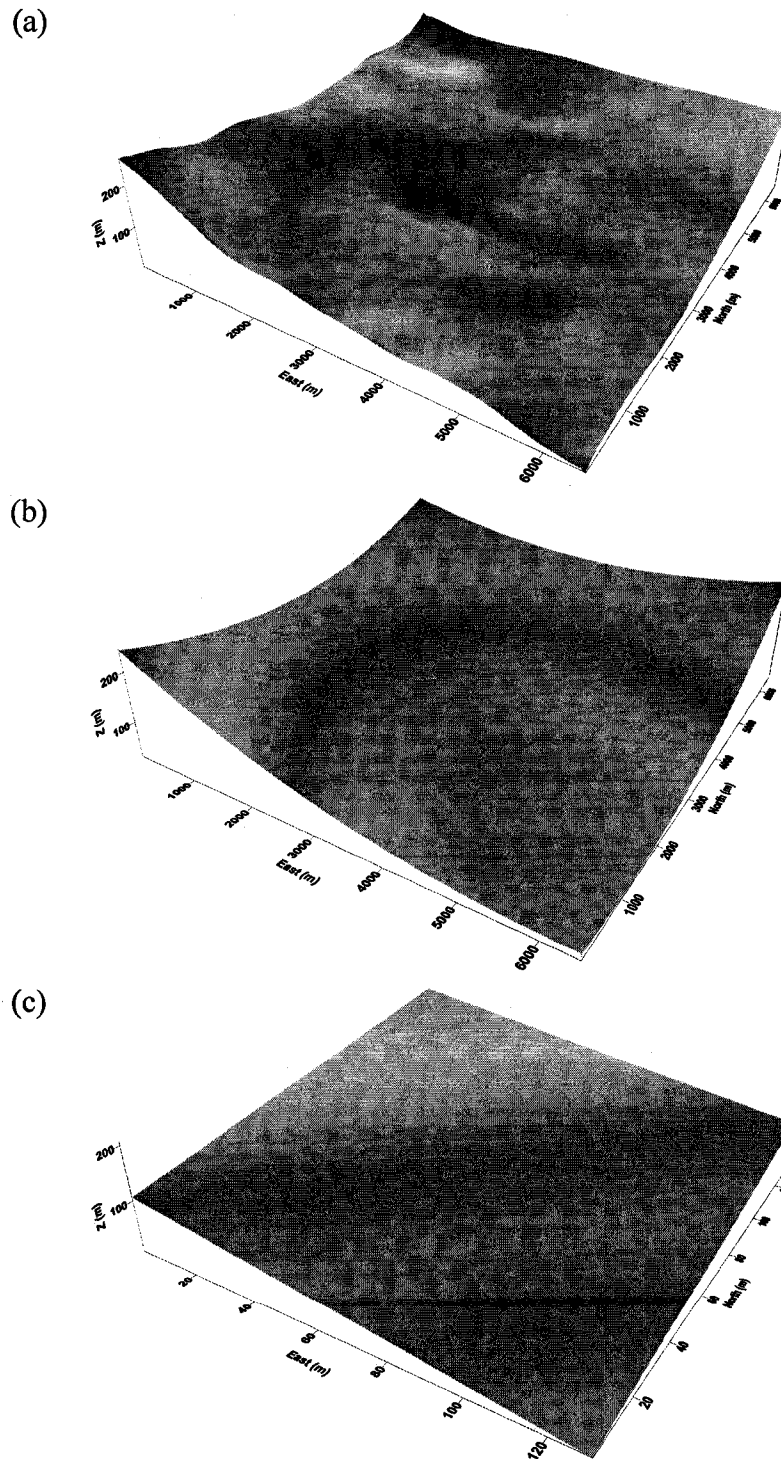
Figure 3-7: An example base surface and transformed base surfaces. (a) original base surface, (b) paraboloid base surface, and (c) incline base surface.

26

An example base surface and the transformed paraboloid and incline are shown in Figure 3-7. Base surface transform should not be performed if there is resolvable local information in the paleobathymetry. For example, if there are ponded minibasins, the base surface transform could remove this information. According to sequence stratigraphy, the idealized base surface is often referred to as global base level.

Some part of base surface may be highly deformed which has great influence on global base level simulation. To mitigate the influence, a marker surface may be used to constrain the area used for surface fitting. The unwanted grid nodes are not considered (Figure 3-8). At present, only non-faulted structures are considered.

When the base surface is transformed, the residuals of the original base surface and the global base level are saved and may be added back after simulation; hence the fluctuation of base surface will be brought to the final surface model.
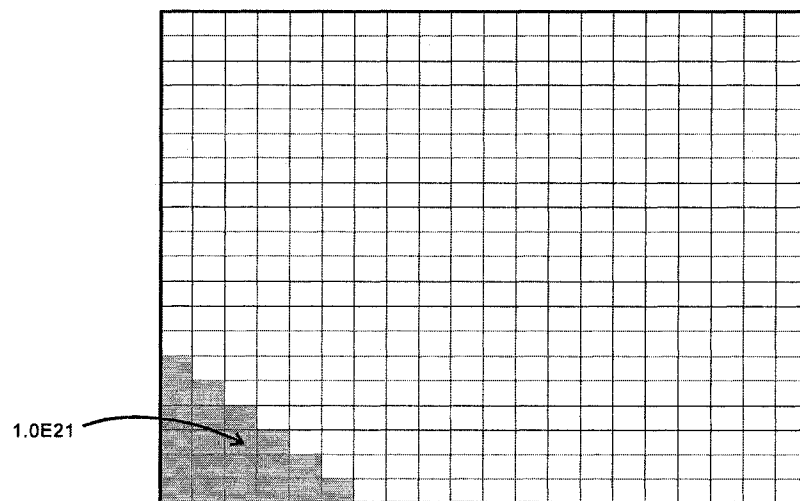
Figure 3-8: Schematic diagram illustrating the mark surface definition. All un-wanted grid cells are signed extremely large values as the indicator of "bad" grids which will not be used for idealized base surface simulation.

3.2.3 Surface positioning

Surface placement includes the determination of attitude and location. For convenience, we will discuss theses two aspects in two sections.

The surface positioning algorithm should: (1) respect geologic information with respect to the interrelationship of the architectural elements described by the surfaces, (2) avoid boundary and vertical surface stacking artifacts, (3) result in a reasonable probability of the candidate surface being accepted, and (4) be computationally efficient (Pyrcz, 2004).

Under the assumption that no erosion happens during surface modeling, base surface is unchanged during simulation. However, the top surface is always treated as a global unconformity; any surface above the top surface will be truncated.

1. Vertical surface positioning rule

According to sequence stratigraphic principles, a candidate surface should ideally be positioned on a base level. Base level is generally regarded as a global reference surface to which long-term continental denudation and marine aggradation tend to proceed (Catuneanu, 2006). The base level is not a real physical surface; it is dynamic, moving upward and downward through time.

(1) Two types of base levels

Global base level is the interactive result of regional basin tectonics, rate, type and source of sediment supply and sea-level fluctuations. Many continental slope base level models and river base level models have been proposed, such as Friedrichs and Wright (2004) and Cronin and Hartley (2000). Usually, the research area for fine-scale deepwater turbidite modeling is only in reservoir scale; therefore, it is difficult to infer and integrate these models into *LE_model* program. As an alternative, a surface fitting methodology is applied to approximate the shape of global base level, which has been illustrated earlier and referred as the initial bathymetry reproduction.

In this thesis, the local base level concept is inferred for fine-scale lobe positioning, but the scale is much smaller than the local level used in sequence stratigraphy research. These base levels are formed by the bathymetric healing process of turbidity current, and not related to any large-scale controlling parameters. Recall the structure of large-scale turbidity current shown in Figure 2-1, along flow path, turbidity current releases loads from both head and tail, and absorbs new load into head by eroding former deposition as compensation. The balance is dynamic and results in the evolution of local base level (Figure 3-9). When loss is greater than compensation, a new lobe starts forming. Under the assumption that turbidity current loses its erosion ability as long as a new lobe forms, the new lobe is positioned on a local base level made by former turbidity currents, not by itself. In practice, a local base level is the final trend of filling topographic lows and smoothing topographic relief.

From above discussion, a local base level is formed by depositional process only. Long-term controlling parameters, such as sea-level change, tectonic movements and depositional supply, control the trend of local base level evolution. Local base level evolution is the driver for global base level formation. There is some literature on the relationship of conventional local base level and global equilibrium profile of the river-marine system, such as Press and Siever (1986) and Catuneanu (2006). In these publications, local profiles are graded fluvial profiles. Under the assumption that erosion is more significant than accommodation, they always move downward to

28

global base level. In *LE_model* program, erosion is assumed to be insignificant; therefore, accommodation is the major component. Under this assumption, local base levels should be always located above global base level and move upward toward the top surface, which represents the final status of global base level.
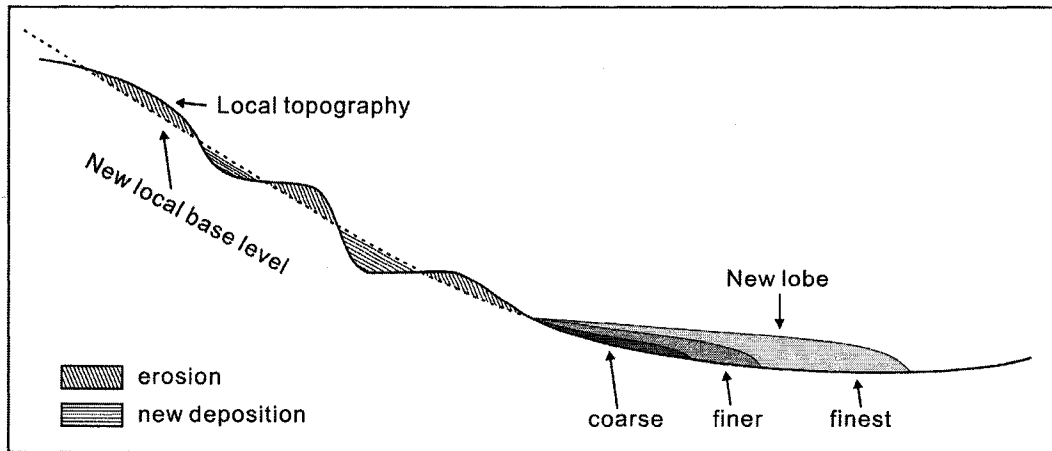
Figure 3-9: A schematic diagram showing the local base profile forming procedure. The vertical scale has been exaggerated to illustrate the local erosion and new deposition process.

(2) Simulation of base levels

For simplification, the same surface fitting methods are applied for both global and local base levels simulation. Paraboloid and incline are selected to represent for base levels. The selection is based on (1) paraboloid or incline mimic the idealized surface shape well, (2) a candidate surface will not change its inclination locally after positioning on a paraboloid or incline, so no surface stacking artifacts arise, and (3) there are many algorithms available in public domain for paraboloid or incline fitting, such as Yu (2001), and the fitting is computationally efficient.

The local base levels are dynamically fitted as functions of former simulated surfaces. The surface shape that best meets proposed surface acceptance criterion is selected and no user interaction is needed. The surface acceptance criteria will be discussed below.

(3) Original surface placement rules

The original *LE_model* program positioned a candidate surface on a datum with the global minimum elevation of former surface. Datum updating rate is much slower than surface stacking rate due to (1) the influence of permissible angle, and (2) no constraints on lobe entry point selection. Therefore, datum is much lower than simulated surface during later simulation stage (Figure 3-10).

29
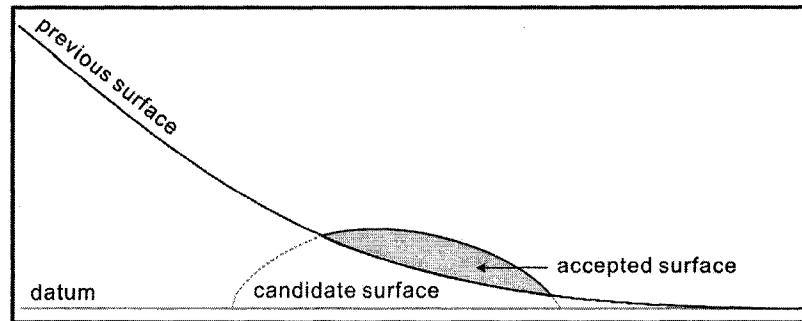
Figure 3-10: Schematic plot showing volume missing problem.

For demonstration, a pair of synthetic bounding surfaces was constructed. The gradient of the base surface is about 2 degrees towards southeast. The bounding surfaces pinch out towards the western and northern edge to mimic the common stratigraphic situation in continental slope environment.

Method I: without transforming base surface

Without base surface transform, 1000 surfaces were generated with final filling proportion of 89.8%. One long section and one cross section are shown in Figure 3-11. In general, the surface model is visually acceptable along the longitudinal direction, but it is not realistic in the transverse direction because of the influence of local bathymetry. It does not reproduce a compensational stacking pattern very well. From the cross plot of filling proportion versus number of surfaces, we can see that the filling proportion is in the direct proportional to the number of surfaces at the initial stage, but more surfaces are needed at the later stage (refer back to the left of Figure 1-4).

Method II: flattening base surface

After flattening the base surface, 1000 surfaces were generated to fill 94.99% of the volume. The surface model is visually acceptable in both directions. Figure 3-12 shows the same long-section and cross-section as in Figure 3-11. The missing volume problem at the later simulation stages still exists (refer back to the right plot in Figure 1-4).

(4) New vertical surface placement rules

The new vertical surface positioning rule amounts to recalculate base level for each surface. The workflow of the rule is: (1) a candidate surface is drawn, (2) the local base level of this candidate surface is fitted based on local topography, (3) the candidate surface is added on the local base level based on its thickness, and (4) the volume below former surfaces is truncated under the assumption that no erosion happens (Figure 3-13).

30
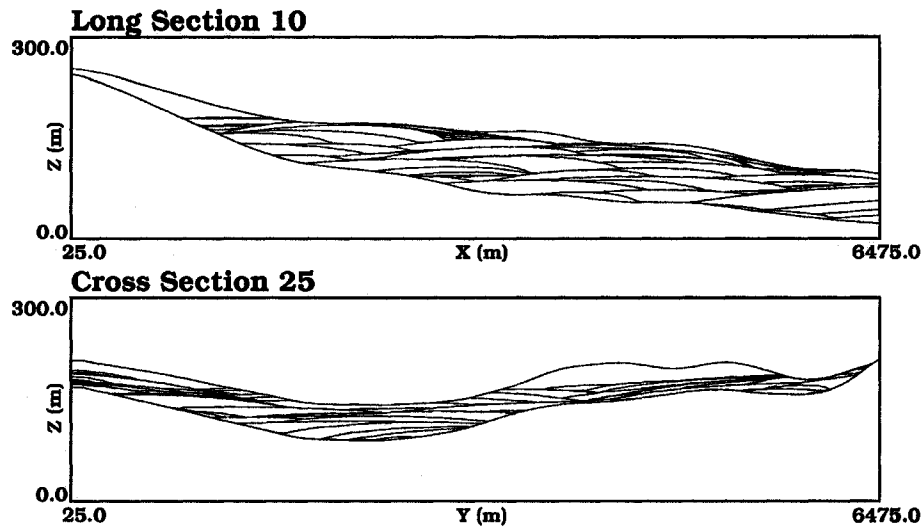
Figure 3-11: A long section and a cross section to illustrate the surface modeling results of original surface placement rules without base surface transformation.
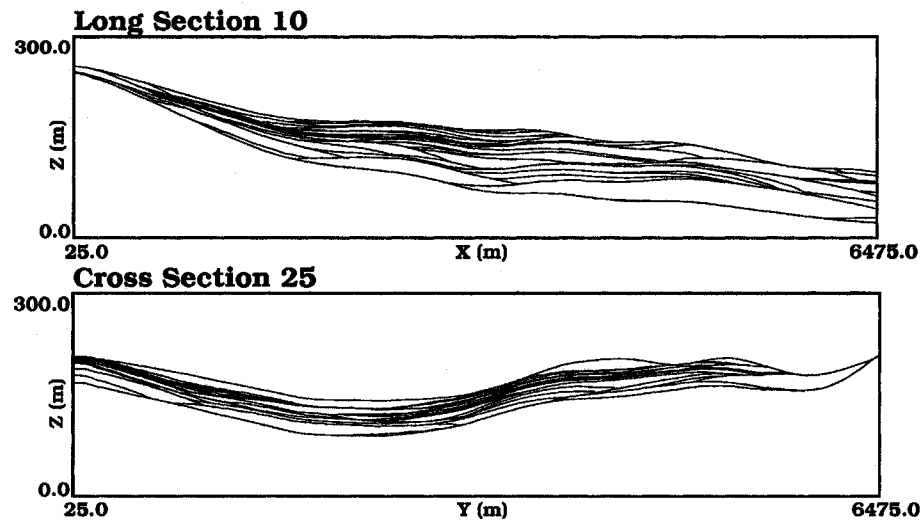
Figure 3-12: A long section and a cross section to illustrate the surface modeling results of original surface placement rules with flattening base surface.
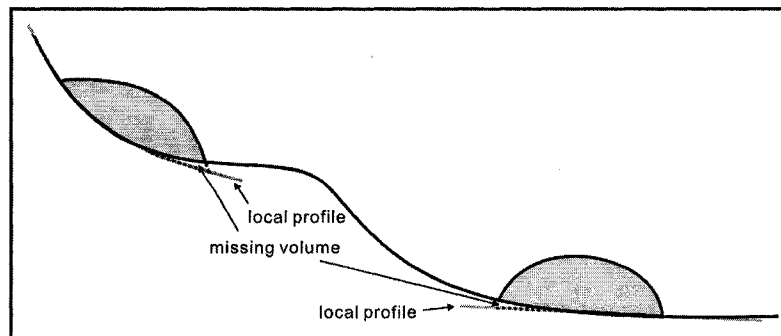
Figure 3-13: Schematic plot showing the vertical surface placement rule.

31

For comparison, the same bounding surfaces and surface simulation parameters used in former case study are applied to demonstrate the new surface position rule. The target filling proportion is also set to 95%. Simulation results are shown in Figure 3-14 through Figure 3-17. Spatial structures are geologically realistic. The cross plots of number of surfaces versus filling proportion are shown in

Figure 3-18. They all have linear shapes, which means that the missing volume problem is essentially solved. Some related statistics are shown in Table 3-2. Incline transform is the best in this case study in the sense that fewer surfaces are needed.

2. Areal surface positioning rule

The areal surface positioning rule amounts to the selection of an entry location. As a gravity-driven flow, local bathymetry has great influence on lobe orientation, geometry and positioning; therefore, the entry location may be a function of previous surface. The entry position may also be independent of previous surfaces, which is applied in *LE_model* program. Since the entry location is selected independently, some additional rules are needed as constraints for a reasonable surface position. A reasonable surface model should honour compensational stacking pattern, which is the tendency of flow event deposit to fill topographic lows and to smooth topographic relief.
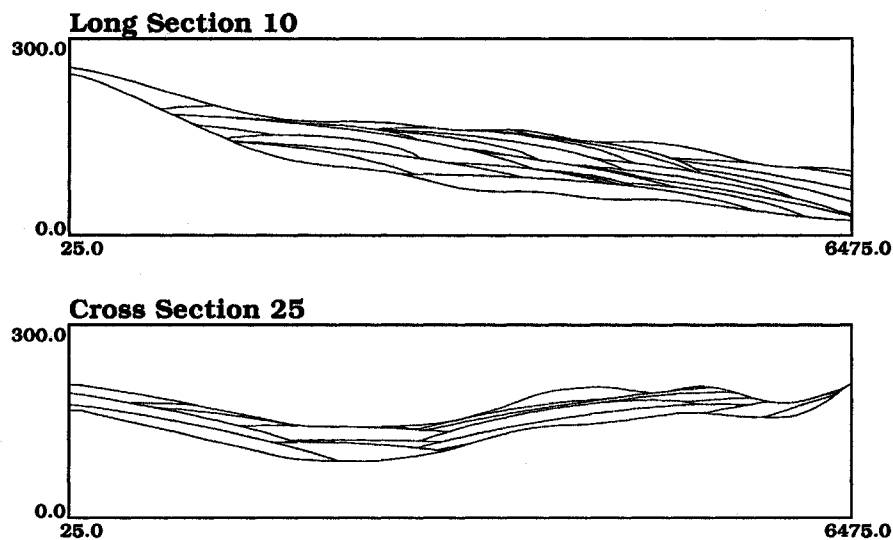
Figure 3-14: Long section 10 and cross section 25. No base surface transform is performed.

32
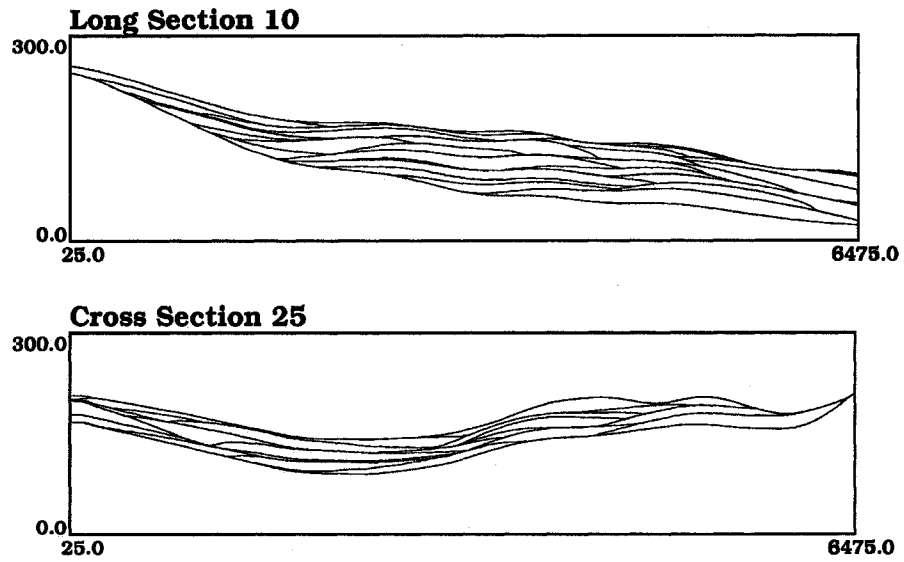
Long Section 10

Figure 3-15: Long section 10 and cross section 25. Base surface is flattened during simulation and then back transformed to original shape.

Long Section 10
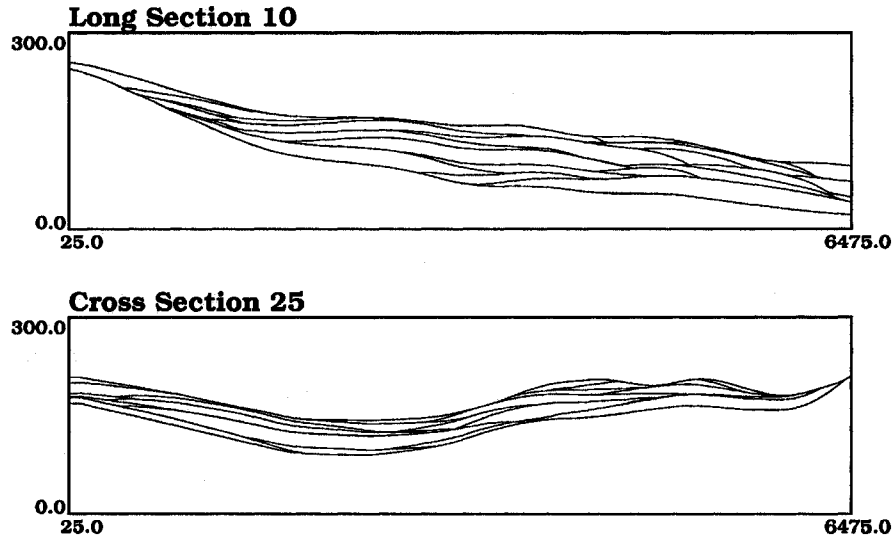
Cross Section 25

Figure 3-16: Long section 10 and cross section 25. Base surface is transformed to a paraboloid during simulation and then back transformed.

33

Long Section 10
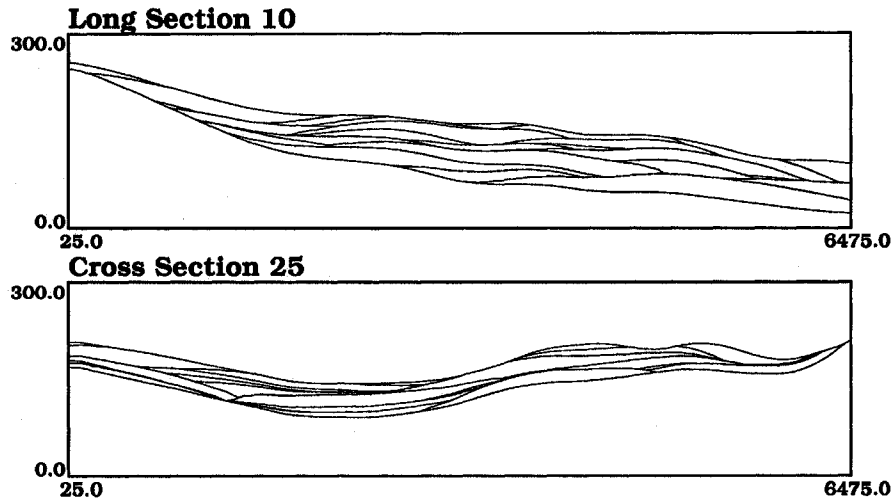
Cross Section 25

Figure 3-17: Long section 10 and cross section 25. Base surface is transformed to an incline during simulation and then back transformed.

(a)

(b)

(c)

(d)
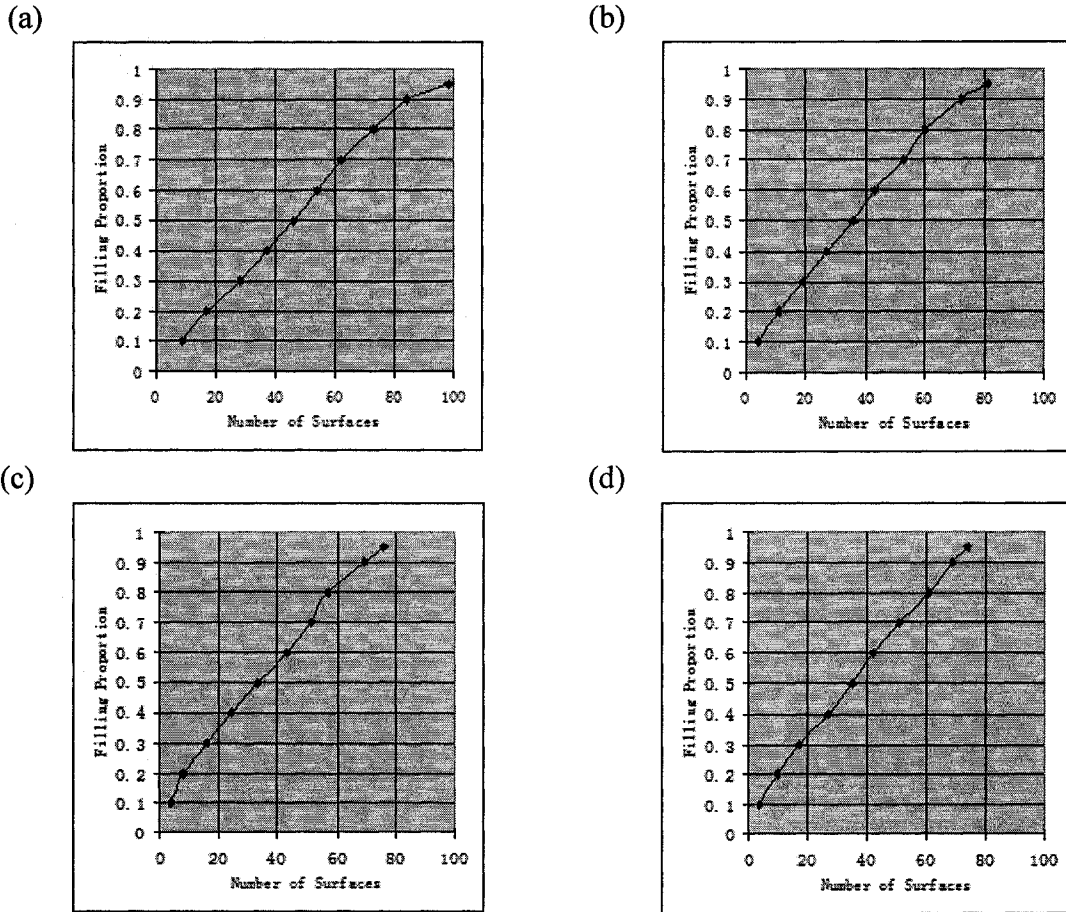
Figure 3-18: The number of surfaces and filling proportion. (a) no base surface transform; (b) flatten base surface; (c) transform base surface to a paraboloid; and (d) transform base surface to an incline.

34

Method	Number of surfaces	Filling Proportion
No base surface transform	99	95.3%
Flatten base surface	82	95.3%
Transform base surface to a paraboloid	78	95.1%
Transform base surface to an incline	75	95.3%

Table 3-2: Some statistics of a synthetic case study with different base surface transform approach.

The areal position is selected by the following procedures: (1) an areal surface occurrence probability field is constructed first. The probability is a function of areal relative positions, already simulated thickness and remaining thickness. A position that is more proximal and close to a channel entry point, with larger remaining thickness or minimum simulated thickness, will have larger occurrence probability; (2) a uniform random number within [0.0, 1.0] is drawn; and (3) the ratio of cumulative probability over total probability is calculated with specific searching path and the position where the ratio is equal to the random number is selected as the entry location.

3.2.4 Well conditioning

An existing well conditioning method for surface-based modeling is the rejection algorithm proposed by Pyrcz (2004). The key steps of the algorithm are: (1) a candidate surface is built, (2) the residual of each available well datum to the candidate surface is calculated, (3) if the sum of the residual is less than a specified tolerance, the surface is accepted; otherwise, it is rejected and the procedure is repeated, and (4) the residual is simulated for all locations and added to the surface to ensure exactitude.

The initial tolerance of rejection algorithm is usually set to a small value for smooth surface models. The tolerance may be increased gradually to improve speed, but unexpected short-scale variations may be introduced.

As an improvement, a dual-spline error surface interpolation algorithm is proposed in *LE_model* program for fast well conditioning. The surface acceptance criteria and optimal surface selection methodology are modified as follows.

Surface acceptance criteria:

1. If the candidate surface does not pass through any wells, it is accepted only when it meets other constraints. For example, the surface A in Figure 3-19.

2. If the candidate surface passes through only one well, it is acceptable only when available surface pick is located within the surface. For example, the surface C in Figure 3-19; surface B is rejected.

35

3. If the candidate surface passes through more than one well, it is acceptable when all available well picks are located within the surface. For example, the surface D in Figure 3-19.

Surface conditioning methodology:

1. If the candidate surface passes through only one well, (1) residual of available well pick to candidate surface is calculated, and (2) the surface is shifted downward based on the residual (Figure 3-20).

2. If the candidate surface passes through multiple wells, (1) the residual of each surface pick to the candidate surface is calculated, (2) the minimum residual r_{min} and maximum residual r_{max} are calculated, (3) the candidate surface is shifted downward by distance $|(r_{max} + r_{min})/2|$, which is the optimal position for the sum of new residuals should be close to zero, and (4) a dual-spline error surface is interpolated based on new residuals and is added back to new candidate surface for exactitude (Figure 3-21).

The optimal surface position is selected by shifting a candidate surface instead of trial-and-error; therefore, it is more efficient than the rejection algorithm.

Figure 3-22 illustrates two possible surface models by conditioning 36 wells in a case study.
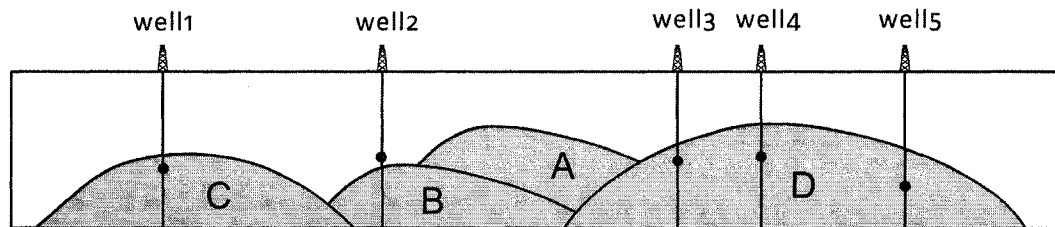
Figure 3-19: A synthetic diagram illustrating the acceptance criteria for well conditioning.
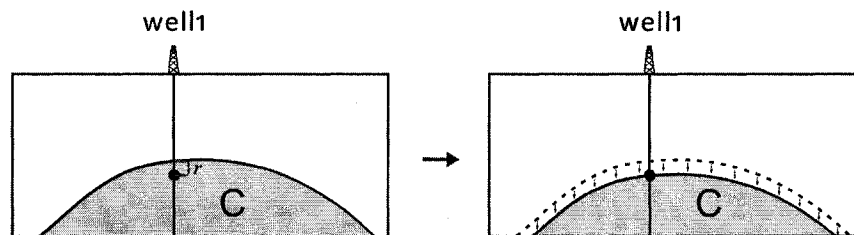
Figure 3-20: Schematic diagram illustrating the well conditioning methodology with one well case. The residual of the available well pick with the candidate surface is calculated first (left plot); then the candidate surface is "lower" down to pass through the available well pick based on the residual (right plot).

36
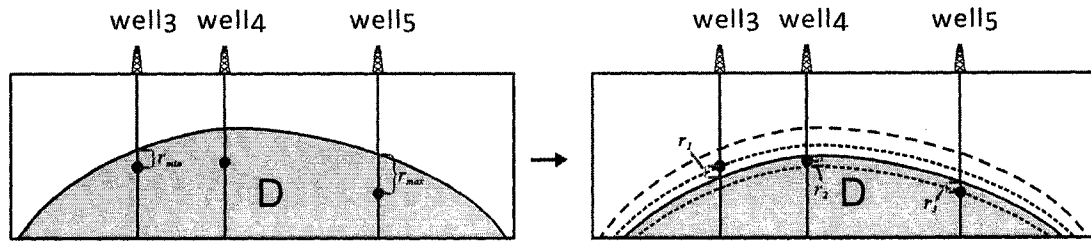
Figure 3-21: Schematic diagram illustrating the well conditioning methodology with multiple wells case. The minimum and maximum residuals are calculated first, i.e., r_{min} and r_{max} on the left plot; then the candidate surface is "lower" down in-between the minimum and maximum residual; after that, the residual of each available well pick to the new surface, r_1, r_2, and r_3, are calculated (the right plot).
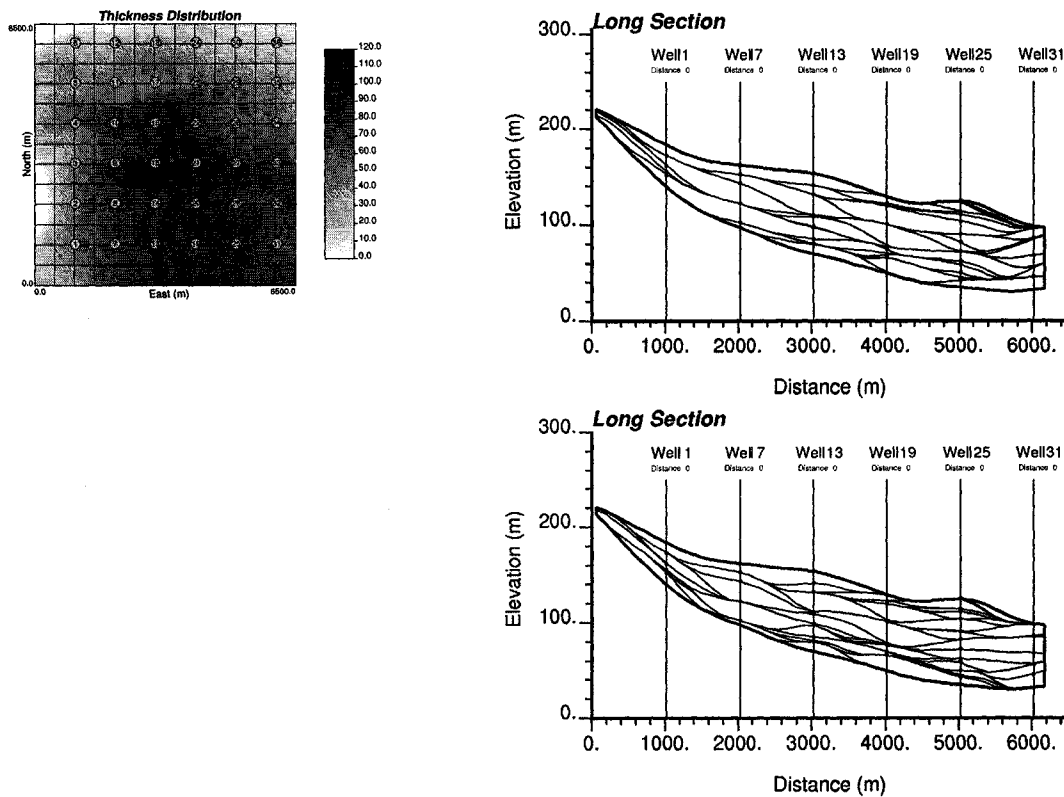
Figure 3-22: The thickness map of the strata and the location map of 36 synthetic wells. Two conditional realizations were built to illustrate possible spatial structures.

37

3.2.5 Surface acceptance criteria

To build geologically realistic surface models, (1) all available surface picks should be honoured, (2) compensational stacking pattern should be honoured, and (3) the input surface geometry statistics should be honoured.

The following surface acceptance criteria should also be met:

Criterion I: *minimum volume ratio* (MVR). MVR is the ratio of lobe volume, V_{lobe}, over the gross strata volume, V_{gross}. Because V_{gross} is problem related, with the same V_{lobe}, MVR may be different for different projects. To establish a reasonable MVR, the modeler needs to set up all surface modeling parameters and run *LE_model* one time. During surface modeling procedure, (1) V_{gross} is calculated, (2) an ideal lobe with geometry of all means parameters is built, (3) ideal lobe volume, V_{ideal}, is calculated, and (4) the ratio of V_{ideal} / V_{gross} is a good reference to set up the MVR parameter. Ideally, $(0.5 - 0.8) \cdot V_{ideal} / V_{gross}$ is a good starting point. Under MVR, a larger surface is likely to be drawn, which accelerates the well conditioning process significantly.

Criterion II: *maximum missed volume ratio* (MMVR). MMVR is the ratio of missed lobe volume, V_{missed}, over the ideal lobe volume, V_{ideal}. Therefore, MMVR is also defined in relative scale. Unlike MVR, MMVR is not related to gross volume. MMVR is calculated by, (1) a candidate surface is drawn and its total volume, V_{total}, is calculated, (2) the candidate surface is positioned on a local base level and the volume below previous surfaces is truncated, (3) the remaining volume, V_{remain}, is then calculated, and (4) MMVR, that is, $(V_{total} - V_{remain}) / V_{total}$, is calculated. Ideally, MMVR should be less than 0.2. Under MMVR, a small surface is likely to be drawn. However, well conditioning may be a problem for these small surfaces.

Both MVR and MMVR will lead to compensational stacking pattern (Figure 3-23). MMVR is easier to establish; however, MVR criterion is applied in *LE_model* for faster well conditioning. Figure 3-24 compares the simulation results of above two surface criteria. All simulation parameters are the same except for the surface acceptance criterion. Only 23 surfaces are needed under MVR; while 113 surfaces are required under MMVR.

3.2.6 Stopping criteria

Surface modeling will stop when,

1) User-specified volume filling proportion is reached, or
2) No available surface pick exists.

38
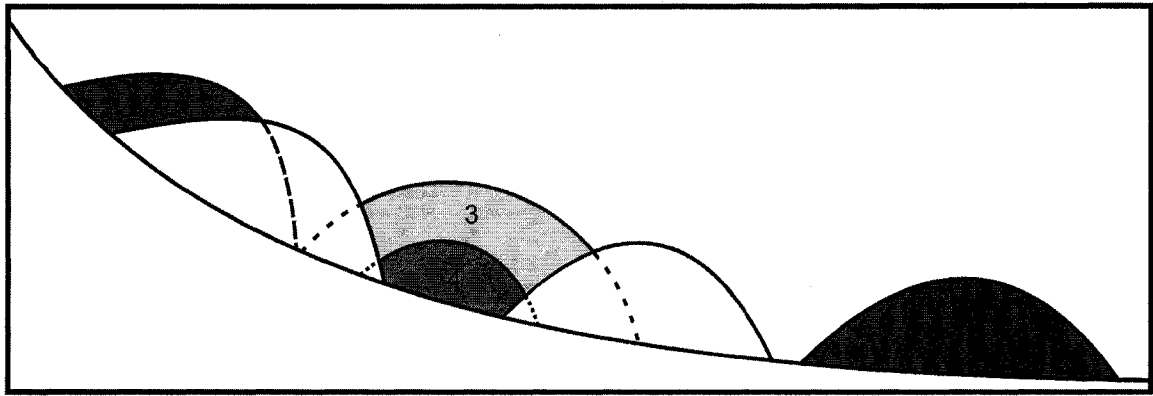
Figure 3-23: Synthetic diagram illustrating acceptable surface under different criterion. Surface 1 is acceptable under both criteria; surface 2 is not acceptable under both criteria; surface 3 is acceptable for MVR only, while surface 4 is acceptable for MMVR only.
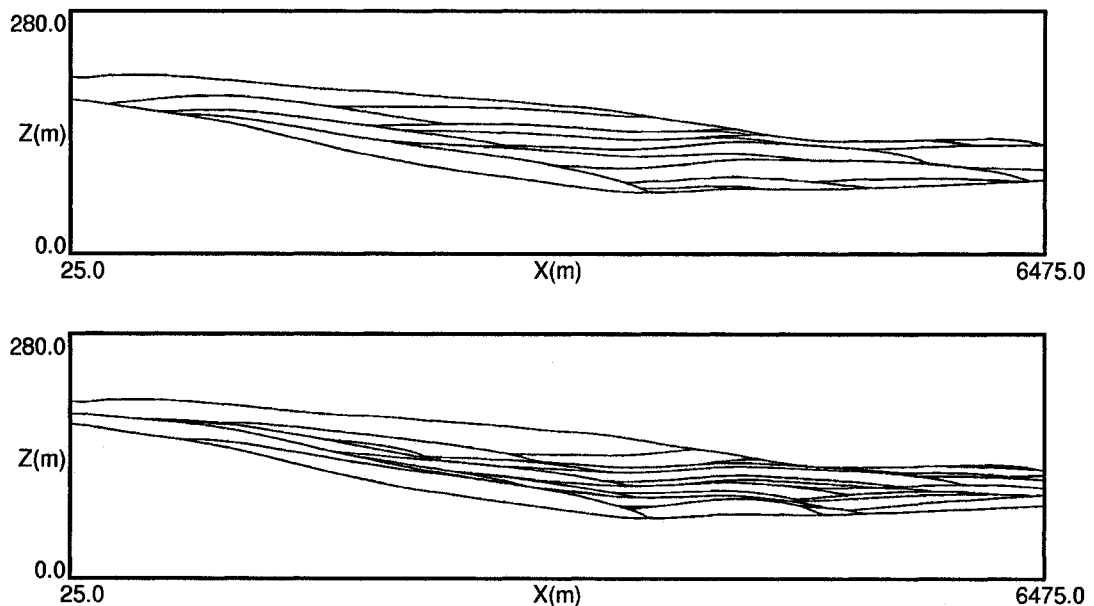
Figure 3-24: Comparison the results of two surface criteria. Above: MVR; Below: MMVR.

3.2.7 Discussion

In this section, prototype research on erosion simulation and the reproduction of stacking patterns will be presented.

1. Erosion simulation

There are two types of erosion in second-order lobes simulation, depositional erosion and unconformities. Although we discussed the formation of local base levels, no erosion and refilling were simulated in former research. Besides depositional erosion, unconformities may also occur. Erosion simulation aims at reproducing more complicated spatial structures.

39

(1) Global unconformities simulation

Global unconformities may be visualized on seismic. They resulted from the variation of long-scale controlling parameters, such as tectonic movements. If an unconformity can be continuously traced on seismic, it can be treated as an additional boundary surface dividing the reservoir into different units for modeling. The following approach may be applied:

a) Both bounding surfaces are transformed to idealized shape, i.e. paraboloid or incline, representing the global base levels at those time stages.

b) We assume that unconformity is located between the global base levels in proportion to time/thickness (Figure 3-25).

c) When wells are available, the unconformity may be locally adjusted to honour wells.

d) All surfaces above the unconformity are truncated until the volume below the unconformity is 100% filled.

e) The procedure is repeated until user-specified global filling proportion is reached.

Figure 3-26 illustrates a global unconformity simulation case study based on above methodology.
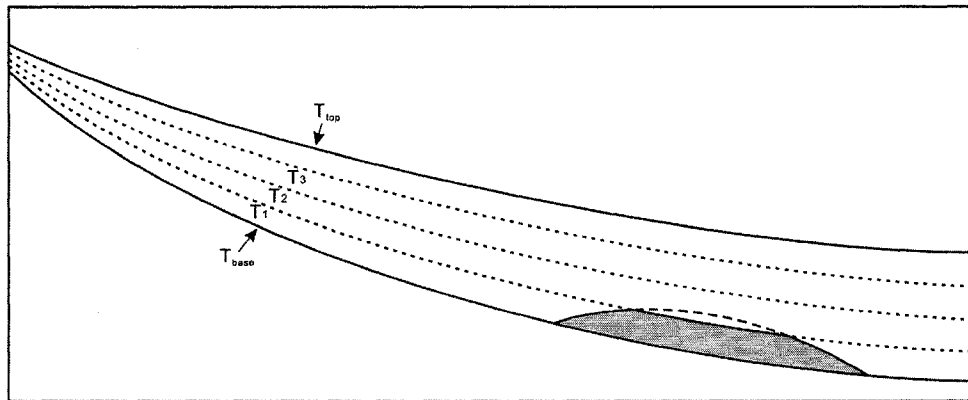
Figure 3-25: Synthetic diagram illustrating the global unconformities modeling methodology. Interim time surfaces T_1, T_2 and T_3 are constructed by their relative positions between T_{base} and T_{top}. A candidate surface above T_1 is truncated to illustrate the erosion effect.
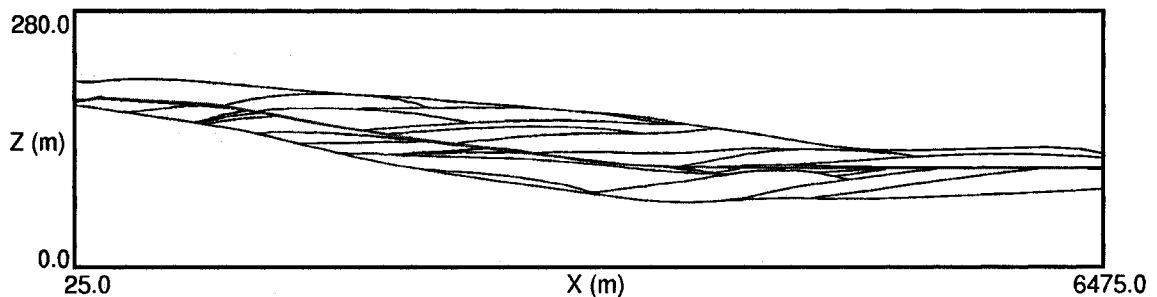
Figure 3-26: A long section to illustrate the global unconformity simulation. Only one global unconformity exists in this synthetic case study.

40

(2) Depositional erosion simulation

As discussed earlier, a local base level results from the bathymetric healing process of turbidity currents. To simulate depositional erosion events, former deposition above the base level should be truncated. The accommodation, that is, the space between the local base level and the former surface, should be refilled (Figure 3-27). We assume that the erosion ability is diminished as long as a new lobe is formed; therefore, a local base level used for depositional erosion simulation will be adjusted to pass through the entry position of the new lobe. A long section is shown in Figure 3-28 to illustrate the depositional erosion methodology. The corresponding section without erosion simulation is shown in the second panel of Figure 3-24. 158 surfaces are generated; while it is 113 for no-erosion case.

The algorithm can only run unconditionally until now.
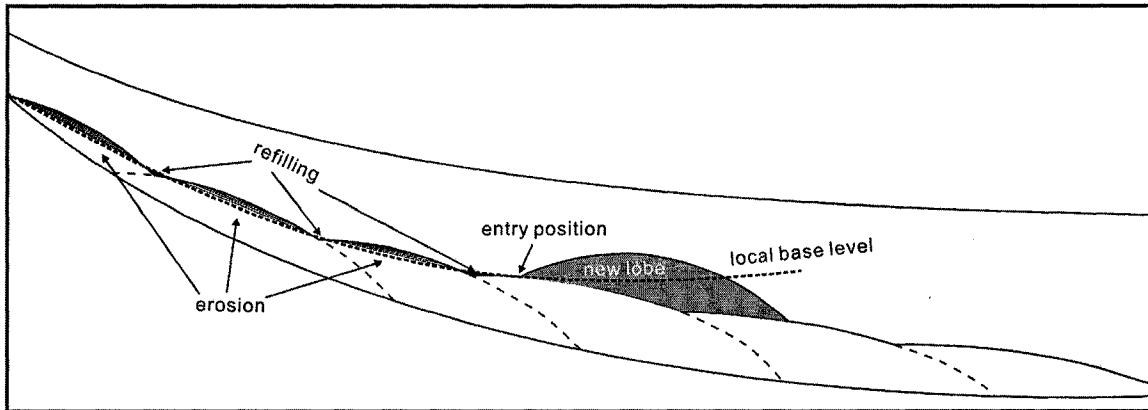
Figure 3-27: Schematic plot showing the erosion rule. Both base and top surfaces have been transformed to paraboloid. The current candidate surface is highlighted with light gray color. The equilibrium is shown with dash line. The local geometry used for equilibrium fitting is illustrated as the heavy gray solid line.
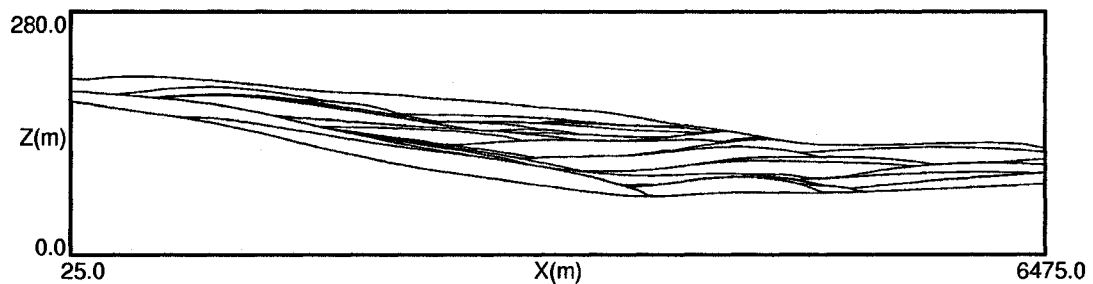
Figure 3-28: A long section to illustrate the depositional erosion simulation results.

2. Honouring stacking patterns

There are three stacking patterns that can be simulated with the *LE_model*, aggradation, progradation and retrogradation. As we mentioned earlier, the entry position in *LE_model* is selected by randomly picking in areal surface occurrence probability field. Therefore, the distribution of the probability field will have significant influence on the selection of surface entry position. Stacking patterns may be honoured by controlling the distribution of a probability field. For example, if proximal positions get higher surface occurrence probabilities, a proximal position will be preferentially picked; therefore, a progradational stacking pattern may be reproduced. The reproduction of different stacking patterns is shown in Figure 3-29.
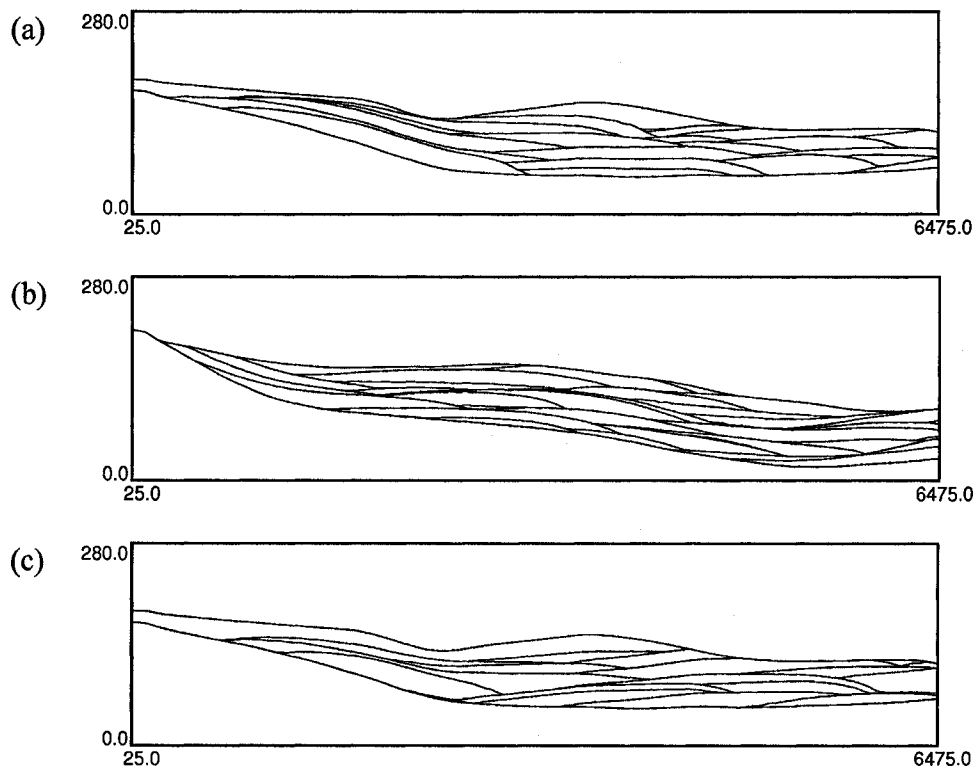
Figure 3-29: The reproduction of different stacking patterns, (a) aggradation, (b) progradation, and (c) retrogradation.

42

3.2.8 An example parameter file of *LE_model*

The parameter file for *LE_model* includes the specification of well data, boundary surfaces, grid definition, lobe geometry and trend definition, and facies trend template. An example parameter file is shown below and an explanation for each parameter is provided in Table 3-3.

Parameters for *LE_model*:

1.	well.dat	- well file
2.	1 2 3 4 5 6 7 8	- data columns
3.	bot.out	- file with base surface
4.	1	- column for variable
5.	top.out	- file with top surface
6.	1	- column for variable
7.	1 bound.dat	- using boundary (0=no, 1=yes), boundary file
8.	3	- flatten method (0=no, 1=base, 2=paraboloid, 3=incline)
9.	0	- honour erosion (0=no, 1=yes)
10.	130 25.0 50.0	- nx, xmn, xsiz
11.	130 25.0 50.0	- ny, ymn, ysiz
12.	280 0.5 1.0	- nz, zmn, zsiz
13.	2	- number of entry locations at Xmin
14.	40 80	- Y locations of entry locations
15.	70	- angle of permissible deposition
16.	0.03	- minimum lobe volume
17.	0.95	- fraction of the model to fill
18.	1	- honour thickness trend? (0=no, 1=yes)
19.	2	- number of trend control points
20.	0.0 15.0 3.0	- depth(1), thickness(1), standard deviation(1)
21.	300.0 35.0 3.0	- depth(2), thickness(2), standard deviation(2)
22.	2500 0.3	- L: length - mean and CV
23.	2000 0.3	- W: width - mean and CV
24.	25.0 0.3	- T: thickness - mean and CV
25.	0.1 0.3	- w/W: width of entry/width - mean and CV
26.	1	- stacking pattern (1=aggradation, 2=retrogradation, 3=progradation)
27.	76067	- random number seed
28.	1 4	- facies proportion, number of facies
29.	0.0 0.7 0.4 0.0	- xx1(1), zz1(1), xx2(1), zz2(1)
30.	0.0 1.0 0.6 0.0	- xx1(2), zz1(2), xx2(2), zz2(2)
31.	0.2 1.0 0.8 0.0	- xx1(3), zz1(3), xx2(3), zz2(3)
32.	1	- output format (1=*BlockSIS*, 2=*sisim_lm*)
33.	LE_model.out	- output surface file
34.	Localmean.out	- output local mean file
35.	3	- debugging level
36.	LE_model.dbg	- debugging file

43

Line	Description
1	Input file with well data. The file should be in GeoEAS format.
2	Column numbers for the well, x, y, z locations and marker code. The x2, y2, z2 are used for no information intervals. The codes are 1 – gradational, and 2 – no information.
3-4	Input file with base surface data, and its column number. The file should be in GeoEAS format.
5-6	Input file with top surface data, and its column number. The file should be in GeoEAS format.
7	Indicator for using boundary file *ibnd*: 0 – no, 1 – yes. If *ibnd* = 1, a boundary file should be specified. The file should be in GeoEAS format, and the data out of interest area will be given extreme large values.
8	Base surface flattening method, 0 – no flattening, 1 – flatten to horizontal, 2 – transform to paraboloid and 3 – transform to incline.
9	Indicator for honouring global unconformity, 0 – no, 1 – yes.
10-12	The regular grid parameters.
13	The number of entry locations at xmin.
14	The Y locations of entry locations.
15	The angle of permissible deposition.
16	The minimum lobe volume. It is in relative scale, and it equals to real lobe volume / gross volume.
17	The fraction of the model to fill.
18	Indicator for honouring lobe thickness trend *ithk*, 0 – no, 1 – yes.
19-21	The lobe thickness trend definition if *ithk* = 1. The trend is defined in real scale and a linear trend template is applied. User needs to specify the number of trend control points, the depth, the mean and standard deviation of lobe thickness at each control point.
22-25	Lobe geometry definition, including lobe length, width, thickness and width ratio w/W.
26	Stacking pattern, 1 – aggradation, 2 – retrogradation, 3 – progradation
27	Random seed
28	Indicator for facies proportion calculation, 0 – no, 1 – yes. Number of facies and facies template type, 0 – 1D vertical trend, 1 – 2D trends. See Chapter 4 for detail.
29-31	Facies trend template definition.
32	Facies proportion output format, 1 – BlockSIS, 2 – sisim_lm.
33	File with output surfaces.
34	File with output facies proportions.
35	Debugging level.
36	File with debugging information.

Table 3-3: A description of the *LE_model* parameter file.

44

3.3 Advances in strataform modeling

Surfsim program was designed by Pyrcz (2004) to build stochastic surface-based realizations that honour surface geometry and erosional and gradational well contacts for strataform deposits.

Original *Surfsim* program assumes:

1) Near parallel bedding; therefore, the surface template is a plane. One possible application of *Surfsim* is to model sheet architectural elements in distal fine grained turbidites.

2) The vertical location is chosen such that an average thickness (drawn from a lognormal distribution with a user defined average and standard deviation) is honoured. Thickness trend modeling is not available.

3) The bounding surfaces are assumed to be nonangular unconformities. A candidate surface will be truncated by bounding surfaces if it tends to extend beyond a boundary.

The improvements developed in this thesis aim at making *Surfsim* more flexible and powerful, so that it can be applied to more complicated geological settings, such as deformed strata.

3.3.1 Boundary surfaces transform

The original bounding surfaces are often planar in distal fine-grained deepwater turbidites. However, geological deformation and faulting are very common in continental slope environments. Therefore, the default assumption will not hold anymore. A common solution is to transform the bounding surfaces to their original shape during simulation, then transform them back after simulation.

1. Methodology

Two boundary surfaces transform approaches are applied:

1) flatten base surface to a horizontal plane,

$$z_{rel} = z - z_{cb} \tag{3.13}$$

where z_{cb} is the correlation base, z is the current elevation, z_{rel} is the relative stratigraphic coordinate. The coordinate z_{rel} is 0.0 at the stratigraphic base and equals the thickness of the bounding surfaces at the stratigraphic top.

This transform may be reversed by:

$$z = z_{rel} + z_{cb} \tag{3.14}$$

2) transform bounding surfaces proportionally,

$$z_{rel} = \frac{z - z_{cb}}{z_{ct} - z_{cb}} \cdot T \tag{3.15}$$

45

where z_{ct} is the correlation top, T is the average thickness of the bounding surfaces. The coordinate z_{rel} is 0.0 at the stratigraphic base and equals T at the stratigraphic top.

This transform may be reversed by:

$$z = z_{cb} + \frac{z_{rel}}{T} \cdot (z_{ct} - z_{cb})$$

(3.16)

2. Demonstration

Figure 3-30 shows a case study example. The strata pinch out proximally, which is common in continental slope environment.

Without boundary surfaces transform, *Surfsim* does not work well (Figure 3-30a). This is due to the intrinsic assumptions of *Surfsim*. After flattening base surface to a horizontal plane, *Surfsim* works very well (Figure 3-30b). The top surface intersects with the base surface in this case, so the simulated surfaces have onlap stratigraphic correlation style. When transforming the bounding surfaces proportionally (Figure 3-30c), new base and top surfaces are parallel with each other. The vertical position of a surface is in proportion to the thickness of the boundary surfaces; therefore the simulated surfaces follow the stratigraphic shape and pinch out proximally.
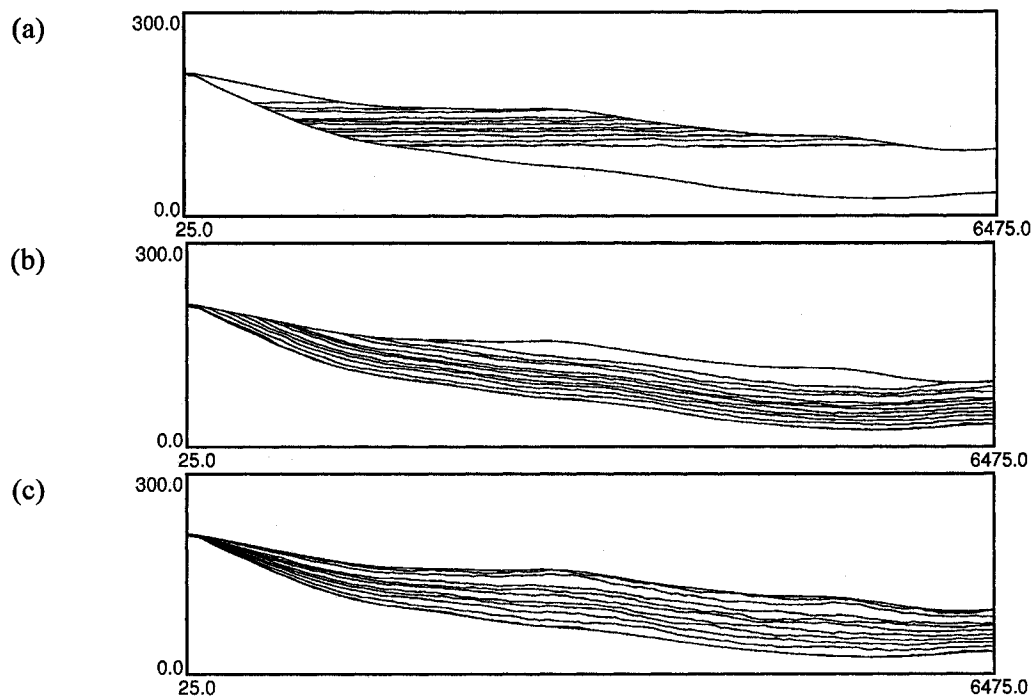
Figure 3-30: Long section 25 to illustrate the surface modeling effect with different boundary surfaces transform algorithms: (a) no transform, (b) flatten the base surface to a horizontal plane, and (c) transform the bounding surfaces proportionally.

46

3.3.2 Piecewise linear trend modeling

A piecewise linear trend template for the layer thickness is proposed and can be reproduced in simulation. The program can be easily modified to honour any types of vertical trend. The trend is defined in relative scale and within the range of [0.0, 1.0] (Figure 3-31). The minimum elevation of the base surface is set as 0.0, and the maximum elevation is set as 1.0. Instead of drawing the thickness mean from a lognormal distribution, it is chosen from the trend template. Note that the thickness of the current surface is a function of former surfaces; therefore, these surfaces are correlated with each other.
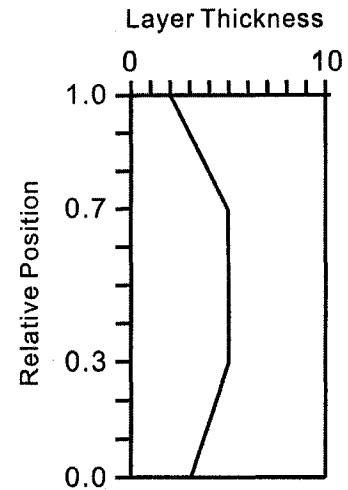
Figure 3-31: Relative thickness trend definition.

1. Demonstration

Figure 3-32 shows two thickness trend reproduction results. The left panel has a standard deviation 0.1, and the thickness is centered on the trend with small fluctuation. The right panel has a standard deviation 1.0; therefore, the thickness shows great dispersion. In both cases, the thickness trends are well reproduced.
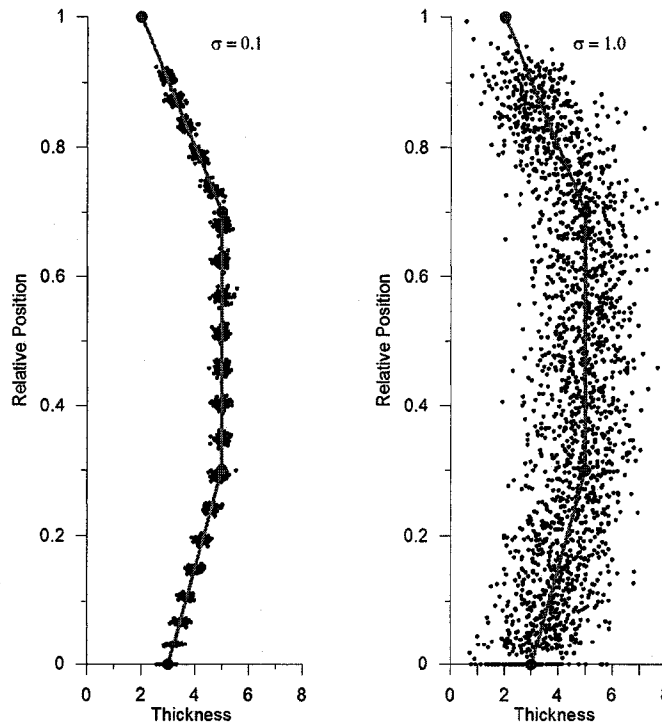
Figure 3-32: Comparing the layer thickness of 99 realizations with the trend definition. The standard deviation for each layer is set to 0.1 for the left panel and 1.0 for the right panel.

47

2. Discussion

Figure 3-33 and Figure 3-34 show 2 profiles simulated with the original algorithm of *Surfsim*, one was conditionally built and the other was unconditionally built. In the conditional case, the conditioning data control the simulation result. Apparent thinning-upward trend exists due to the distribution of well data. On the unconditional profile, 4 cycles exist. However, no vertical trends should exist according to the algorithm. It shows that an unrealistic trend template may be inferred with limited data.
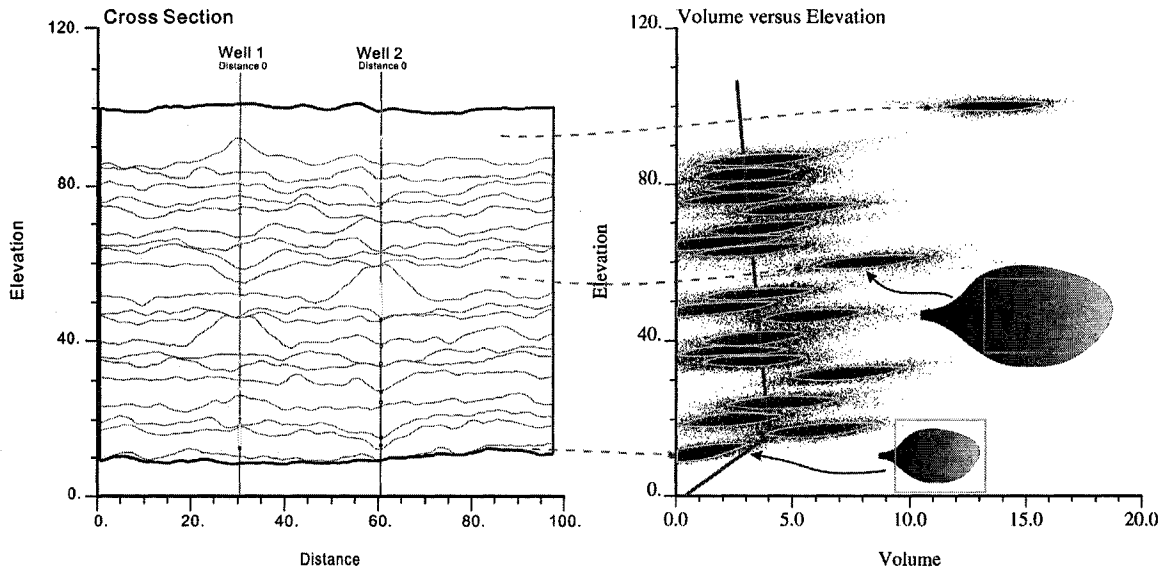
Figure 3-33: The vertical thickness trend of a section with conditional *Surfsim* realization. Thinner upward trend is very clear due to the conditioning data.
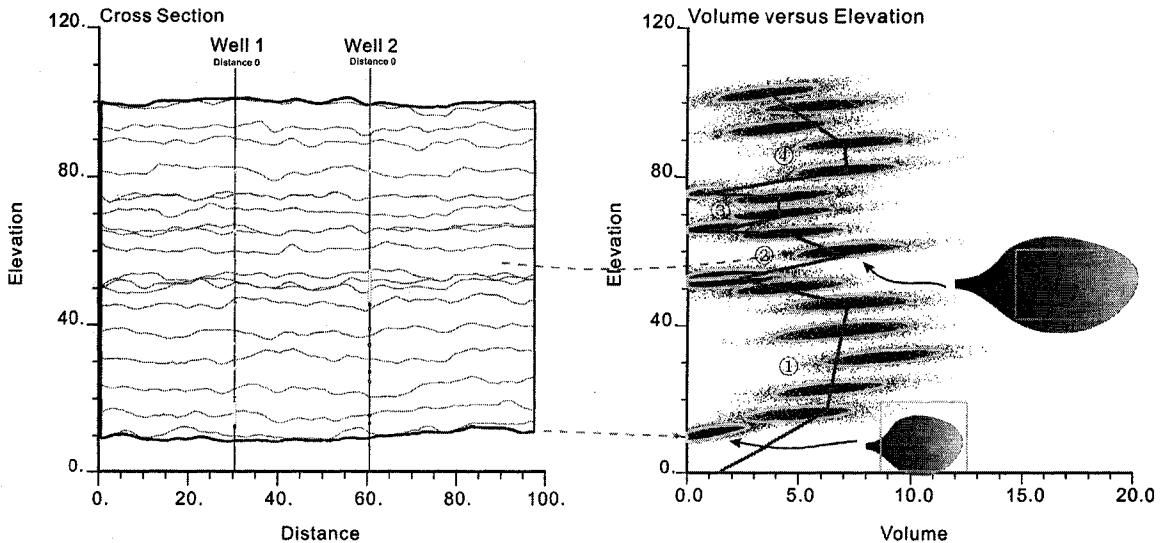
Figure 3-34: The vertical thickness trend of a section with unconditional *Surfsim* realization. It looks that 4 cycles (sequence) exist. The boundaries are the same as those in Figure 3-32 and wells are also plotted to show that this is an unconditional realization.

48

3.3.3 Honour common stratigraphic correlation style

The assumption of *Surfsim* is that the base surface is always a nonangular unconformity, and the top surface is an unconformity. This is not always true. The common stratigraphic correlation styles, including unconformity, onlap, downlap, stratigraphic pinch out, may all be reproduced with the new *Surfsim* program.

1. Unconformity and conformity

When top surface is not parallel to base surface, it is assumed to be an unconformity, or it is assumed to be a nonangular unconformity. The conformity contact of top surface can be honoured by setting a smaller filling proportion. Angular unconformity can be honoured by using an incline surface template, instead of a planar template (Figure 3-35). The dip can be specified by the user.

2. Onlap

When top surface is not parallel to base surface, onlap can be honoured by flattening the base surface to a plane. When top surface is parallel to base surface, onlap can be honoured by using an incline surface template.

3. Downlap

Downlap can be honoured by using an incline surface template only.

4. Stratigraphic pinch-out

It can only be honoured by using proportional bounding surfaces transform when the bounding surfaces pinch out somewhere.
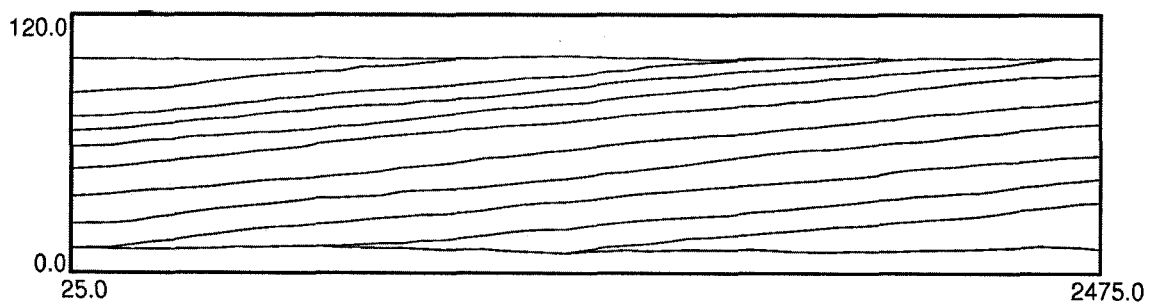
Figure 3-35: An angular unconformity modeling example. Onlap and downlap contacts are also reproduced.

49

3.3.4 An example parameter file of *Surfsim*

Some new parameters are introduced into *Surfsim* for these newly developed functions. The new *Surfsim* parameter file includes well data, boundary surfaces, flattening method, grid definition, filling proportions, vertical trend definition and simulation parameters (search and semivariogram) for the 2D simulation of the residual. An example parameter file is included below and an explanation for each parameter is provided in Table 3-4.

Parameters for *Surfsim*:	
1. well.dat	- file with data
2. 1 2 3 4 5 6 7 8	- well, x1, y1, z1, x2, y2, z3, code
3. 1	- well conditioning (0=no, 1=yes)
4. top.out	- file with top surface
5. bot.out	- file with bottom surface
6. 0	- flatten method (0=no, 1=base, 2=proportional)
7. 100 0.5 1.0	- nx, xmn, xsiz
8. 50 0.5 1.0	- ny, ymn, ysiz
9. 150 0.5 1.0	- nz, zmn, zsiz
10. 1	- number of realizations to generate
11. 69069	- random number seed
12. 0.90	- fraction of the model to fill
13. 5.0 2.0	- mean and stdev of thickness
14. 1 4	- vertical trend? (0=no, 1=yes), no. of control points
15. 0.0 3.0 2.0	- 1st: relative depth, thickness, stddev
16. 0.3 5.0 2.0	- 2nd: relative depth, thickness, stddev
17. 0.7 5.0 2.0	- 3rd: relative depth, thickness, stddev
18. 1.0 2.0 2.0	- 4th: relative depth, thickness, stddev
19. 20	- maximum number of surfaces
20. 1.0	- gradient of surface in degrees
21. 0	- output option (0=process, 1=all surfaces)
22. surfsim.out	- file for simulation output
23. surfsimgrid.out	- file for simulation grid output
24. surfvol.out	- file for surface volume output
25. 0	- debugging level: 0, 1, 2, 3
26. surfsim.dbg	- file for debugging output
27. 12	- number of simulated nodes to use
28. 1 3	- multiple grid search (0=no, 1=yes), num
29. 10.0 10.0	- maximum search radii (hmax, hmin)
30. 0.0	- angle for search ellipsoid
31. 51 51	- size of covariance lookup table
32. 1 0.1	- nst, nugget effect
33. 1 0.9 0.0	- it,cc,ang1
34. 10.0 10.0	- a_hmax, a_hmin

50

Line	Description
1	Input file with well data. The file should be in GeoEAS format.
2	Column numbers for the well, x, y, z locations and marker code. The x2, y2, z2 are used for no information intervals. The codes are 0 – erosional, 1 – gradational, and 2 – no information.
3	Indicator for well conditioning, 0 – no, 1 – yes.
4-5	Input files with boundary surfaces data. Files should be in GeoEAS format.
6	Flatten method, 0 – no, 1 – flatten base surface, 2 – proportional flattening.
7-9	Regular grid definition.
10	Number of realizations to generate.
11	Random seed.
12	Fraction of the model to fill.
13	Mean and standard deviation of thickness.
14	Indicator for honouring vertical trend, 0 – no, 1 – yes. Number of controlling points. Piecewise linear trend template is applied at present.
15-18	The depth, thickness and standard deviation for each controlling point. The depth is in relative scale.
19	Maximum number of surfaces.
20	Gradient of surface in degrees. 0 degree means horizontal surface template.
21	Output option. 0 – output interim surfaces for each stage for surface evolution checking, 0 – output final surface model only.
22	File with surface model.
23	File with simulation grid.
24	File with volume of each surface.
25	Debugging level.
26	File with debugging info.
27-34	2D simulation parameters.

Table 3-4: A description of the *Surfsim* parameter file.

3.4 Summary

Advances in turbidite lobes modeling and strataform surface modeling are presented in this chapter. An automatic surface picks identification approach is proposed as a preprocessor of turbidite lobes modeling. A series of rules are proposed for turbidite lobe events modeling, including (1) global and local base levels modeling, (2) vertical and areal surface positioning, (3) well conditioning, (4) erosion events modeling and (5) stacking patterns reproduction. Several global coordinates transform approaches are introduced into strataform surface simulation; therefore the *Surfsim* program may be applied to more geological settings. Piecewise linear thickness trend can be honoured and inclined surface template is introduced to reproduce common strata correlation styles.

51

Chapter 4

Surface-based Facies Modeling

Facies modeling is the process of creating a discrete 3D facies distribution within a geological grid. Facies models are often cell based and focus on reproducing one- and two-point statistics, so complicated spatial structures are not often reproduced. As illustrated in Chapter 3, the proposed surface modeling approach may build complicated and geologically realistic surface models that honour available surface picks at wells. Therefore, utilizing the simulated surface models to capture curvilinear reservoir structures becomes a natural solution to produce realistic curvilinear facies structures.

In this chapter, facies modeling is developed in the context of simulated surface models. Depositional trends information is utilized. Section 4.1 reviews the idealized deepwater turbidite facies distributions, which is the geological basis of the proposed approaches. Section 4.2 illustrates the approach for integrating geological conceptual models and 2D facies trends template. Section 4.3 presents facies modeling approaches that can integrate facies proportions. Section 4.4 demonstrates the proposed methodologies with a realistic case study.

4.1 Introduction

In terms of waning flow regime from bottom to top and with increasing path across a basin, turbidity current loses both energy and sediment; hence the distal turbidites, as well as deposits on the levees, do not show the complete turbidite sequences (Figure 4-1; Reineck and Singh, 1980). The resulting hypothetical facies plan distribution is shown in Figure 4-2. This is also the idealized facies distribution within a second-order turbidite lobe. The loss of energy results in progressively less basal erosion, deposition of progressively finer sediment and thickening of the finer part of the sandstone / mudstone couplet. Most importantly, accompanying the downcurrent (lateral) grading of size and bed thickness, there is a change in the internal structure of the sand component of the couplet, with progressively higher parts of the Bouma sequence forming the base of the turbidite bed (Figure 4-3; MacDonald, 1992). Based on above analysis, the idealized facies distribution of a second-order turbidite lobe is shown in Figure 4-4. Three facies are assumed in this diagram.

52
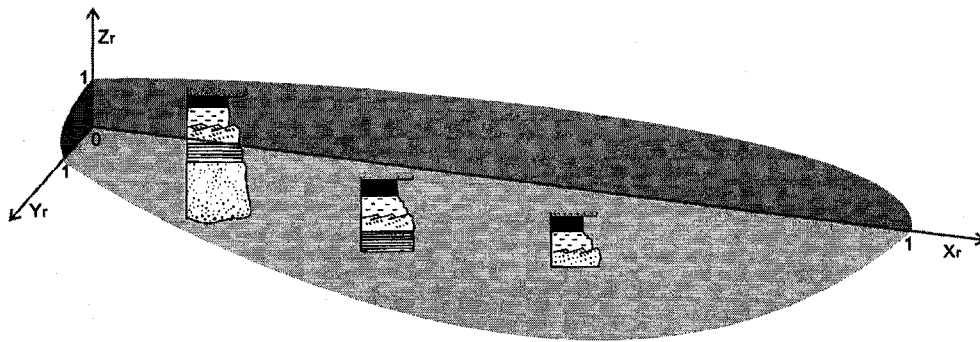
Figure 4-1: Schematic diagram depicting Bouma sequences change in terms of distance across basin and flow conditions (after Reineck and Singh, 1980). Background is a second-order turbidite lobe.
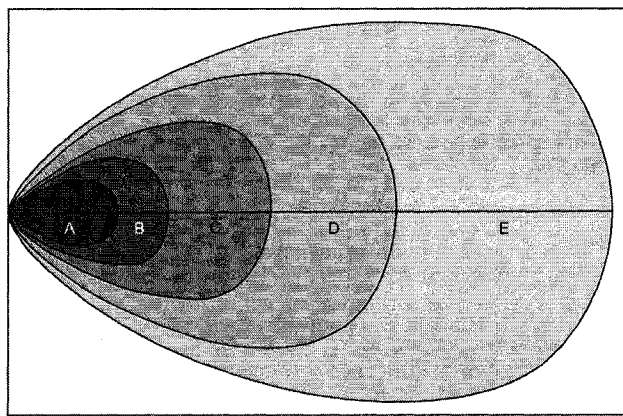
Figure 4-2: Hypothetical plan view showing geographic distribution of intervals in a flysch profile from Bouma division A at the base to E at the top (after Reineck and Singh, 1980).
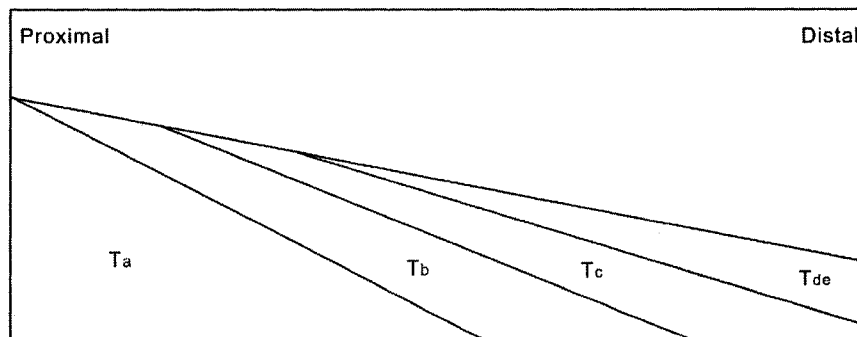
Figure 4-3: Schematic diagram showing upper parts of the Bouma sequence (Ta-Te) coming to rest on turbidite bed base distally (after MacDonald, 1992).

53
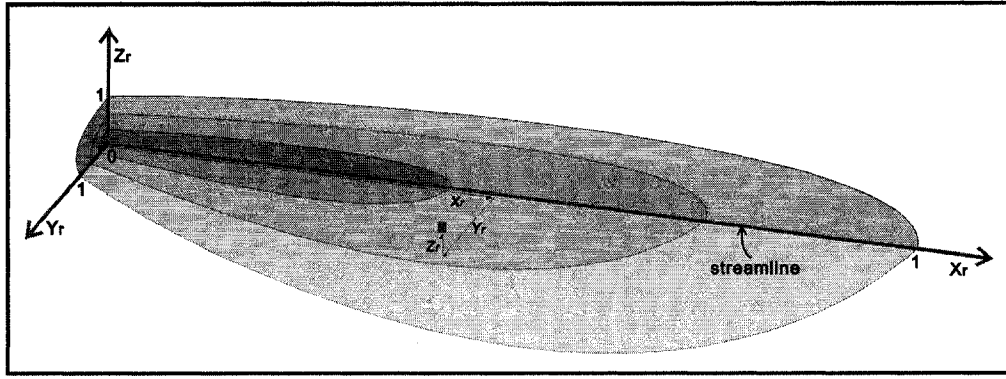
Figure 4-4: Schematic diagram depicting idealized facies distribution in a second-order turbidite lobe. This plot also shows how to calculate depositional coordinates for a given cell (after Pyrcz, 2004).

4.2 Surface-based facies proportion calculation

Facies models are often cell based. For a given cell, its depositional coordinates can be easily determined based on its vertical, longitudinal and transverse relative position within a second-order lobe. If facies trends are known, the position information may be transformed to facies proportions and taken into account in facies modeling process. Therefore, surface shape information will be brought into facies modeling stage.

4.2.1 Integration of geological conceptual models

The vertical facies trend may be available from well logs. Areal facies trend inference is difficult due to widely spaced wells. Therefore, an areal facies conceptual model is used often in practice, which may come from experienced geologists. These models are problem specific and therefore no universal solutions exist. In this research, the areal facies distribution in Figure 4-2 is applied to illustrate the proposed methodology.

Conceptual models may also be defined analytically. There are several analytical turbidite lobe models available. One popular model is the "simple" lobe model proposed by Deutsch (2002). Assuming that the inner facies distribution follow the lobe boundary shape, the facies boundary may be expressed as:

$$
y = \begin{cases} w + 4 \cdot (W - w) \cdot [\frac{x}{2\ell}(1 - \frac{x}{2\ell})], & 0 \le x \le \ell \\ W \cdot \sqrt{1 - (\frac{x - \ell}{\mathcal{L} - \ell})^2}, & \ell \le x \le \mathcal{L} \end{cases}
\tag{4.1}
$$

54

where x, y are the X, Y coordinates of facies boundary, w, W are the minimum and maximum facies width, ℓ is the X position of maximum width, and $\mathcal{L}$ is the maximum length. An idealized areal facies distribution is shown in Figure 4-5.

(a)

(b)
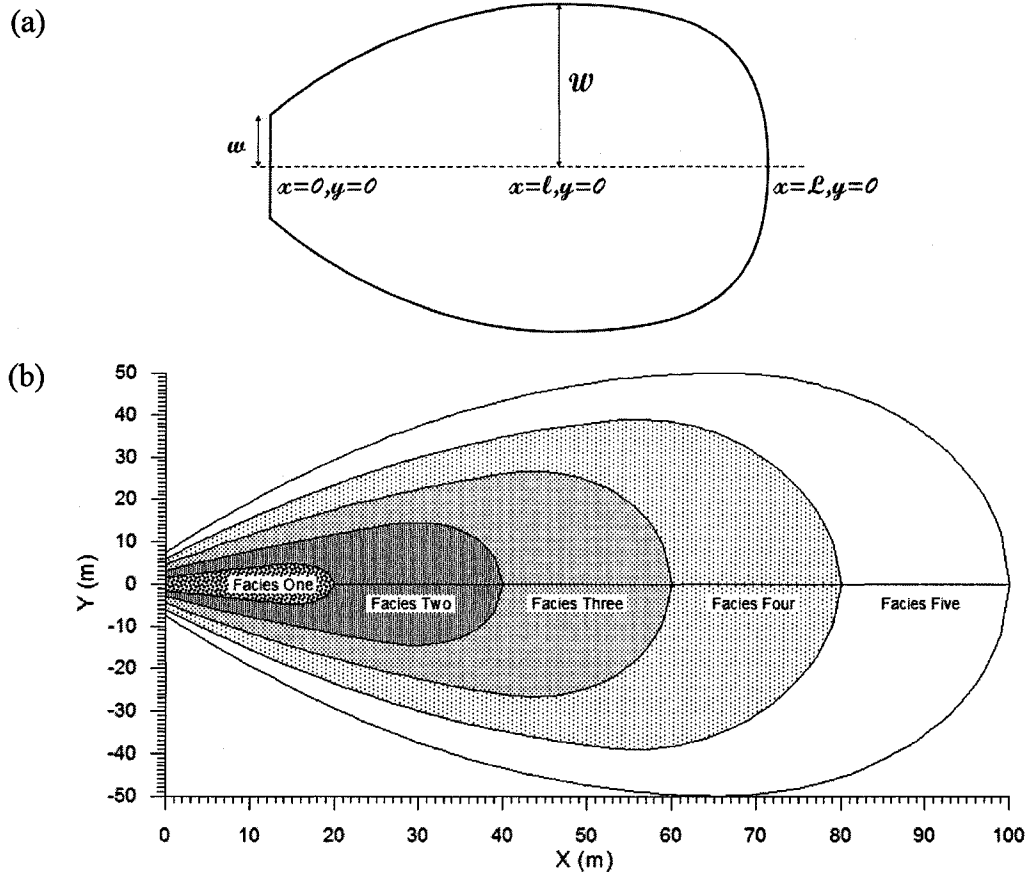
Figure 4-5: Schematic diagrams illustrating an analytical conceptual facies template, (a) parameters used in "simple" facies template, and (b) the idealized facies distribution described with Formula (4.1).

For a given cell within a second-order lobe, its depositional coordinates may be denoted as Xr, Yr and Zr. It may have the same vertical trend as some position on the centerline. The location can be inferred under some assumptions. Therefore, the 3D facies trend calculation problem may be simplified to a 2D facies trend calculation problem. One convenient assumption is that for any point on axis, it has the same facies changing rate longitudinally and laterally (Figure 4-6), that is,

$$\frac{X_1}{X_2} = \frac{Y_1}{Y_2} = \frac{Y_1}{1} \tag{4.2}$$

where Y_1 is the distance from P_1 to its perpendicular projection on centerline, A; Y_2 is the lateral facies width of Facies Two from A; X_1 is the distance from A to P_2, the position has same vertical facies trend as P_1; and X_2 is the longitudinal distance from A to the boundary of Facies Two.

55

A linear vertical facies trend model may be applied to simulate the facies change proximally according to proximity theory. For convenience, the facies trend is defined in relative scale. Since the areal lobe shape is known, only vertical trend definition is needed in facies proportion calculation. An example linear vertical trend template is shown on the left plot in Figure 4-7.
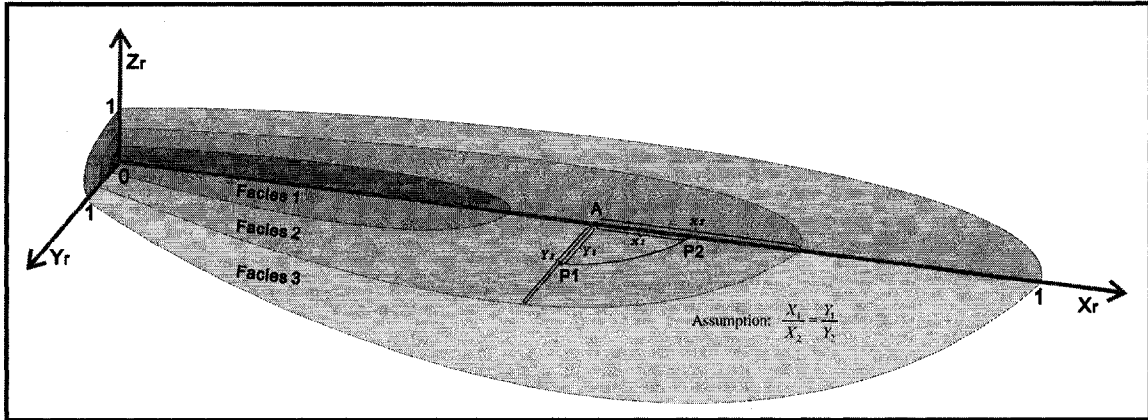
Figure 4-6: Schematic diagram illustrating the axis relative position determination procedure.
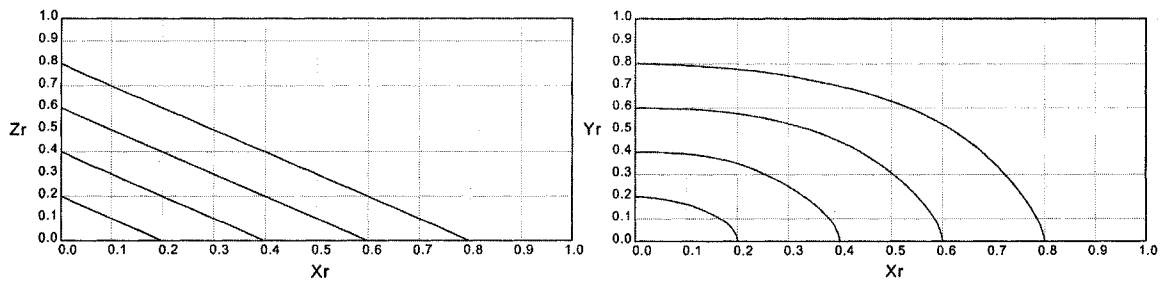
Figure 4-7: Schematic diagrams illustrating the linear and elliptical axis-vertical facies trend definition.

The calculated facies proportions may be rescaled to honour global proportions,

$$p_k^{1D}(z_r) = P_k \cdot p_k(z_r) \qquad (4.3)$$

where k denotes for the kth facies, $p_k^{1D}(z_r)$ is the updated facies proportion, P_k is the global proportion, and $p_k(z_r)$ is the calculated facies proportion.

4.2.2 Integration of statistical trends

When well spacing is close enough, areal facies trends may be inferred. In this case, both areal and vertical facies trends may be applied. For simplification, both vertical and areal facies trends are defined in relative scale. An elliptical areal facies trend and a linear vertical facies trend are applied in this thesis. The elliptical shape is selected because it is simple and the facies distribu-

56

tion follows the shape of the lobe outline very well (Figure 4-8). An example 2D trend template is shown in Figure 4-7.
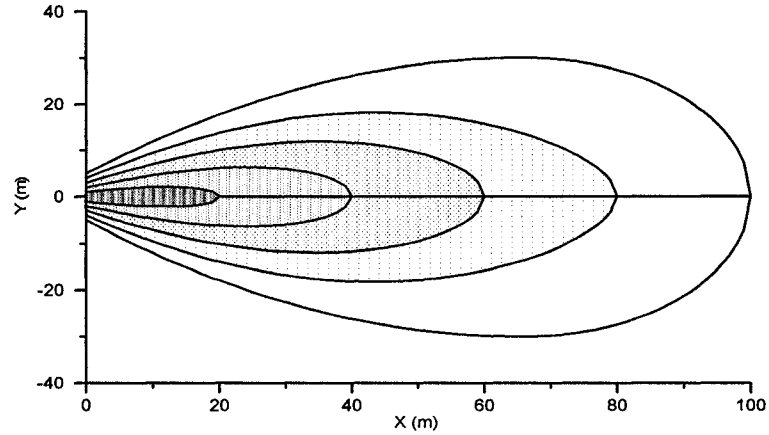
Figure 4-8: An analytical diagram showing the areal facies distribution with elliptical areal facies trends.

Under the assumption that the areal and vertical facies trends are conditionally independent, the final facies trend may be expressed as,

$$p_k^{CI}(y_r, z_r) = P_k \cdot p_k(y_r) \cdot p_k(z_r) \tag{4.4}$$

where k denotes for the kth facies, $p_k^{CI}(y_r, z_r)$ is the updated facies proportion under conditional independence assumption, P_k is the global proportion, and $p_k(y_r)$ and $p_k(z_r)$ are the calculated areal and vertical facies proportions, respectively.

A common shortcoming of the conditional independence assumption is that the high values may be extremely high and low values may be extremely low (Deutsch, 2002). To overcome this drawback, the permanence ratio approach (Journel, 2002) is applied to integrate the two types of trends,

$$p_k^{PR}(y_r, z_r) = \frac{\dfrac{1-P_k}{P_k}}{\dfrac{1-P_k}{P_k} + \dfrac{1-p_k(y_r)}{p_k(y_r)} \cdot \dfrac{1-p_k(z_r)}{p_k(z_r)}} \tag{4.5}$$

where $p_k^{PR}(y_r, z_r)$ is the updated facies proportion under permanence ratios assumption.

The calculated facies proportions are also scaled to honour global facies proportions.

57

4.3 Application of facies proportions

Programs available in the public domain to integrate calculated facies proportions include *GTSIM*, *BlockSIS* and *sisim_lm*. *GTSIM* applies facies proportions directly to truncate continuous Gaussian values to build facies model. *BlockSIS* and *sisim_lm* integrate facies proportions as secondary data.

For surface-based facies modeling, both facies types and facies proportions are known at wells, so the corresponding Gaussian values may be easily calculated by reversely transforming the centroid *ccdf* value of the facies (Figure 4-9). A Fortran 90 program, *CalcSgsData*, was written to perform the proposed methodology. The program parameters are shown below; the description of each parameter is included in Table 4-1.
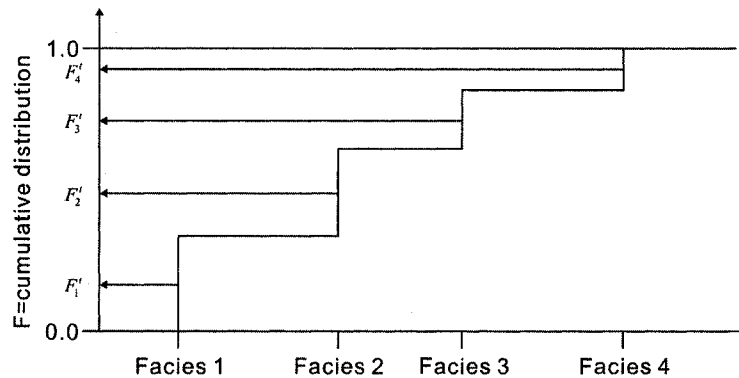
Figure 4-9: Schematic diagram illustrating the *ccdf* value of each facies.

Parameters for *CalcSgsData*:

1.	well.dat	- well file
2.	1 2 3 4 5	- Columns for keyout, x, y, z, facies
3.	lm.out	- local mean file
4.	upwell.dat	- output file
5.	4	- number of facies
6.	130 25.0 50.0	- nx,xmn,xsiz
7.	130 25.0 50.0	- ny,ymn,ysiz
8.	280 0.5 1.0	- nz,zmn,zsiz

Line	Description
1	Input file with wells data. The file should be in GeoEAS format.
2	Column numbers for the keyout array, x, y, z location and facies code.
3	Input file with facies proportions / local means data.
4	The file with updated wells data. An additional column with the transformed Gaussian values is added.
5	The number of facies.
6-8	The regular grid definition.

Table 4-1: A description of the *CalcSgsData* parameter file.

58

A comparison of above transformation approach and conventional transformation approach is shown in Figure 4-10. Although the transformed values do not have perfect Gaussian shape, they are consistent with the facies proportions at wells. A typical *GTSIM* workflow with integrating facies proportions information is shown in Figure 4-11. The *GTSIM* program was modified to have the ability to read keyout array, so the volume out of the bounding surfaces will not be modeled. If a cell is located within the strata, its keyout value equals to 1; otherwise it equals to 0. An example *GTSIM* parameter file is shown below and each parameter is included in Table 4-2.
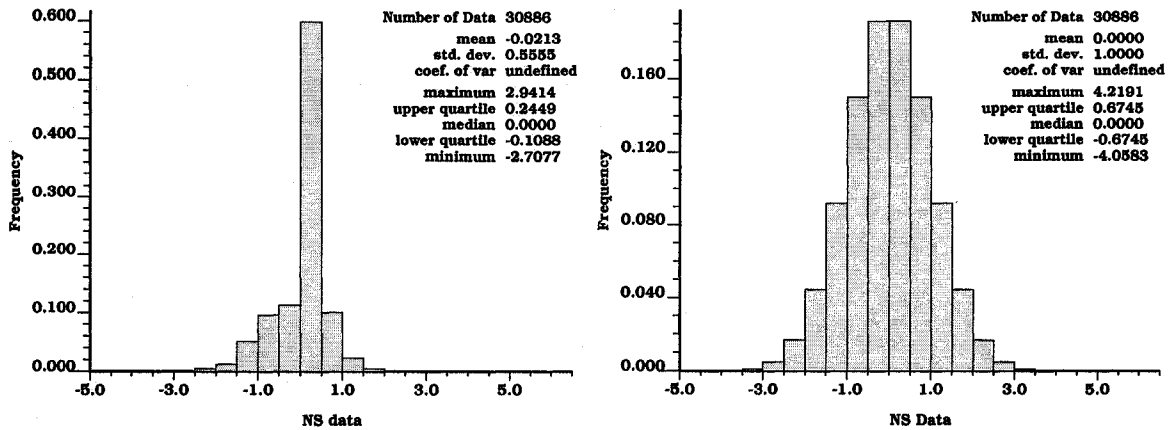
Figure 4-10: Comparison of calculated Gaussian values with *CalcSgsData* and conventional Normal score transformed Gaussian values. Left: *CalcSGSData*; right: *nscore*.

Parameters for *GTSIM*:	
1. sgsim.out	- input file with Gaussian values
2. gtsim.out	- output file with categorical values
3. 1	- number of realizations
4. 50 50 1	- nx, ny, nz
5. 3	- number of categories
6. 1 0.25	- cat(1) - global proportion(1)
7. 2 0.25	- cat(2) - global proportion(2)
8. 3 0.50	- cat(3) - global proportion(3)
9. 1	- proportion curves (0=no, 1=yes)
10. propc.dat	- file with local mean values
11. 1 2 3 4	- keyout, column number for p1, p2, p3...

Line	Description
1	Input file with Gaussian values. The file should be in GeoEAS format.
2	Output file with categorical values. The file should be in GeoEAS format.
3	Number of realizations
4	Total grid number in x, y, z directions.
5	Number of categories.
6-8	Global proportions of each category. The total lines equal to the number of categories.
9	Indicator for using proportion curves, 0 – no, 1 – yes.
10	If proportion curves are used, the file with the proportion curves needs to be specified here.
11	The columns for keyout array, probability for each category.

Table 4-2: A description of the *GTSIM* parameter file.

59
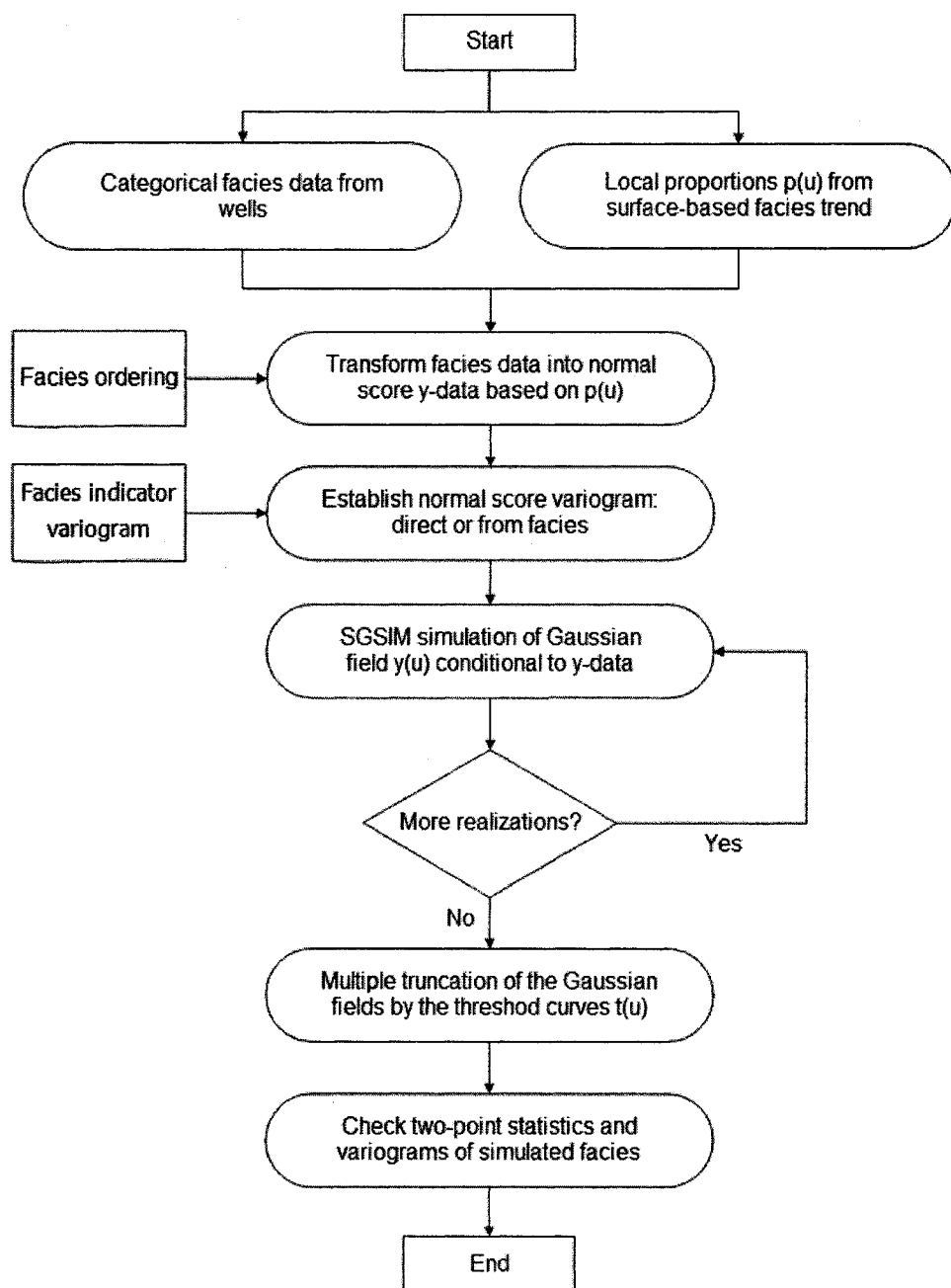
Figure 4-11: Schematic diagram illustrating the workflow of GTSIM with facies proportion curves.

60

There are two algorithms that can integrate facies proportions as secondary data. One is the non-stationary simple kriging with residuals from the locally varying mean probabilities,

$$i_{LVM_1}^* \left(\mathbf{u}; k \right) - p_k \left(\mathbf{u} \right) = \sum_{\alpha=1}^{n} \lambda_\alpha^{SK} \left(\mathbf{u}; k \right) \cdot \left[i \left(\mathbf{u}_\alpha; k \right) - p_k \left(\mathbf{u}_\alpha \right) \right] \qquad (4.6)$$

Another one uses one minus the sum of the weights assigned to the local mean,

$$i_{LVM_2}^* \left(\mathbf{u}; k \right) = \sum_{\alpha=1}^{n} \lambda_\alpha^{SK} \left(\mathbf{u}; k \right) \cdot i \left(\mathbf{u}_\alpha; k \right) + \left[1 - \sum_{\alpha=1}^{n} \lambda_\alpha^{SK} \left(\mathbf{u}; k \right) \right] \cdot p_k \left(\mathbf{u} \right) \qquad (4.7)$$

When locally varying mean values are smooth, the differences between Function (4.6) and (4.7) are minor (Deutsch, 2006).

sisim_lm program is not recommended for it cannot utilize the keyout array; therefore, the volume above the top surface or below the base surface will be filled up with background facies.

4.4 Synthetic case study

In this section, a case study will be presented to illustrate the surface-based facies modeling approach. The case study aims at illustrating and comparing two common facies modeling techniques, *GTSIM* and *BlockSIS*, by integrating the same facies proportions model. Therefore, only one surface model and facies proportions model were built. The global coordinates have been rotated to parallel to the major paleocurrents. Within the 5 Kilometers by 5 Kilometers study area, 81 vertical wells are equal-distance sampled (Figure 4-12). A long section and a cross section are shown in Figure 4-13 to illustrate the reservoir spatial structures.
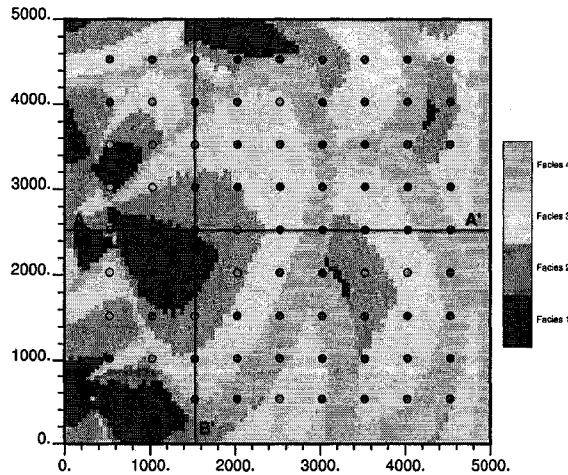
Figure 4-12: The surface distribution on base surface and the location map of 81 vertical synthetic wells. The position of a long section (A-A') and a cross section (B-B') are also marked.

61
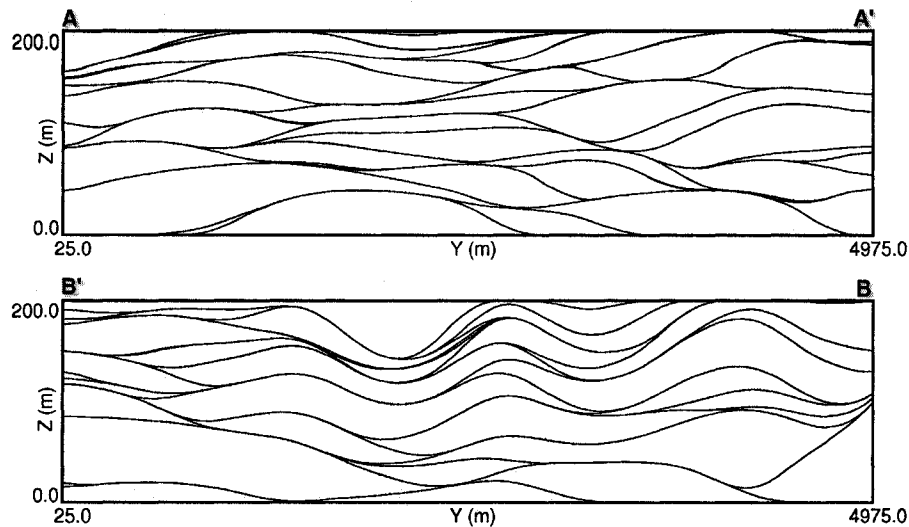
Figure 4-13: The long section A-A' and cross section B-B' to illustrate the reservoir spatial structures.

Lobe geometry is the most important control on facies distribution. When areal and vertical facies trends can be inferred, facies proportions can be calculated using the developed methodologies. Four facies types are assumed in this case study, which represent the typical facies components of Bouma sequence (Figure 4-14). They are summarized in Table 4-3. Declustering may be applied to estimate the global facies proportions (Figure 4-15).

	Grain Size	Divisions	Interpretation
	Mud	E Laminated to homogeneous mud	Low density tail of turbidity current
	Silt	D Upper mud/silt laminae	Shear sorting of grains & flocs
	Sand	C Ripples, climbing ripples, wavy or convolute laminae	Lower part of lower flow regime
		B Plane laminae	Upper flow regime - plane bed
	Coarse Sand	A Structureless or graded sand to granule	Non-equilibrium flow quick bed

Figure 4-14: Ideal sequence of sedimentary structures in a turbidite bed (after Pickering *et al.*, 1989).

Category	Grain Size	Bedding	Bouma (1962) Divisions
Facies 1	Coarse Sand	Structureless or graded sand to granule	A
Facies 2	Sand	Plane laminae and ripples, climbing ripples, wavy or convolute laminae	B and C
Facies 3	Silt	Upper mud/silt laminae	D
Facies 4	Mud	Laminated to homogeneous mud	E

Table 4-3 A summary of the lithofacies definition used in the synthetic case study.

62

Well Data

Number of Data 16200
mean 3.0523
std. dev. 0.7860
coef. of var 0.2575

maximum 4.0000
upper quartile 4.0000
median 3.0000
lower quartile 3.0000
minimum 1.0000

Declustered Data

Number of Data 16200
mean 3.0631
std. dev. 0.7879
coef. of var 0.2572

maximum 4.0000
upper quartile 4.0000
median 3.0000
lower quartile 3.0000
minimum 1.0000

weights used
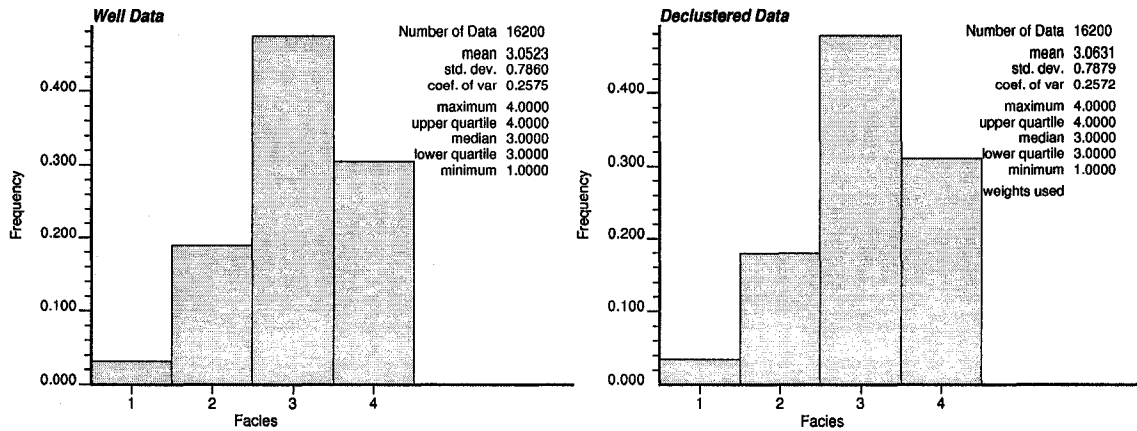
Figure 4-15: The distribution of original and declustered facies distribution from synthetic well logs.

4.4.1 *BlockSIS*

A SIS-based facies modeling approaches, *BlockSIS*, is applied first.

1. Variogram calculation

Like other SIS-based facies modeling approaches, the variogram of each facies should be modeled to specify maximum facies continuity direction and range (Figure 4-16 and Figure 4-17). With many wells, variogram inference is straightforward. In practice, variogram inference may be a big challenge because (1) there are usually not so many densely sampled wells, and (2) stratigraphic framework is usually highly deformed.

2. Facies modeling

A long section and a cross section of a facies model built with *BlockSIS* are shown in Figure 4-18. No image cleaning is performed in this case study for it may alter the spatial structure. Therefore, the facies model appears a little patchy.

3. Model Validation

The histogram reproduction of *BlockSIS* is shown in Figure 4-19. The histogram reproduction is very good.

Each indicator variogram is checked (Figure 4-20 and Figure 4-21). Short-scale variation is well reproduced, but long-scale structure is not well captured, especially in the vertical direction. In general, the variogram reproduction is very good.

A quantitative measure of closeness to the true probabilities may be calculated by,

$$C = \frac{1}{N}\sum_{i=1}^{N}\left\{p(u;k)\,|\,true = k\right\} \tag{4.8}$$

This measure is interpreted as the average predicted probability of the true facies. C value describes how "right" the probabilities are for the true facies. The limitation of C is that it gives no

63

credit when a similar facies is predicted nor does it penalize the case when drastically different facies are predicted (Deutsch, 2002). In this case study, the C value is 0.3355.

Another indicator is the local probabilities. The local probabilities are "accurate" or "fair" if they accurately reflect the true fraction of the predicted facies occurs (Deutsch, 2002). Cases where the actual fraction departs significantly from the predicted probabilities are a problem. The corresponding accuracy plots are shown in Figure 4-22. In general, the accuracy is very good.

Figure 4-16: 3D Variograms of facies one and facies two.

64

Facies 3

Facies 4

Azimuth: 0 Dip: 0

1	0.183				- nst, nugget effect
2	0.817	90.0	0.0	0.0	- it,cc,ang1,ang2,ang3
	481.190	743.730	25.774	- a_hmax,a_hmin,a_vert

Distance (m)

Azimuth: 0 Dip: 0

1	0.183				- nst, nugget effect
2	0.817	90.0	0.0	0.0	- it,cc,ang1,ang2,ang3
	942.220	1307.300	43.512	- a_hmax,a_hmin,a_vert

Distance (m)

Azimuth: 90 Dip: 0

1	0.183				- nst, nugget effect
2	0.817	90.0	0.0	0.0	- it,cc,ang1,ang2,ang3
	481.190	743.730	25.774	- a_hmax,a_hmin,a_vert

Distance (m)

Azimuth: 90 Dip: 0

1	0.183				- nst, nugget effect
2	0.817	90.0	0.0	0.0	- it,cc,ang1,ang2,ang3
	942.220	1307.300	43.512	- a_hmax,a_hmin,a_vert

Distance (m)

Azimuth: 0 Dip: 90

1	0.183				- nst, nugget effect
2	0.817	90.0	0.0	0.0	- it,cc,ang1,ang2,ang3
	481.190	743.730	25.774	- a_hmax,a_hmin,a_vert

Distance (m)

Azimuth: 0 Dip: 90

1	0.183				- nst, nugget effect
2	0.817	90.0	0.0	0.0	- it,cc,ang1,ang2,ang3
	942.220	1307.300	43.512	- a_hmax,a_hmin,a_vert

Distance (m)

Figure 4-17: 3D variograms of Facies Three and Facies Four.

65

Figure 4-18: A long section and a cross section illustrating the facies modeling results with *BlockSIS*. Above: long section; and below: cross section.
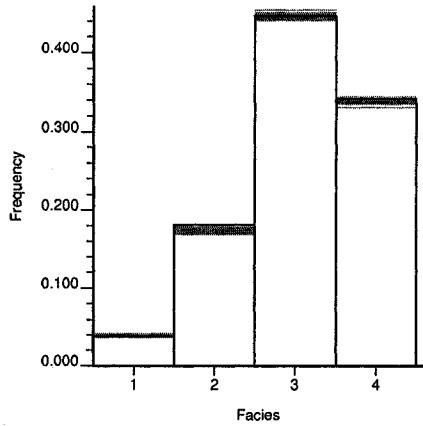
Figure 4-19: Histogram reproduction of 25 realizations.
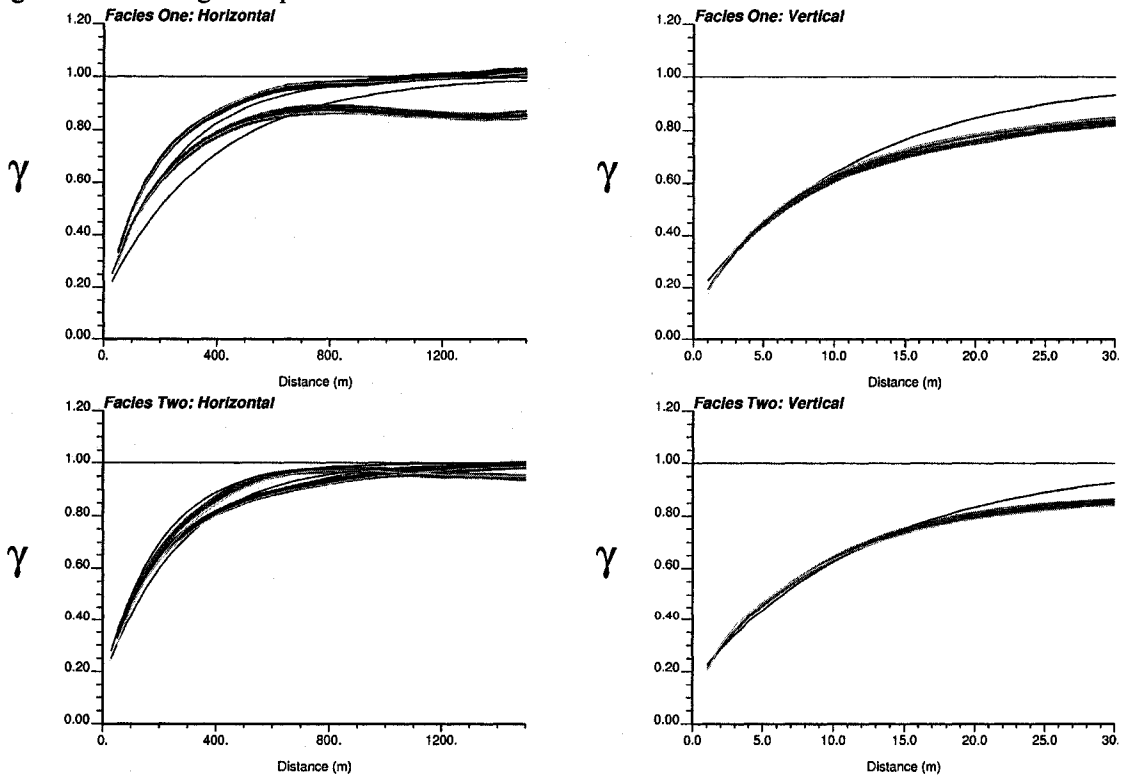
Figure 4-20: Variogram reproduction of Facies One and Two.

66
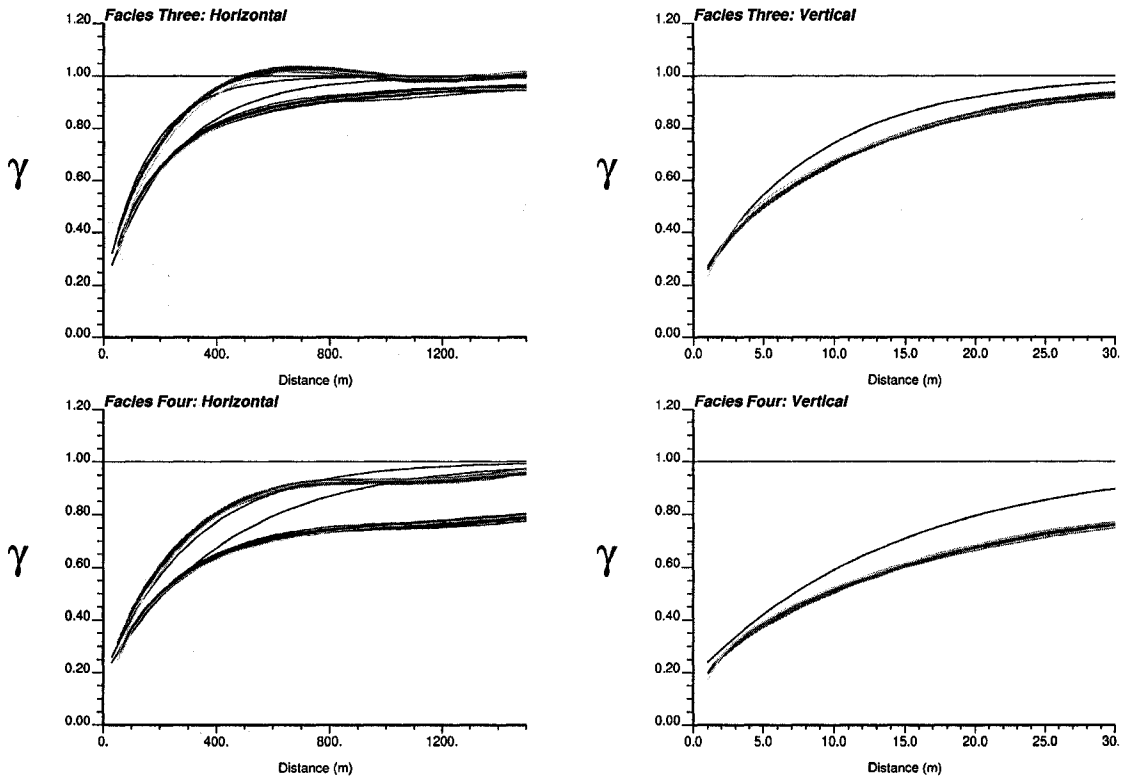
Figure 4-21: Variogram reproduction of Facies Three and Four.
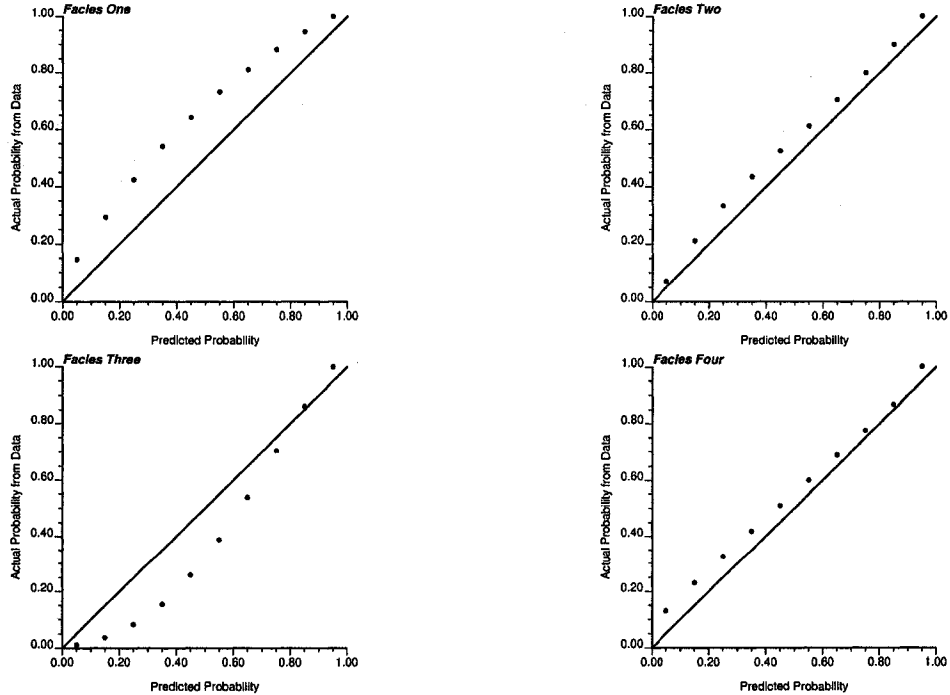
Figure 4-22: Accuracy plots of four facies.

67

This measure is interpreted as the average predicted probability of the true facies. C value describes how "right" the probabilities are for the true facies. The limitation of C is that it gives no credit when a similar facies is predicted nor does it penalize the case when drastically different facies are predicted (Deutsch, 2002). In this case study, the C value is 0.3355 with *BlockSIS* approach.

Another indicator is the local probabilities. The local probabilities are "accurate" or "fair" if they accurately reflect the true fraction of the predicted facies occurs (Deutsch, 2002). Cases where the actual fraction departs significantly from the predicted probabilities are a problem. The corresponding accuracy plots are shown in Figure 4-22. The accuracy is very good.

4.4.2 *GTSIM*
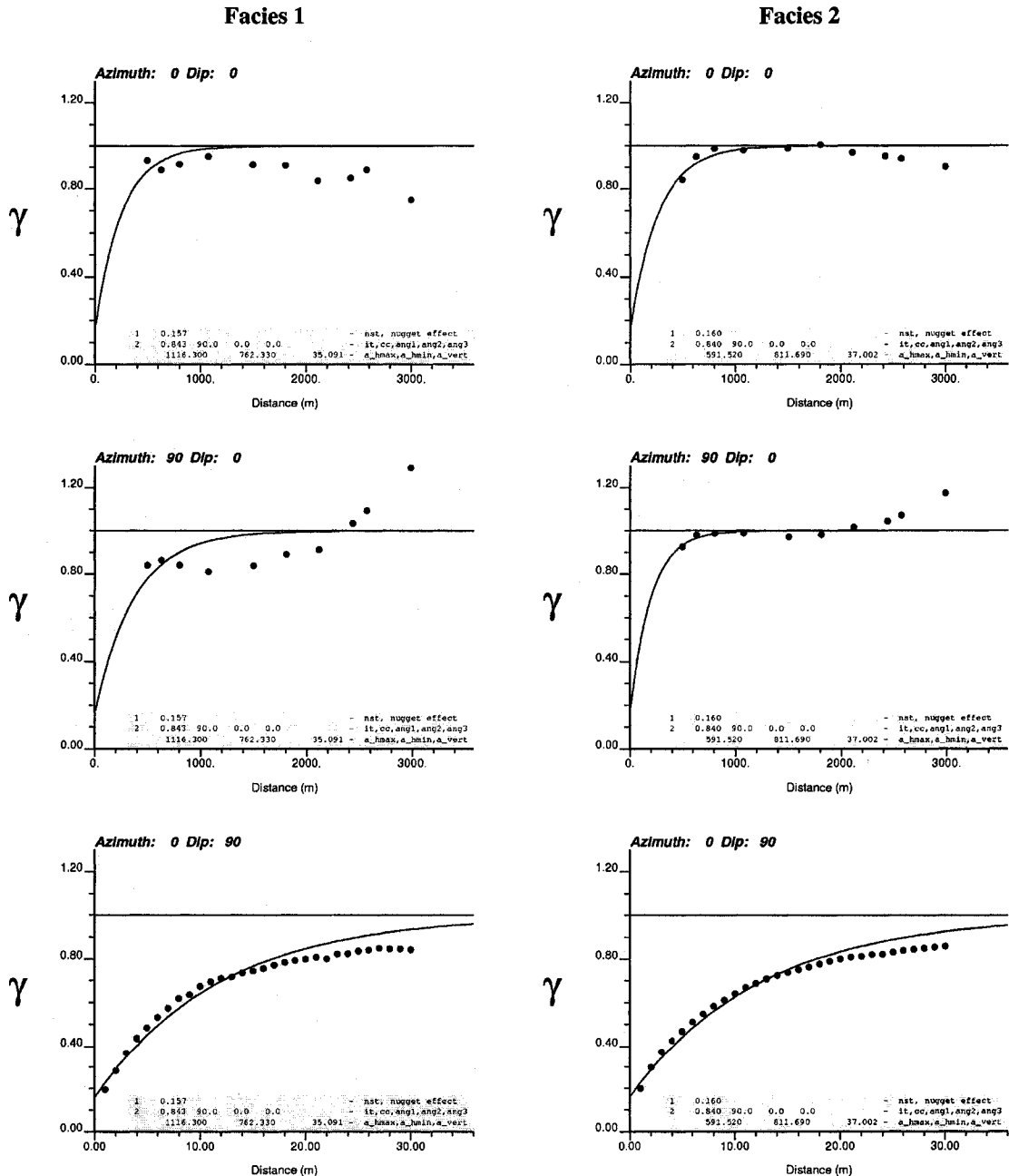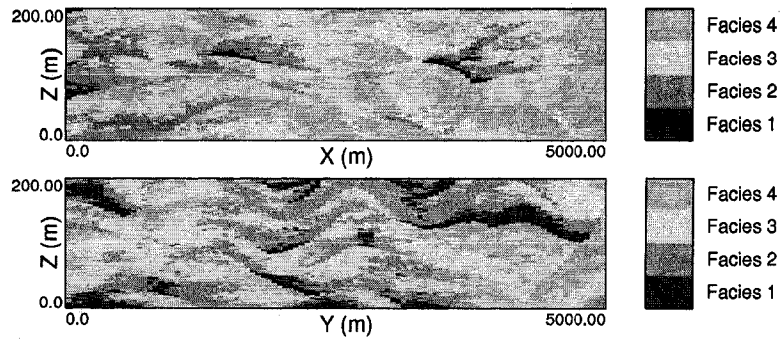
1. Normal score transform

As mentioned earlier, conventional normal score transform is not appropriate when local proportions are available. *CalcSGSData* program is applied to transform facies data to normal score values (Figure 4-23).

NS Data

Number of Data	16200
mean	-0.0367
std. dev.	0.5740
coef. of var	undefined
maximum	3.0018
upper quartile	0.2183
median	0.0000
lower quartile	-0.1746
minimum	-3.5447

Gaussian Value for SGS
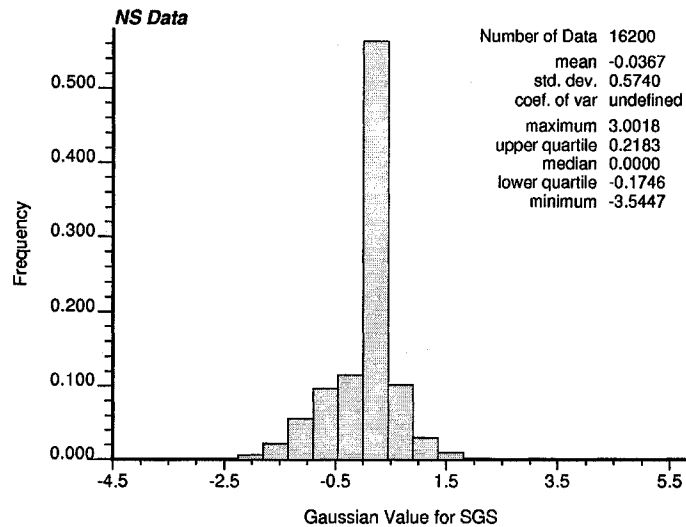
Figure 4-23: The normal score transformed facies data based on collocated facies proportions. A high spike exists.

2. Variogram calculation

Truncated Gaussian simulation requires a single variogram for the normal score transformed facies variable. In general, it is not a good idea to directly calculate and fit the transformed facies variogram for the spikes. The recommended approach is to:

- Take the most important indicator variogram.

- "Invert" it numerically by *bigaus2* program to the corresponding normal score variogram (Figure 4-24).

- Fit the normal score variogram to get input variogram model (Figure 4-25)

The fitted Gaussian variogram is more parabolic at short distance comparing with the original variogram.

3. Facies modeling

The advantage of *GTSIM* is that the simulated facies model is very clean. The spatial structure is well honoured (Figure 4-26).

4. Model checking

The histogram reproduction of 25 realizations is shown in Figure 4-27. The lowest facies proportion (Facies One) is reproduced very well. In general, the histogram reproduction is very good, but it is not as good as *BlockSIS*.

For *GTSIM*, the input variogram is the normal score variogram. Therefore, the variogram of the simulated Gaussian models were checked, instead of indicator variograms of facies models (Figure 4-28). In general, the variograms are very close to the input.

The *C* value is the same as *BlockSIS*, 0.3355, in this case study.

The accuracy plots are made on the by-facies basis (Figure 4-29). Accuracy plots show it is better than *BlockSIS*.
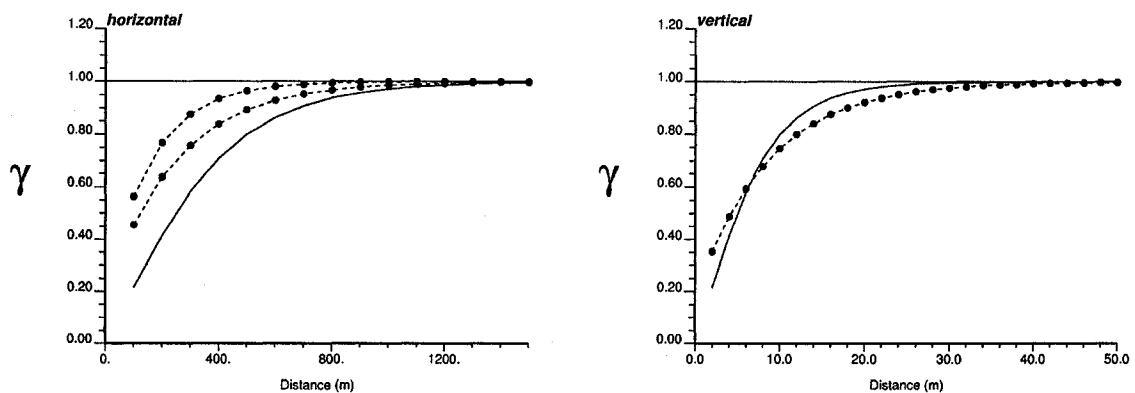
Figure 4-24: The results of *bigaus2* transform. The dash lines show the input indicator variograms and solid lines show the transformed variogram.

69
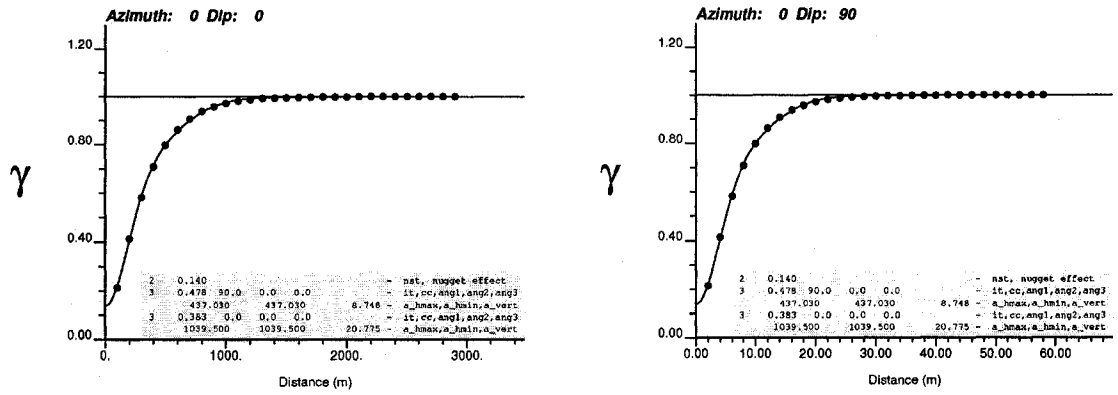
Figure 4-25: The fitted Gaussian model of the *bigaus2* variogram.
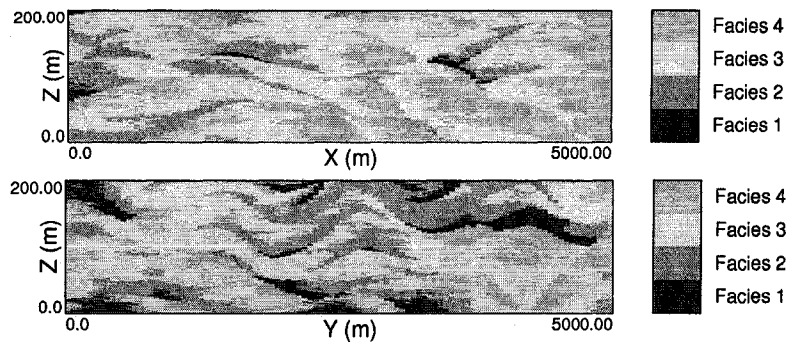
Figure 4-26: The long and cross sections of a truncated Gaussian realization. Above shows the long section and below shows the cross section.
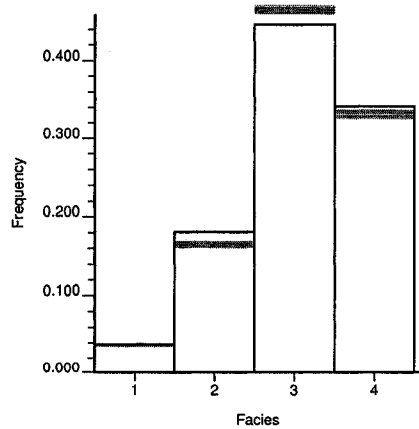
Figure 4-27: The histogram reproduction of 25 *GTSIM* realizations.

70
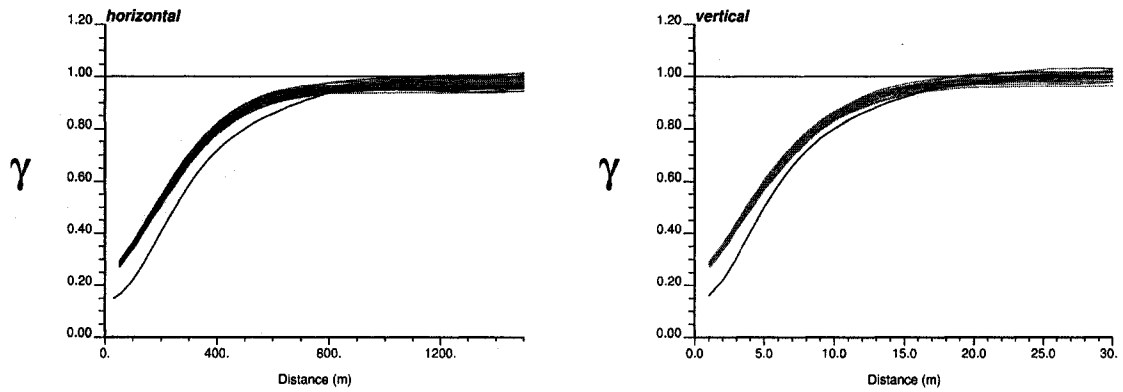
Figure 4-28: The variogram reproduction results of 25 GTSIM realizations.
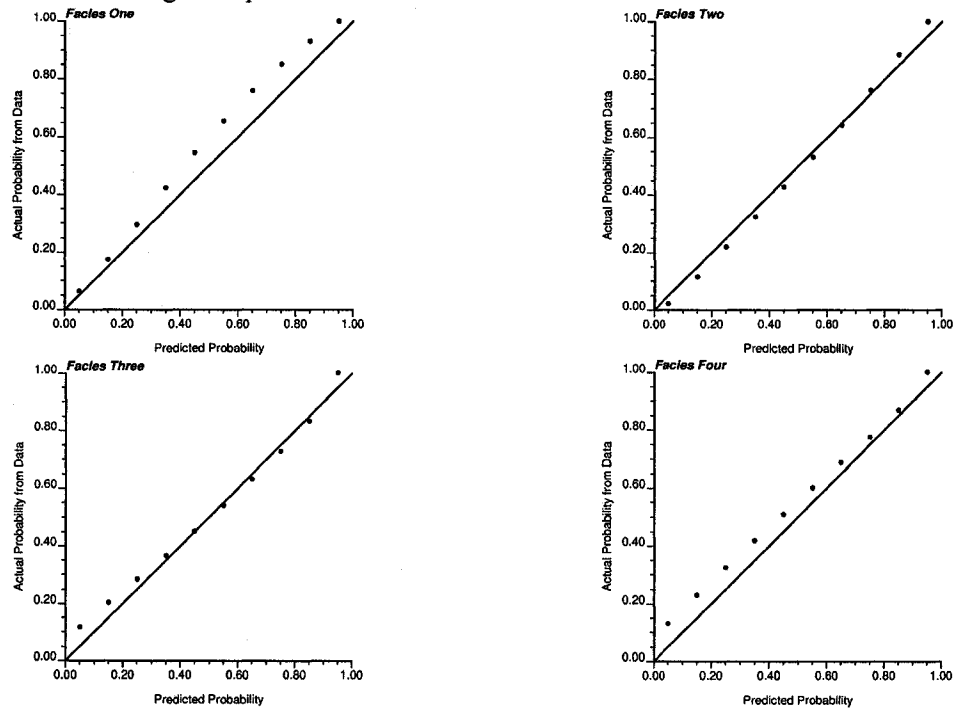
Figure 4-29: Accuracy plots of four facies.

4.4.3 Conclusions

Comparing the simulated facies model and model checking results, the following conclusions can be drawn:

1. The facies model of truncated Gaussian simulation is cleaner. For deepwater turbidite systems, the facies correlation is very strong; therefore, truncated Gaussian simulation approach appears more suitable.

2. In general, both simulation approaches honour well data and spatial structures. *BlockSIS* shows more short-scale spatial variability.

71

Chapter 5

Surface-based Turbidite Modeling Case Study

In this chapter, the application of stochastic surface-based simulation to a synthetic turbidite reservoir is demonstrated.

5.1 The data

The bounding surfaces were synthetically constructed. The slope gradient is about 2 degrees, which is common in distal continental slope environment. The stratum is roughly 60m (198ft) thick and pinches out towards west and north (Figure 5-1 and Figure 5-2). The initial bathymetry is a northwest-southeast-trending submarine depression, and it is assumed that 36 vertical wells are available (Figure 5-3). 36 wells are chosen as a reasonable high level of conditioning in a typical deepwater reservoir study. The 36 wells are regularly distributed (1000 m). A large amount of wells are used in this case study for better variogram inference and enough well data for controlling facies, porosity and permeability distributions. As we discussed earlier in Chapter 3, the newly developed dual-spline error surface interpolation approach works efficiently with a relatively large number of wells. All available data will be honoured, including well picks, facies, porosity and permeability at wells. No large-scale seismic trend and areal trend are applied.

The turbidite reservoir is dominated by compensational cycles that constrain the distribution of lithofacies. Facies along wells were sampled from an unconditional SIS-based realization for modelling the facies distribution at wells. Four facies types are recognized (Table 5-1 and Figure 5-4) and linear vertical facies trend is assumed from proximal to distal based on proximality theory. Declustering technology is applied to rebuild global facies distribution (Figure 5-5). In this synthetic case study, the "true" facies model is assessable, so we know the "real" facies proportions.

Porosity and permeability along the wells were synthetically sampled on a by-facies basis. Permeability is commonly related to porosity. For simplicity, an experimental logarithm relationship between porosity and permeability is applied to build the porosity-based permeability distribution (Deutsch, 2002). The regression equation takes the form:

$$log(K)^* = a_0 + a_1 \cdot \phi \qquad (5.1)$$

where $log(K)^*$ is the predicted logarithm of permeability, a_0 and a_1 are regression coefficients, and ϕ is porosity.

72

The reservoir is assumed to be a mud-rich turbidite fan. Therefore, mudstone is the most important facies component under this geological background. Porosity and permeability histograms are shown in Figure 5-6. The scatter plots of permeability and porosity are shown in Figure 5-7.
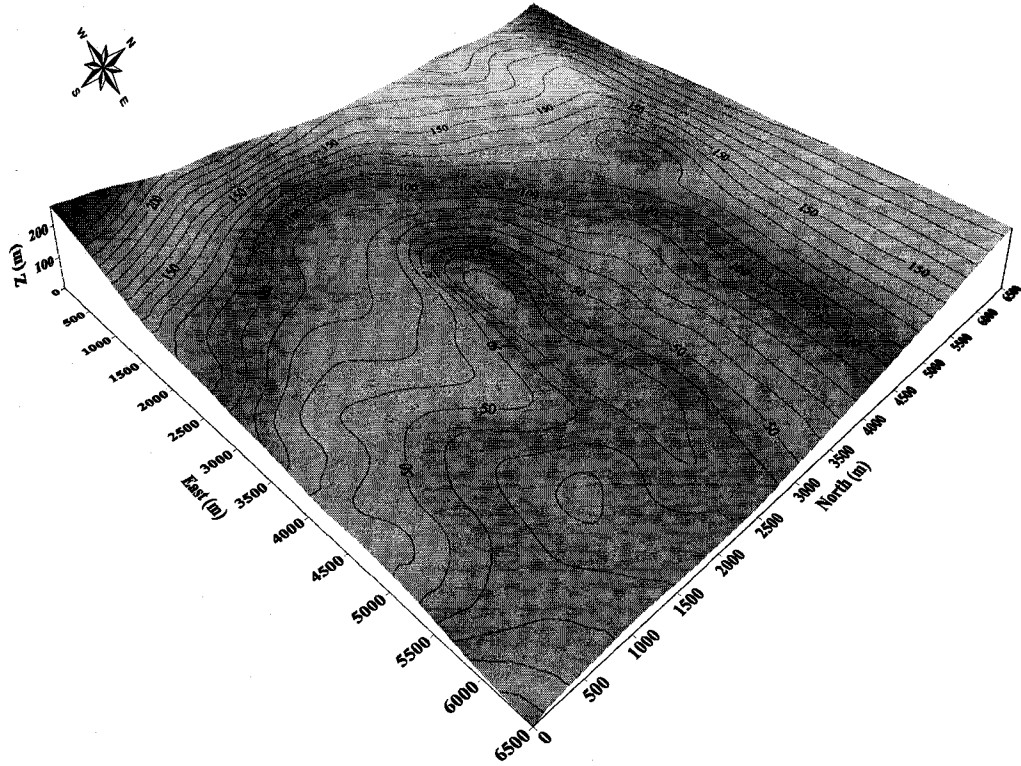
Figure 5-1 The initial bathymetry for the synthetic case study. The contour lines show the elevation distribution of the base surface.
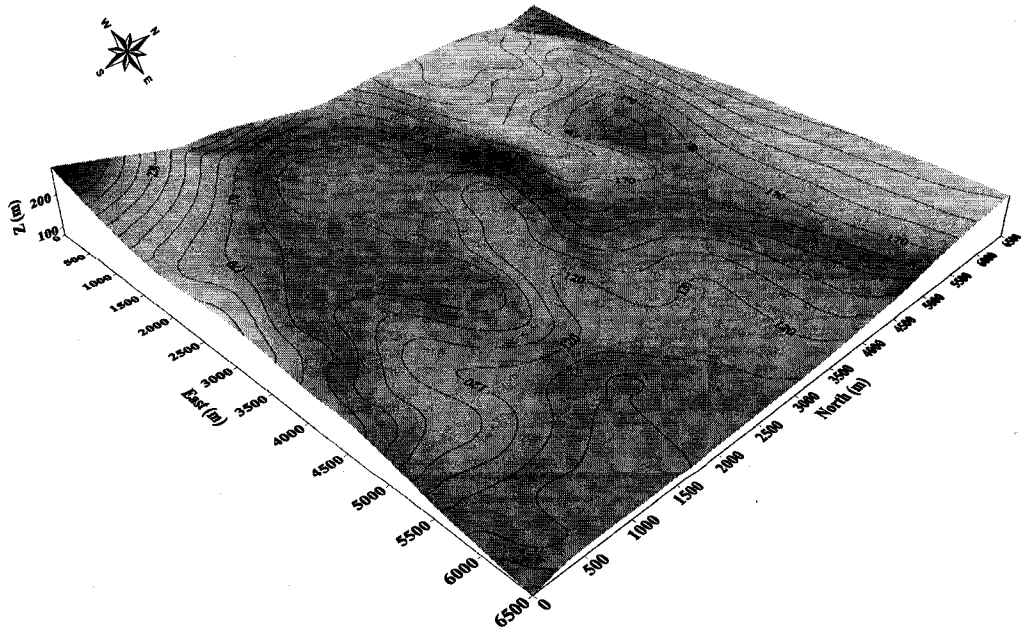
Figure 5-2 The terminal bathymetry for the synthetic case study. The contour lines show the elevation distribution of the top surface.

73
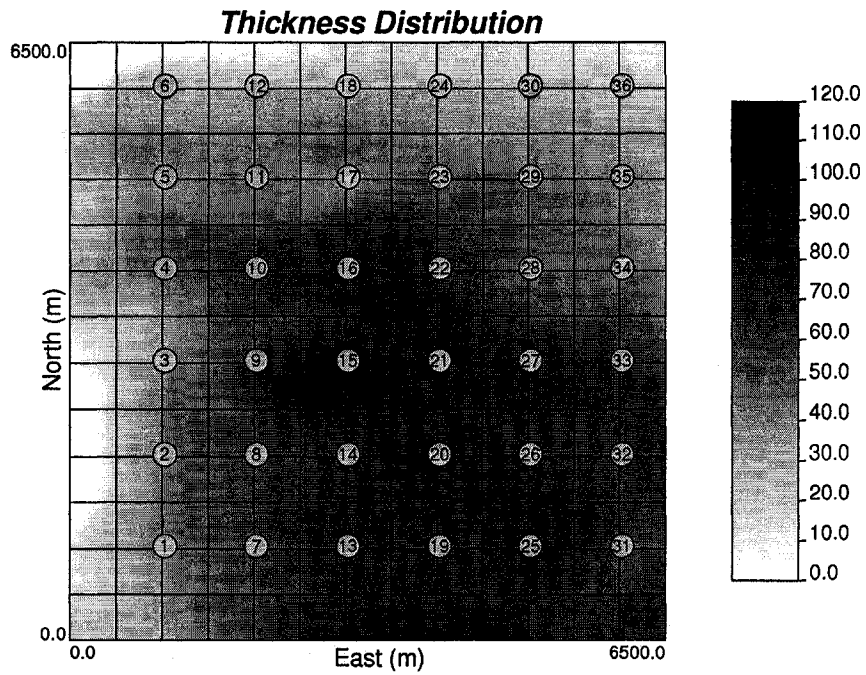
Figure 5-3 The thickness distribution of the strata and the well positions of 36 synthetic wells.

Category	Dominant Lithology	Bedding	Bouma Sequence
Facies 1	Sandstone	Thick – massive, crudely graded	A-division
Facies 2	Sandstone	Thin – medium, subtly graded	B, C-division
Facies 3	Siltstone	Thinly bedded siltstone	D-division
Facies 4	Mudstone	Devoid of mudstone	E-division

Table 5-1: A summary of the lithofacies defined in this case study.
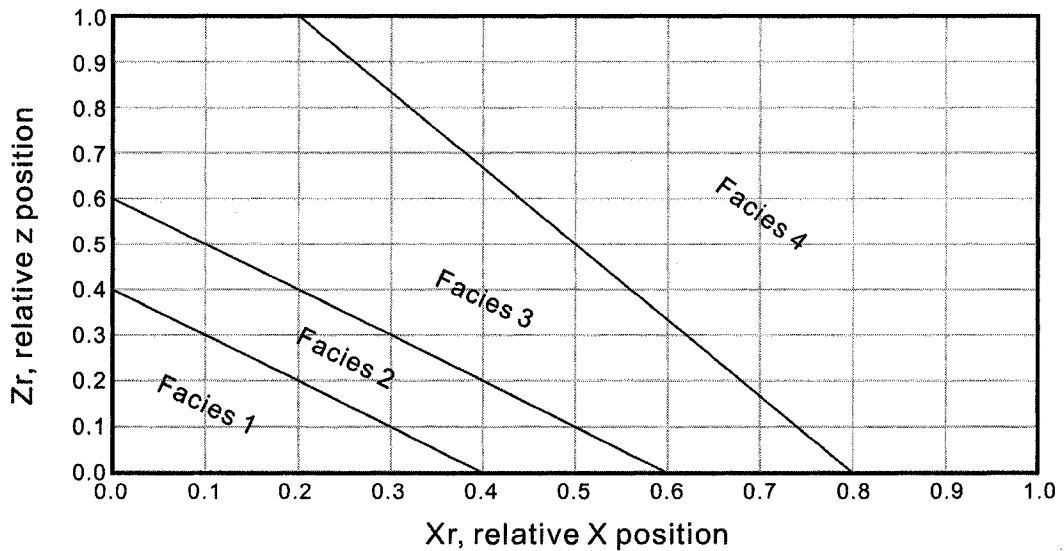
Figure 5-4 The axis-vertical trend definition. The distance is measured in relative scale, and linear facies transitions are assumed. Xr is the relative position along main streamline; Zr is the relative position along vertical direction.
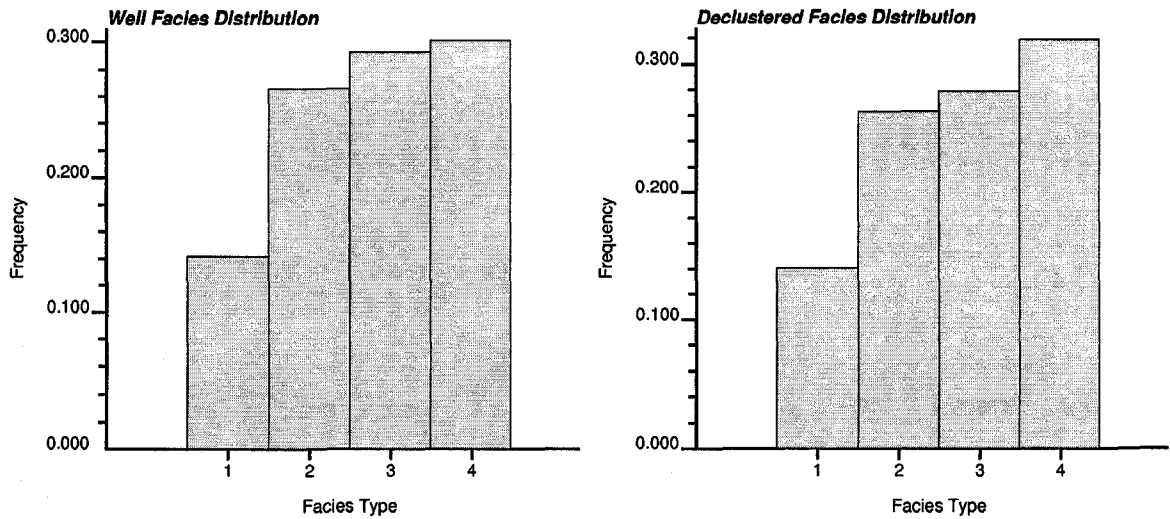
Figure 5-5 Histograms of facies type variable. The four facies, thick sand, thin sand, siltstone and mudstone are equal to 1, 2, 3 and 4, respectively.
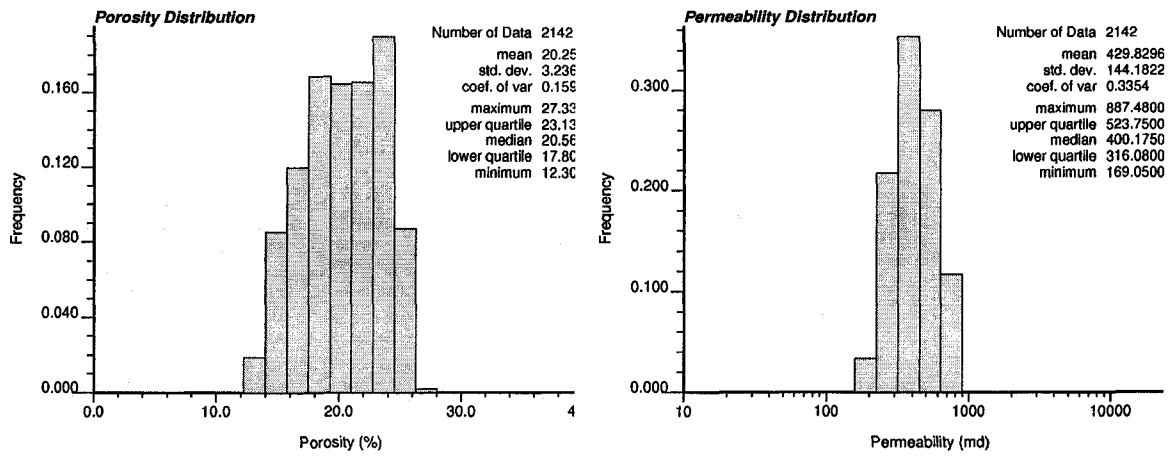
Figure 5-6 The distribution of porosity and permeability from synthetic well logs.
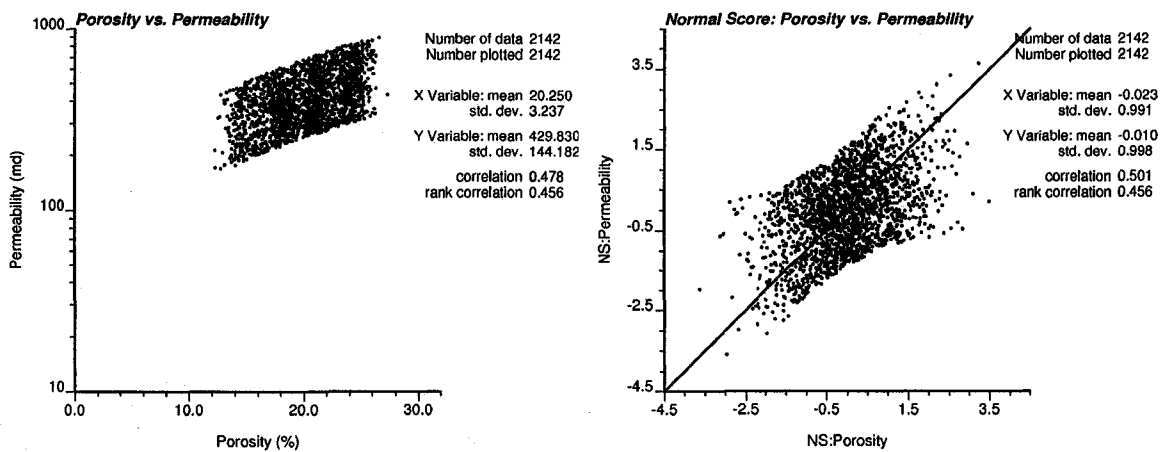
Figure 5-7 The scatter plots of well permeability and porosity before and after Gaussian transform.

75

5.2 Geostatistical work flow

A common geostatistical workflow for surface based modeling is to model: (1) reservoir geometry that honours available wells picks based on geological concept models and related statistical information; cell-based facies proportions model will be built at the same time based on modeled surfaces distribution; (2) lithofacies considering facies proportions model as secondary data; (3) porosity distribution within each facies; and (4) permeability distribution within each facies considering porosity as a secondary variable (Deutsch, 2002; Pyrcz, 2004, 2005). These models are conditioned to all available well data and analog information. Figure 5-8 illustrates the geostatistical workflow of surface-based modeling.

5.2.1 Model of reservoir geometry

Large-scale reservoir geometry can be visualized with seismic and are known for subsequent surfaces modeling. In this case study, two source locations for the turbidite lobes are selected based on global base surface geometry. There are four facies types: graded sandstone, laminated sandstone, siltstone and mudstone (Table 5-1). Mudstone has the largest proportion (Figure 5-5). Subsequent flow event deposits have persistent internal lithofacies trends which are defined by a linear proximal-distal facies trend template (Figure 5-4). An idealized areal facies distribution is assumed.

Surface picks were automatically identified on porosity curves. As a curve identification approach, only shape information is used. Porosity is a function of lithology (shale content), diagenesis, epigenesist, and also other influences. The identified sandstone boundaries are good starting point for further analysis. Experienced geologists may adjust the results based on their geological understandings and by integrating other information that cannot be easily quantified, such as fine-scale depositional structures from core images.

Figure 5-9 illustrates the automatic surface picks identification results of Well 13. The synthetic porosity curve has many short-scale fluctuations, but it is usually very smooth in practice if it is interpreted with well logs.

25 conditional surface models were built to demonstrate the surface-based modeling approach. Although all conditional surface models honour available well picks, the number of surfaces and spatial structures are different, which indicates that the fine-scale reservoir structure has significant uncertainty. The number of surfaces is a good indicator of spatial structure uncertainty (

Figure 5-10); it changes from 61 to 100 with a lognormal shape. The median number of surfaces is 78. Three conditional surface models are shown in Figure 5-11 to compare different spatial structures, which comprising 61, 79 and 100 flow events, respectively.

76

The surface models affect reservoir production performance. This is the initial motivation of quantitative stratigraphic forward modelling (Cross and Lessenger, 1998). Each realization of the reservoir structure is passed through the entire subsequent process of geostatistical reservoir characterization.
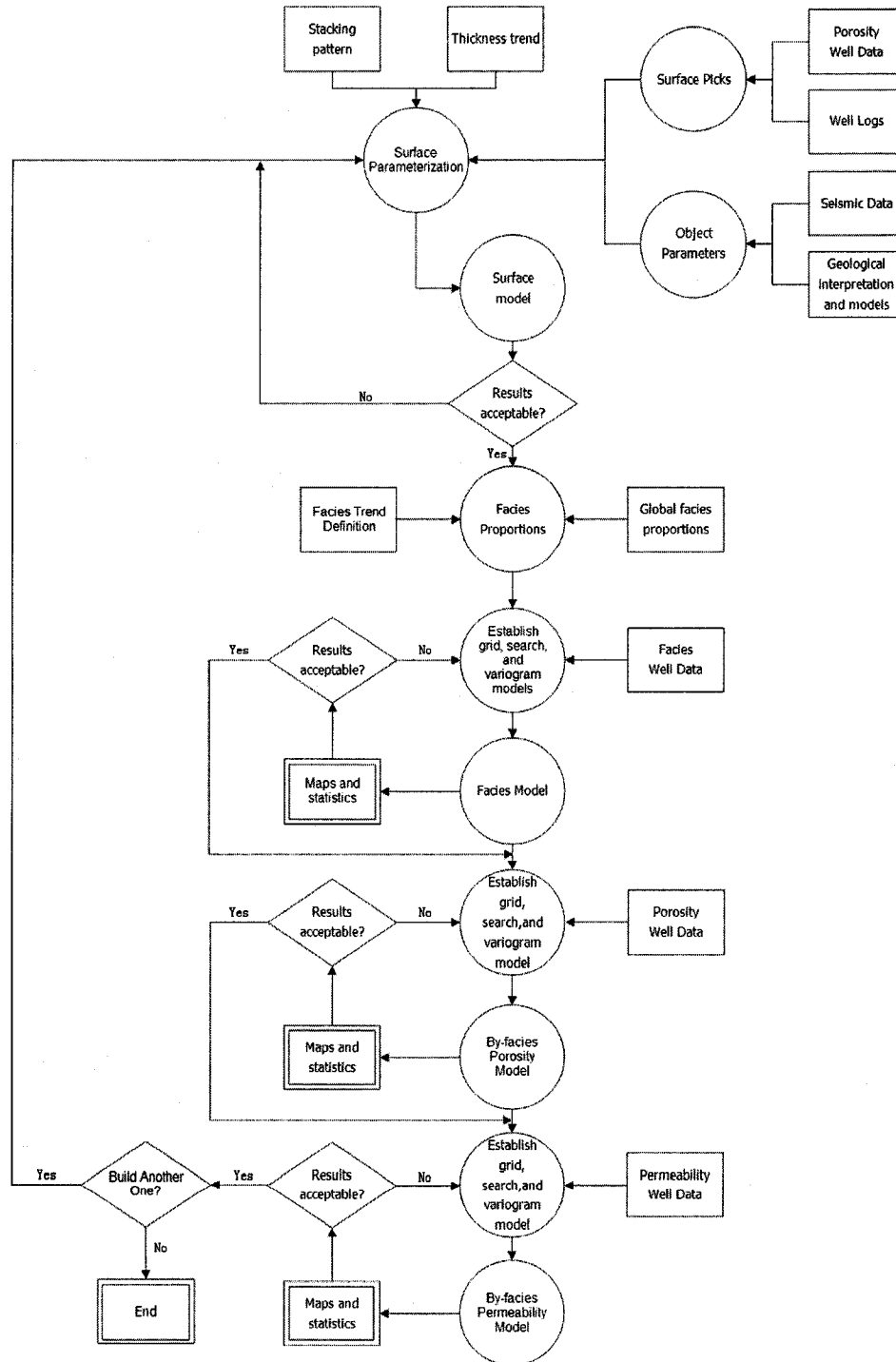
Figure 5-8 Geostatistical workflow of surface based modeling.
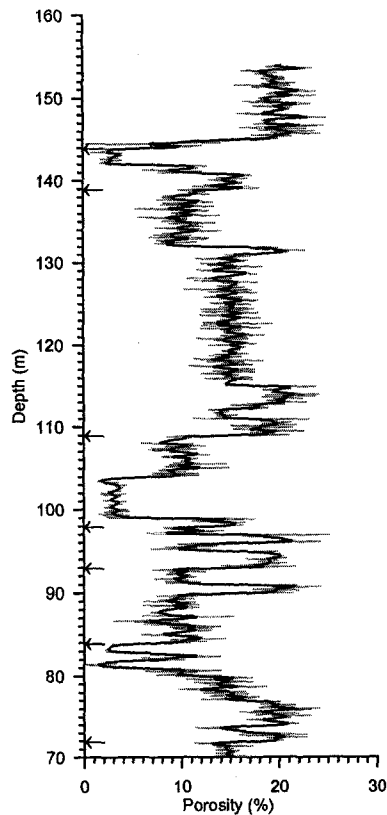
Figure 5-9 The auto surface picks identification results of Well 13. The gray curve is the original porosity curve. The dark curve is the moving window smoothed curve. The left arrows show the identified surface picks. The lowest surface pick is deleted during surface modeling based on visual checking.
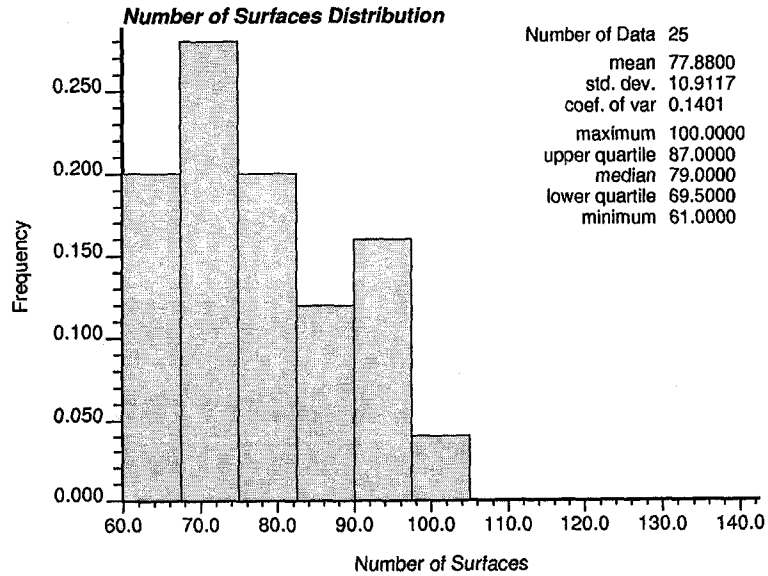
Figure 5-10: The number of surfaces distribution of the 25 conditional surface models.

78

(a)

(b)

(c)
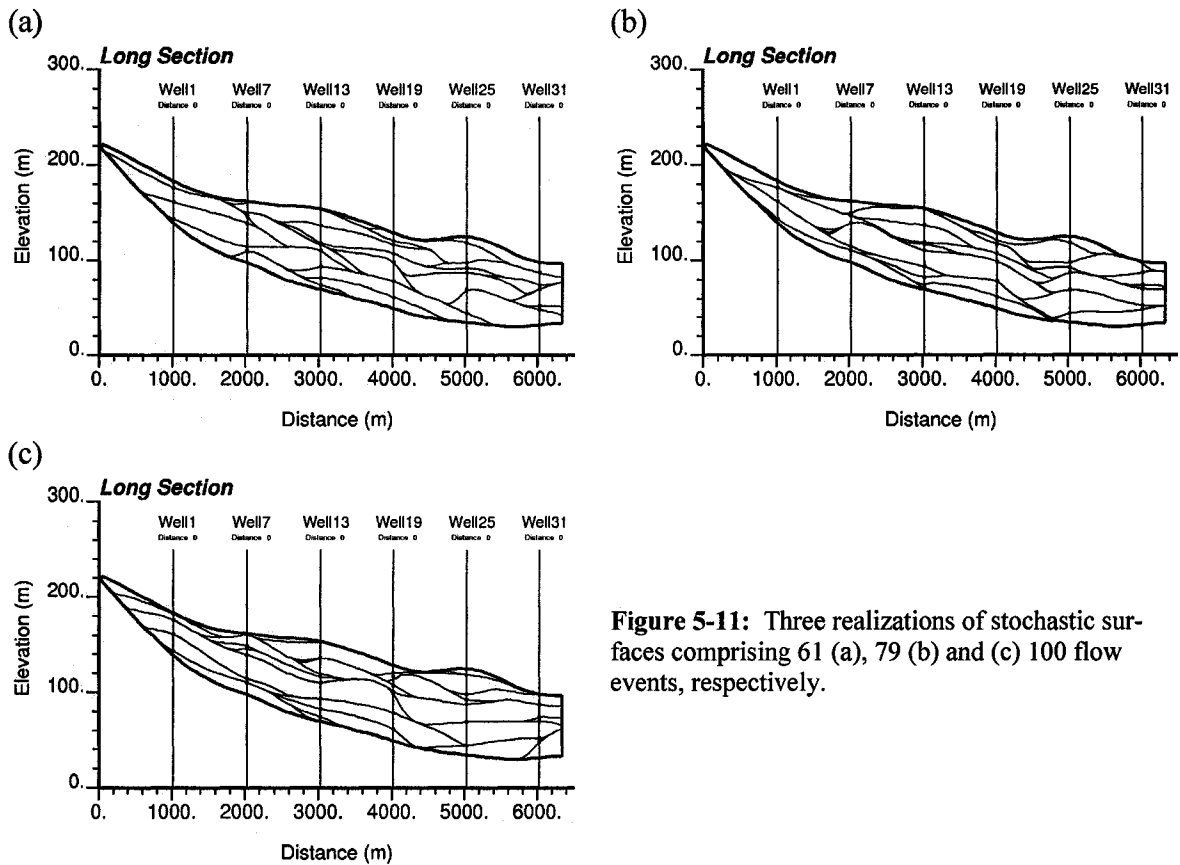
Figure 5-11: Three realizations of stochastic surfaces comprising 61 (a), 79 (b) and (c) 100 flow events, respectively.

5.2.2 Lithofacies models

There are progressively finer sediments and thickening of the finer part of the sandstone / mudstone as the sediments go from proximal to distal direction. The trend information is integrated into cell-based facies model as facies proportions information. The details of facies proportions calculation methodologies were demonstrated in Chapter 4. *BlockSIS* is applied in this case study.

The facies distribution inferred from log and core available at the wells are shown in Figure 5-6. The facies semivariograms are shown in Figure 5-12. The vertical variogram is well informed, but the horizontal variogram inference is a challenge for the continuity within each facies is much smaller than the average well distance. Three facies models comprising 61, 79 and 100 flow events are shown in Figure 5-13 to illustrate the surface-based facies modeling results.

Although both models honour available well data, the spatial distribution of facies changes from realization to realization. The distribution of facies is controlled by the reservoir structure. The distribution of facies will affect reservoir production performance. Uncertainty of each realization of the facies passes through the entire geostatistical reservoir characterization procedure by controlling the reservoir petrophysical properties distributions. The combined contribution of

structural uncertainty and facies distribution uncertainty to production uncertainty can be quantified in terms of production performance.

Figure 5-12: Horizontal and vertical semivariograms of different facies.

Figure 5-13: Fence diagrams of three facies models comprising 61 (a), 79 (b) and 100 (c) flow events, respectively.

81

5.2.3 Petrophysical properties

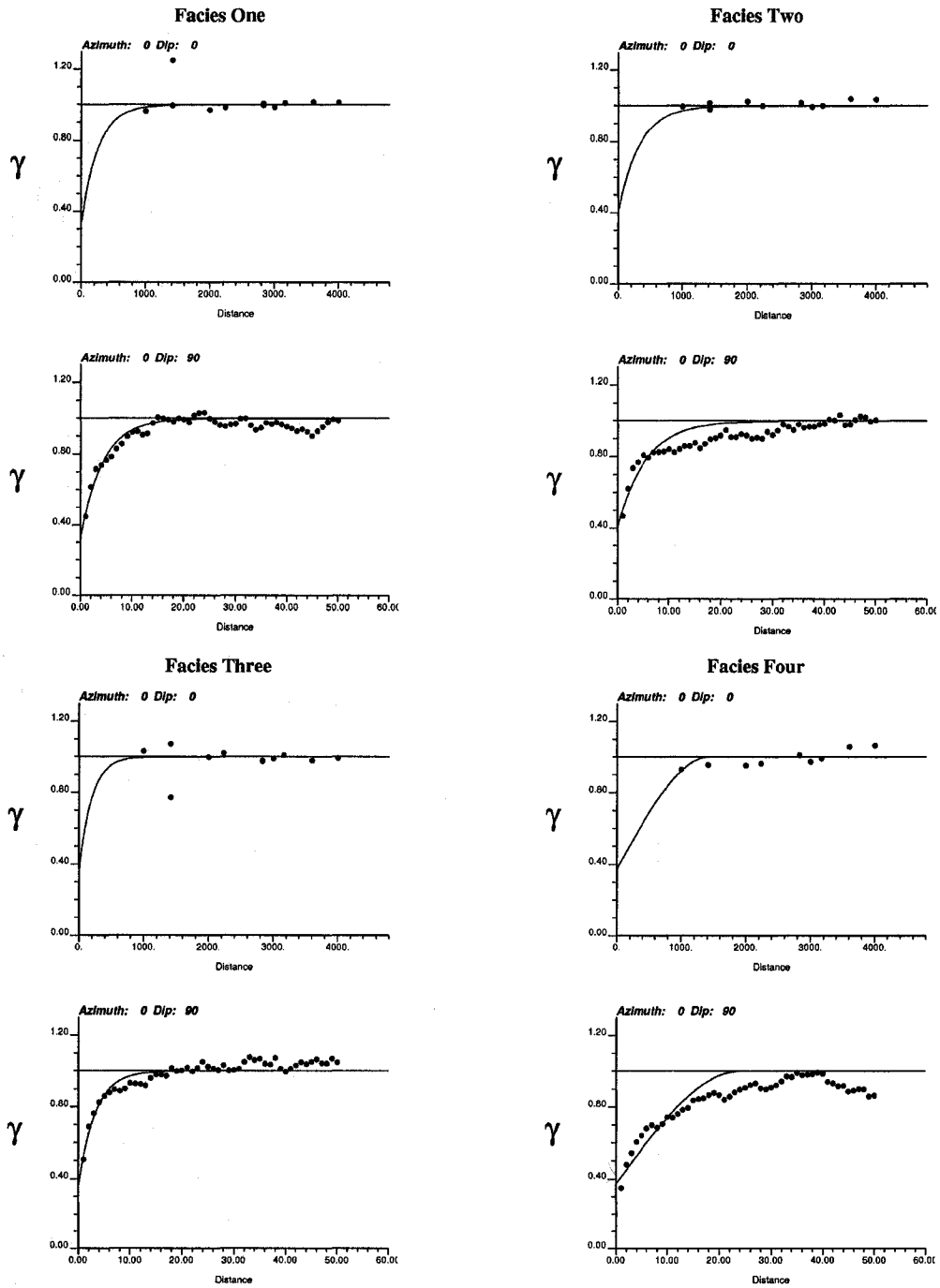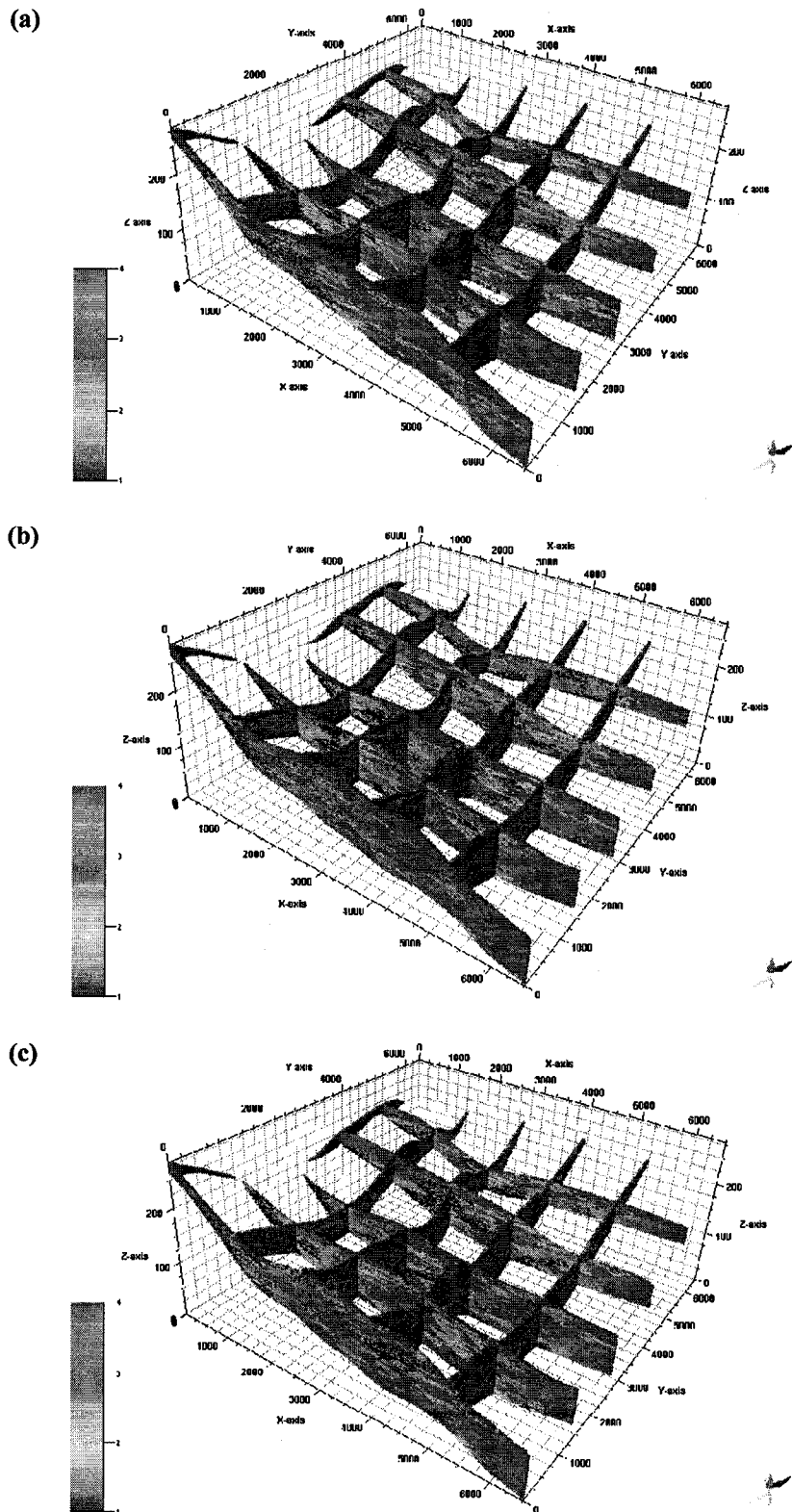Porosity and permeability are continuous variables within each facies. Porosity is simulated independently for each facies type. The results are merged on the by-facies basis. Then permeability is simulated with the corresponding porosity realization as second variable for collocated cokriging on the by-facies basis (Deutsch, 2002; Deutsch and Journel, 1998).

For geological uncertainty assessment purposes, each geological model consists of a single realization of all parameters; therefore, a single realization of porosity and permeability are modeled in associated with each reservoir structure model and facies model. A single geological realization is then defined by a surface (reservoir structure) model, a facies model, a porosity model and a permeability model. The approach is computationally efficient to quantify geological uncertainty (Deutsch, 2002; Pyrcz, 2004). 25 reservoir petrophysical models were built.

The same grid specification used for surface and facies modeling is used for porosity and permeability modeling. The same cells populated with simulated facies codes are populated with simulated properties values. Therefore, the reservoir properties are only simulated between bounding surfaces.

The porosity and permeability distribution inferred from log and core available at the wells are shown in Figure 5-6. The correlation coefficient between the Gaussian transform of porosity and permeability may be inferred from available conditioning data and it is used for permeability modeling with collocated cokriging (Figure 5-7). The experimental porosity and permeability semivariograms were calculated in the plane of the flow events and orthogonal to the flow events (Figure 5-14).

25 by-facies porosity and permeability models were constructed (Figure 5-15, Figure 5-16). The uncertainty in porosity and permeability, i.e. the fluctuation from realization to realization, makes the last contribution to geological uncertainty.

The realizations of reservoir petrophysical properties may be applied for reservoir production uncertainty assessment. The geological uncertainty will be transformed into production uncertainty with flow simulation. Each geological realization is passed into the flow simulator to get a realization of reservoir production performance.

5.3 Some comments

Adequate horizontal and vertical discretization is required to capture geological details. Facies and reservoir properties are often cell-based; therefore finer grid definition is needed to capture geological details and variability, especially along the transition zones of flow events. On the other hand, fine grid definition will create huge simulation grids that need much longer running

time on facies and reservoir properties simulation. In this case study, a 50m×50m×1m grid was applied and the major depositional characteristics were well captured.

The proposed surface conditioning approach works efficiently with large amount of wells. The convergence procedure may be slow if the well density is very high.

The by-facies reservoir petrophysical properties semivariograms inference may be a big challenge in practice. In this case study, it is a serious problem even when the average well distance is only 1000 m.

5.4 Summary

A workflow for surface-based simulation is proposed with a synthetic example in this chapter. The workflow is proposed for geological uncertainty assessment, so each geological realization compromises a surface model, a facies model, a porosity model and a permeability model. The uncertainty in each step will be brought into next simulation stage and the entire geological uncertainty will be brought into reservoir production uncertainty.

With honouring the same available surface picks, surface models show great uncertainty. The number of flow events changes in a broad range. The reservoir properties models reflect the structural uncertainty by honouring facies distribution, which is controlled by surface distribution.

The proposed methodology works very well with relatively dense well pattern. The reservoir structural model will control the later facies and reservoir petrophysical properties distribution. The proposed methodology may be applied to other fan-shaped depositional systems, such as small-scale delta fans and alluvial fans. The default assumption is that the facies trend is understood.

The proposed methodology can be easily modified for more complicated geological settings. For example, streamlines may be modeled based on local bathymetry. The starting point of a flow event should be located on a streamline, instead of by random drawing.

83
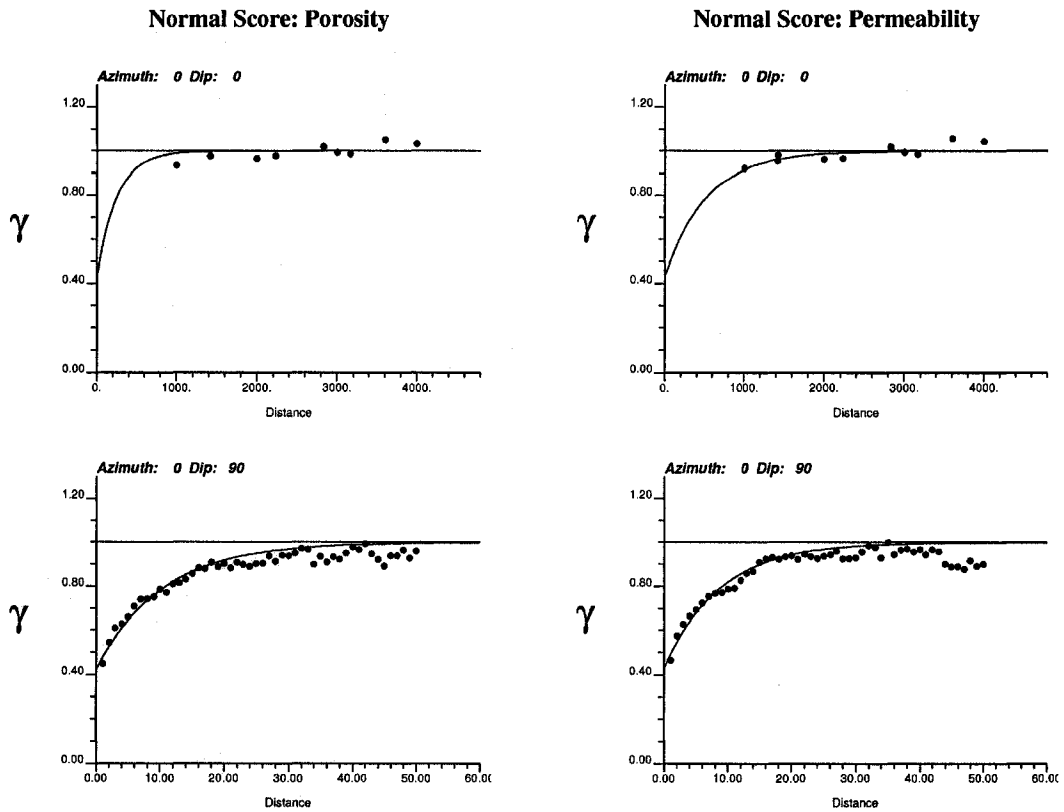
Figure 5-14: Horizontal and vertical semivariograms of the Gaussian transform of the porosity and permeability data.
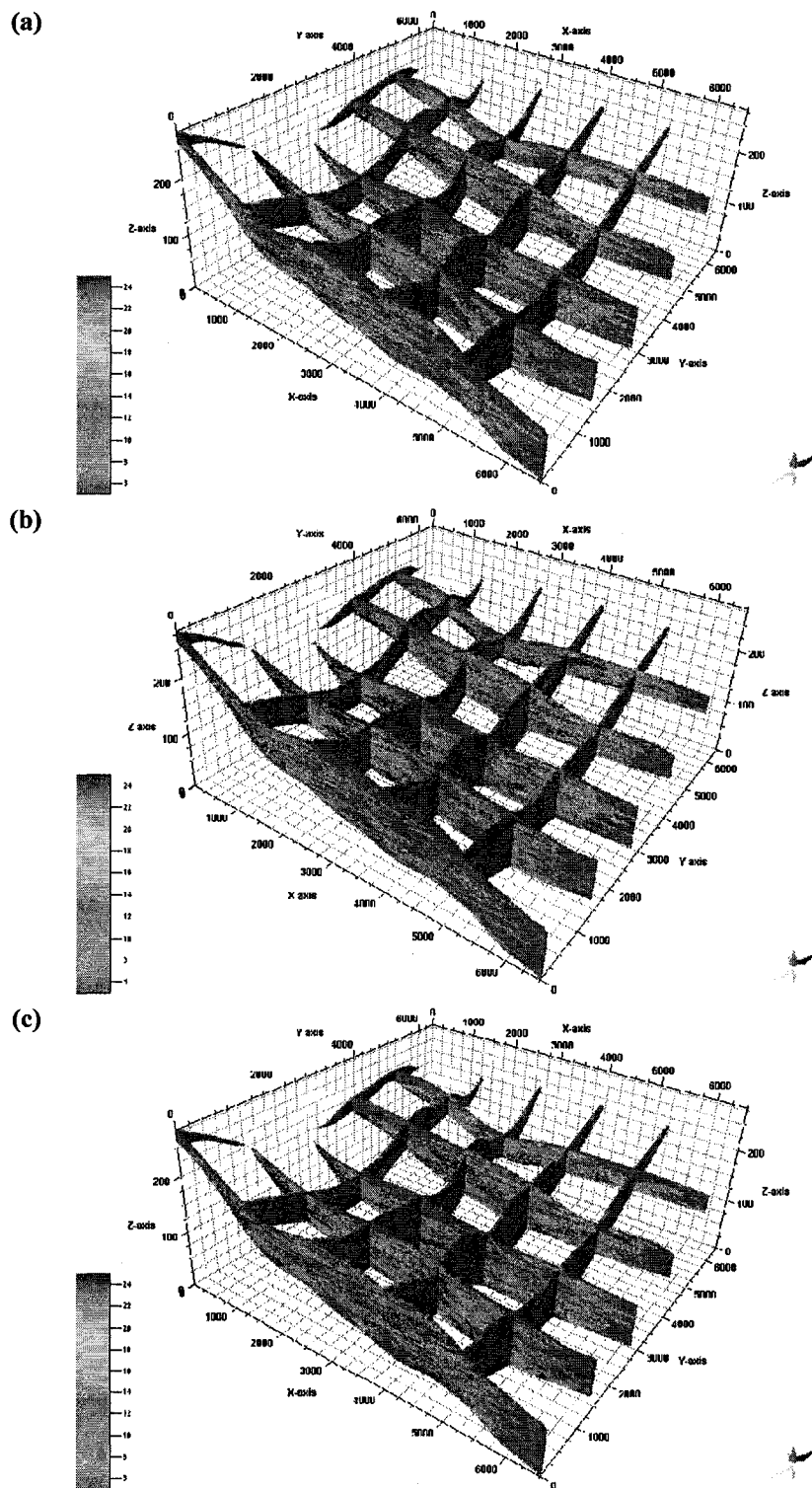
(a)

(b)

(c)

Figure 5-15: Fence diagrams of three porosity models comprising 61 (a), 79 (b) and 100 (c) flow events, respectively.

85

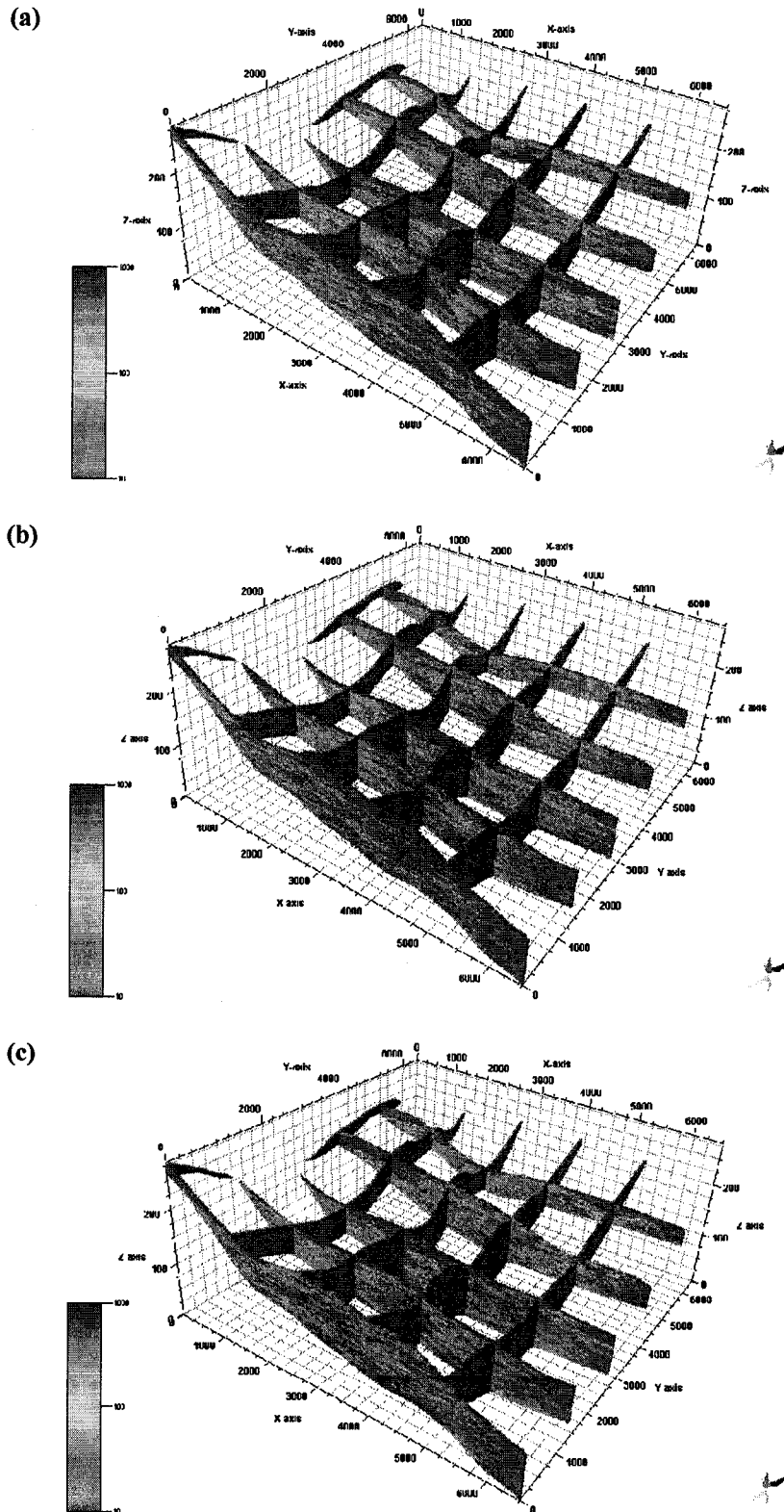**(a)**

(b)

(c)

Figure 5-16: Fence diagrams of three permeability models comprising 61 (a), 79 (b) and 100 (c) flow events, respectively.

Chapter 6

Concluding Remarks

Stochastic surface modeling is applied in this research to capture complicated deepwater turbidite reservoir structures that has been a historic limitation of conventional geostatistical simulation approaches. The spatial structures of deepwater turbidite are complicated with clear curvilinear shapes. Conventional geostatistical simulation approaches focus on reproducing one- and two-point statistics only; therefore, they do not work well for these deepwater depositional systems. There are usually too few wells to control the spatial distribution of reservoir properties over the study area due to the high drilling costs in deepwater environments. This makes deepwater turbidite reservoir uncertainty assessment more difficult. The unique flow mechanism of such depositional systems results in lobes with similar spatial structures; therefore, modeling the lobe topography shapes becomes possible with the development of surface-based modeling techniques.

6.1 Summary

This research aims at developing a lobe event modeling program improving on former research. The original contributions made in this thesis include: (1) the base level concept from sequence stratigraphy is introduced into stochastic surface modeling to guide for surface positioning; (2) improved surface conditioning method for efficiently honoring large amount of wells; (3) stochastic stacking patterns reproduction; and (4) surface-based facies proportions calculation methodologies to integrate both geological conceptual model and areal and vertical facies trends.

1. Equilibrium profile

Equilibrium profile is an important concept in sequence stratigraphy analysis. There are lots of papers discussing large-scale equilibrium profile shapes in various depositional environments, such as beach, continental slope and fluvial environments. For small-scale turbidite lobe events modeling, it is difficult to build equilibrium profiles analytically. A local base level is assumed based on depositional mechanism analysis and applied in this research.

2. Improved surface conditioning method

The improved surface conditioning method is based on the rejection algorithm developed by Pyrcz (2004). To accelerate the optimal surface searching process, a larger candidate surface is drawn with all available well picks located within it. Then the surface is adjusted to an optimal

87

position. To avoid introducing short-scale fluctuation, a dual-spline error surface fitting method is applied to model the error surface.

3. Honour stacking patterns

Stacking pattern has strong influence on facies connectivity and flow patterns. When transforming base surface to paraboloid or incline, the global surface gradient information is kept. This information is utilized in constructing surface probability distribution. Controlling the probability distribution allows common stacking patterns to be reproduced, including aggradation, progradation and retrogradation.

4. Surface based facies modeling

Surface models cannot be used directly in conventional cell-based facies simulation. Surface information has to be transformed to related information that can be integrated by cell-based simulation approach. The relative position information is transformed to facies proportions that can be integrated by conventional SIS-based facies modeling approaches. Both conceptual facies model and vertical and areal trends may be integrated. The spatial structure uncertainty is brought into facies modeling stage.

6.2 Future work

Complicated depositional environments and flow mechanisms make it difficult to design a universal lobe events modeling program. There are some limitations for the current LE_model program that need to be addressed in future research.

1. Streamline construction

No streamlines are explicitly constructed in LE_model. The geometry is constructed based on the center line of a lobe. As a gravity driven turbidity current flow, local geometry strongly controls streamlines distribution and entry point location. It is also the major controlling factor of lobe orientation. The simulated streamlines could also honour the recognized streamlines on high-resolution seismic image.

2. Honour incomplete surface information

Small-scale surface can not be continuously traced on seismic, but part of the surface may be visualized clearly on seismic. The incomplete surface information and recognized surface contacts have to be honored.

3. Conditional modeling depositional erosion events

Local depositional erosion events due to the strong destruction ability of turbidite current happen often in geological history. Therefore, the idealized spatial structures seldom exist. Erosion simulation is important on reproducing complicated reservoir structures. The proposed method can only work unconditionally at present.

4. Honour 3D facies trend directly

3D facies trend may be recognized on seismic. At present, only longitudinal and lateral facies trends information can be integrated using user-specified trend templates.

89

Bibliography

Allen, P. A., and J. R. Allen, 2005, Basin analysis: principles and applications: Malden, Blackwell Scientific Publications, 549 p.

Baas, J. H., W. D. McCaffrey, and R. J. Knipe, 2005, The deep-water architecture knowledge base: towards an objective comparison of deep-marine sedimentary systems: Petroleum Geoscience, v. 11, p. 309 - 320.

Boggs, S., 2001, Principles of sedimentology and stratigraphy: Upper Saddle River, Prentice Hall, 3rd edition, 726 p.

Bouma, A. H., 1962, Sedimentology of some flysch deposits: a graphic approach to facies interpretation: Amsterdam, Elsevier Publication Corporation, 168 p.

Catuneanu, O., 2006, Principles of sequence stratigraphy: developments in sedimentology: Amsterdam, Elsevier, 375 p.

Cronin, B. T., and A. J. Hartley, 2000, Equilibrium profile development in graded deep-water slopes: Eocene, Eastern Turkey: Journal of the Geological Society, v. 157, p. 943 - 955.

Cross, T. A., and M. A. Lessenger, 1998, Sediment volume partitioning: rationale for stratigraphic model evaluation and high-resolution stratigraphic correlation, in K. O. Sandvik, F. Gradstein, and N. Milton, eds., Predictive high resolution sequence stratigraphy, Norwegian Petroleum Society Special Publication, p. 171 - 196.

Deutsch, C. V., and L. Wang, 1996, Hierarchical Object-based stochastic modeling of fluvial reservoirs: Mathematical Geology, v. 28, p. 857 - 880.

Deutsch, C. V., and A. G. Journel, 1998, GSLIB: geostatistical software library and user's guide: New York, Oxford University Press, 2nd edition, 369 p.

Deutsch, C. V., and T. T. Tran, 1999, Simulation of deepwater lobe geometries with object-based modelling, CCG Annual Report One, University of Alberta, Edmonton.

Deutsch, C. V., Y. Xie, and A. S. Cullick, 2001, Surface geometry and trend modeling for integration of stratigraphic data in reservoir models, 2001 Society of Petroleum Engineering Western Regional Meeting, Bakersfield, California, SPE 68817.

Deutsch, C. V., 2002, Geostatistical reservoir modeling: New York, Oxford University Press, 376 p.

Deutsch, C. V., 2006, A sequential indicator simulation program for categorical variables with point and block data: BlockSIS: Computers & Geosciences, v. 32, p. 1669 - 1681.

Friedrichs, C. T., and L. D. Wright, 2004, Gravity-driven sediment transport on the continental shelf: implications for equilibrium profiles near river mouths: Costal Engineering, v. 51, p. 795 - 811.

Ghosh, B., and D. R. Lowe, 1993, The architecture of deep-water channel complexes, Cretaceous Venado Sandstone Member, Sacramento Valley, California, in S. A. Graham, and D. R. Lowe, eds., Advances in the sedimentary geology of the Great Valley Group, Sacramento Valley, California, SPEM Pacific Section, Special Publication, p. 51 - 65.

Haldosen, H. H., and L. W. Lake, 1984, A new approach to shale management in field-scale model: Society of Petroleum Engineering Journal, p. 447 - 457.

Haldosen, H. H., and D. W. Chang, 1986, Notes on stochastic shales; from outcrop to simulation model, in L. W. Lake, and H. B. Caroll, eds., Reservoir characterization: London, Academic Press, p. 445 - 485.

Hesse, R., 1992, Turbiditic and non-turbiditic mudstone of Cretaceous flysch sections of the East Alps and other basins, in D. A. V. Stow, eds., Deep-Water Turbidite systems: Oxford, Blackwell Scientific Publications, 473 p.

Journel, A. G., 2002, Combining knowledge from diverse sources: an alternative to traditional data independence hypotheses: Mathematical Geology, v. 34, p. 573 - 596.

Krsek, P., G. Lukacs, and R. R. Martin, 1998, Algorithms for computing curvatures from range data, in R. R. Martin, and T. Varady, eds., RECCAD Deliverable Document 4 Copernicus Project, no. 1068, Budapest, Computer and Automation Institute, Hungarian Academy of Sciences.

MacDonald, D. I. M., 1992, Proximal to distal sedimentological variation in a linear turbidite through: implications for the fan model, in A. V. Stow, eds., Deep-water turbidte systems: Oxford, Blackwell Scientific Publications.

Middleton, G. V., and M. A. Hampton, 1976, Sediment gravity flows: mechanics of flow and deposition, in G. V. Middleton, and A. H. Bouma, eds., Turbidites and deep-water sedimentation, SEPM Pacific Section, Special Publication.

Mulder, T., J. P. M. Syvitski, and K. I. Skene, 1998, Modeling of erosion and deposition by turbidity currents generated at river mouths: Journal of Sedimentary Research, v. 68, p. 124 - 137.

Natland, M. L., and P. H. Kuenen, 1951, Sedimentary history of the Ventura Basin, California, and the action of turbidity currents: Soc. Ec. Pal. and Min., Special Publication, v. 2, p. 77 - 107.

Pickering, K. T., R. N. Hiscott, and F. J. Hein, 1989, Deep-marine environments: clastic sedimentation and tectonics: London, Unwin Hyman, 416 p.

Press, F., and R. Siever, 1986, Earth, W. H. Freeman and Company, 567 p.

Pyrcz, M. J., and C. V. Deutsch, 2003, Stochastic surface modeling in mud rich, fine-grained turbidite lobes (abs.), AAPG Annual Meeting, Salt Lake City, Utah.

Pyrcz, M. J., 2004, Integration of geologic information into geostatistical models: Ph.D. thesis, University of Alberta, Edmonton, 293 p.

Pyrcz, M. J., O. Catuneanu, and C. V. Deutsch, 2005, Stochastic surface-based modeling of turbidite lobes: AAPG Bulletin, v. 89, p. 177 - 191.

Reading, H. G., and M. Richards, 1984, Turbidite systems in deepwater basin margins classified by grain size and feeder system: AAPG Bulletin, v. 78, p. 792 - 822.

Reineck, H., and I. B. Singh, 1980, Depositional sedimentary environments, with reference to terrigenous clastics: New York, Springer-Verlag, 2nd, revised and updated edition, 549 p.

Stelting, C. E., A. H. Bouma, and C. G. Stone, 2000, Fine-grained turbidite systems: Overview., *in* A. H. Bouma, and C. G. Stone, eds., Fine-grained Turbidite Systems, AAPG Memoir 72 / SEPM Special Publication, no. 68, American Association of Petroleum Geologists, p. 1 - 8.

Stow, D. A. V., 1992, Deep-water turbidite systems: Oxford, Blackwell Scientific Publications, 473 p.

Stow, D. A. V., H. G. Reading, and J. D. Collinson, 1996, Deep seas, *in* H. G. Reading, eds., Sedimentary environments: processes, facies and stratigraphy: Oxford, Blackwell Science, 3rd edition, 688 p.

Stoyan, D., W. S. Kendall, and J. Mecke, 1987, Stochastic geometry and its applications: New York, John Wiley & Sons, 345 p.

Strebelle, S., 2002, Conditional simulation of complex geological structures using multiple-point statistics: Mathematical Geology, v. 34, p. 1 - 21.

Xie, Y., and C. Deutsch, 2000, Surface geometry and trend modeling for integration of stratigraphic data in reservoir models, Sixth International Geostatistics Congress, Cape Town.

Yu, Z. W., 2001, Surface interpolation from irregularly distributed points using surface splines with Fortran program: Computers & Geosciences, v. 27, p. 877 - 882.